Supporting Information for

The Structure-Activity Relationship of Peptide Conjugated Chloramphenicol for Inhibiting *E. coli*

Jiaqing Wang,[†] Adrianna Shy,[†] Difei Wu,[†] Deani Cooper ,[‡] Jiashu Xu,[†] Hongjian He,[†] Wenjun Zhan,[†] Shenghuan Sun,[†] Susan T. Lovett,[‡] Bing Xu[*,†]

[†]Department of Chemistry, Brandeis University, 415 South Street, Waltham, Massachusetts 02454, United States.

[‡]Department of Biology, Brandeis University, 415 South Street, Waltham, Massachusetts 02454, United States.

Correspondence to: Email: bxu@brandeis.edu

Table of Contents

S1. Experimental materials and instruments

All the solvents and chemical reagents were used directly as received from the commercial sources without further purification unless otherwise stated. Porcine liver esterase (PLE) was purchased from Sigma-Aldrich (lyophilized powder, ≥15 units/mg solid; Unit definition: One unit will hydrolyze 1.0 μmole of ethyl butyrate to butyric acid and ethanol per min at pH 8.0 at 25 °C). All conjugates were purified with Agilent 1100 Series Liquid Chromatography system, equipped with an XTerra C18 RP column and Variable Wavelength detector. The LC-MS spectra were obtained with a Waters Acquity Ultra Performance LC with Waters MICROMASS detector. ^{1}H NMR spectra were obtained on Varian Unity Inova 400, and TEM images on a Morgagni 268 transmission electron microscope.

S2. Synthesis and characterizations

We synthesized CLsu by acidifying the commercially available chloramphenicol succinate sodium. Chloramphenicol succinate sodium (150 mg) was dissolved in distilled water (3 mL), and HCl (1 M) was added dropwise until the pH of the mixture was adjusted to 2.0. The precipitate was washed several times with distilled water and dried for further use.

We used solid phase peptide synthesis (SPPS)[26] for the synthesis of all pepetide-conjugated prodrugs. 2-Chlorotrityl chloride resin (500 mg, 0.5 mmol) was swelled in 10 mL of DCM for 20 min. The attachment of the first Fmoc protected amino acid (0.5 mmol) to the resin was achieved by adding *N,N*-diisopropylethylamine (DIPEA) (413 μL, 2.5 mmol) to the beads in the reaction vessel, which was allowed to shake at room temperature for 1 h. After that, the reaction solution was drained, followed by washing with DMF (10 mL × 3) and DCM (10 mL × 3). The unreacted 2-chlorotrityl chloride moieties were capped with a solution of methanol/DIPEA/DCM (v/v/v:

3/1/16) for 30 min. The beads were washed with DMF (10 mL × 3). The Fmoc group was removed by treating beads with 20% piperidine/DMF (v/v) solution for 20 min at room temperature. The solution was drained and washed with DMF (10 mL × 3). The beads were reacted with next Fmoc protected amino acid or CLsu (0.5 mmol) by adding HBTU (190 mg, 0.5 mmol) and *N,N*-diisopropylethylamine (DIPEA) (413 μL, 2.5 mmol) to the beads in the reaction vessel, which was allowed to shake at room temperature for 1 h, and the solution was drained. Then the product was cleaved from resin with 10 mL of trifluoroacetic acid for 2 h. The solution was collected, and the remaining beads were washed with 5 mL of trifluoroacetic acid three times. All the solution was combined and trifluoroacetic acid was removed with the N_2 flow. The residue was then precipitated with diethyl ether. The crude product was purified by reverse phase HPLC using HPLC grade acetonitrile and water with supplement of 0.1% trifluoroacetic acid as the eluents.

Synthesis of compound 4b. CLsu was dissolved in DCM. After that, bromotrimethylsilane (TMSBr) was added dropwise to afford compound 4b, which was purified by reversed phase HPLC using HPLC grade acetonitrile and water with supplement of 0.1% trifluoroacetic acid as the eluents.

Synthesis of compound 4c. CLsu (0.1 mmol), HBTU (0.11 mmol) and DIEA (0.5 mmol) were dissolved in DMF (1 mL). The mixture was stirred at room temperature for 30min. Followed by, taurine (0.2 mmol) was added to the stirring mixture and stirred continually at room temperature for overnight. The solvent was removed by air dry, and then final product was purified by reversed phase HPLC using HPLC grade acetonitrile and water with supplement of 0.1% trifluoroacetic acid as the eluents.

Synthesis of compound 4d. CLsu (0.1 mmol), HBTU (0.11 mmol) and DIEA (0.5 mmol) were dissolved in DMF (1 mL). The mixture was stirred at room temperature for 30min. Followed by, o-phosphorylethanolamine (0.2 mmol) was added to the stirring mixture and stirred continually at room temperature for overnight. The solvent was removed by air dry, and then final product was purified by reversed phase HPLC using HPLC grade acetonitrile and water with supplement of 0.1% trifluoroacetic acid as the eluents.

S3. Hydrolysis assay

Wild-type *E. coli* strains (K12) were harvested by centrifugation and the cell pellets were lysed using a sonic device. After centrifugation, the supernatant was collected and the proteinase inhibitor was added in the *E.coli* lysate. The concentration of *E. coli* lysate was normalized by the fluorescence intensity of 5-carboxyfluorescein diacetate (CFDA). Briefly, different concentrations of CES (4 U/mL, 2 U/mL, 1 U/mL, 0.5 U/mL, 0.25 U/mL, 0.125 U/mL, 0.0625 U/mL, 0.03125 U/mL, 0.015625 U/mL and 0 U/mL) and different amount of *E. coli* lysates were prepared in PBS buffer. Followed by, 25 μM of CFDA was added in and incubated at room temperature for 1 h. Then the fluorescence was tested to draw a fluorescence-concentration dependent curve for figuring out the concentration of *E. coli* lysates. Solutions of CLsuGG (3) (200 μM) were prepared in pH 7.4 PBS buffer. CES and *E. coli* lysate (0.1 U/mL) were added and incubated with above solutions at 37 ℃ for 24 h. At different time points, the solution was taken out, extracted with an equal volume of butanol, concentrated to dryness, and resuspended with butanol for HPLC analysis.

S4. TEM sample preparation

In this paper, we used negative staining technique to study the TEM images. We first glowed discharge the 400 mesh copper grids coated with continuous thick carbon film (~ 35 nm) prior to use to increase the hydrophilicity. After loading samples (7 μL) on the grid, we then rinsed grid by dd-water for twice or three times. Immediately after rinsing, we stained the grid containing sample with 2.0 % w/v uranyl acetate for three times. Afterwards, we allowed the grid to dry in air.

S5. Light scattering sample preparation

The static light scattering experiments were performed by using an ALV (Langen, Germany) goniometer and correlator system with a 22 mW HeNe (λ = 633 nm) laser and an avalanche photodiode detector. All samples were dissolved in PBS buffer. The addition of PLE to the solution of the conjugates for 24 h, we obtained corresponding enzymatic hydrolyzed samples. The SLS tests were carried out at room temperature, and the angles of light scattering we chose were 30^{o}, 60^{o}, 90^{o} and 120^{o}, respectively. The resulting intensity ratios are proportional to the amount of aggregates in the samples.

S6. Bacteria culture and inhibitory activity assay

Single esterase (*bioH*, *yjfP*, *frsA*, *ybfF*, *yfbB*, *yqiA*, *yeiG*, or *ypfH*) deletion mutants, bacterial transporter (*ydgR*, *fepA* and *ompF*) deletion mutants and the efflux pump (*acrA*) deletion mutant were all purchased from Dharmacon Horizon Discovery (Cambridge, United Kingdom). The K12 wild-type *E. coli* strain (MG1655) was cultured in autoclaved LB medium (25 g/L LB broth/water) in a shaker-incubator overnight to stationary growth phase, and then sub-cultured in

the same medium after dilution to OD_{600} of 0.05. Compounds were added at different concentrations. The mixture of bacteria and compounds were placed (200 μL/well) into 96-well clear flat bottom plates. In all plates, the OD_{600} was measured before and after 16 h incubation at 37 °C.[2]

S7. Cell culture and cell viability assay

All cell lines were purchased from the American Type Culture Collection (ATCC, Manassas, VA, USA). The HS-5 cells were propagated in Dulbecco's Modified Eagle's Medium (DMEM) supplemented with 10% fetal bovine serum (FBS) and 1% antibiotics in a fully humidified incubator containing 5% CO_2 at 37 °C, HepG2 and HEK293 cells in Eagle's Minimum Essential Media (MEM) supplemented with 10% FBS and 1% antibiotics in a fully humidified incubator containing 5% CO_2 at 37 °C.

Cells in exponential growth phase were seeded in a 96 well plate at a concentration of 1×10^4 cell/well, and were allowed to attach to the well for 24 h at 37°C, 5% CO_2. The culture medium was removed and 100 μL culture medium containing corresponding compounds (immediately diluted from fresh prepared stock solution) at gradient concentrations (0 μM as the control) was placed into each well. After culturing at 37 °C, 5% CO_2 for 24h, 48h and 72h, each well was added with 10 μL of 5 mg/mL MTT ((3-(4,5-dimethylthiazol-2-yl)-2,5-diphenyltetrazolium bromide), and the plated cells were incubated at dark for 4h. 100 μL 10% SDS with 0.01M HCl was added to each well to stop the reduction and to dissolve the purple. After incubation of the cells at 37 °C for overnight, the OD at 595 nm of the solution was measured in a microplate reader. Data represent the mean ± standard deviation of three independent experiments.

S8. Supplemental figures

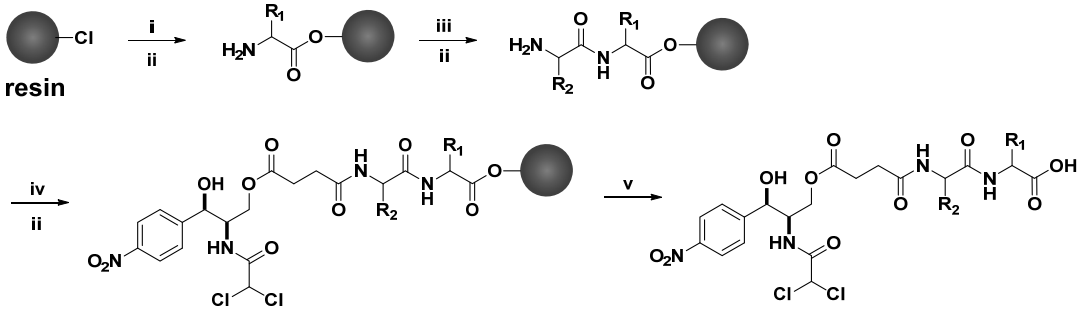

Scheme S1. Synthesis of peptide conjugated chloramphenicol by SPPS.

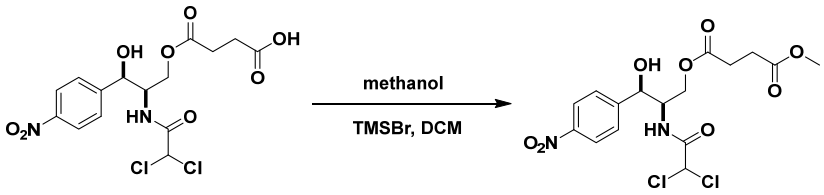

Scheme S2. Synthesis of CLsu-OMe (**4b**).

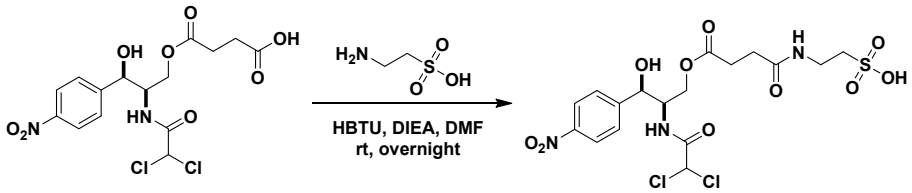

Scheme S3. Synthesis of CLsu-Tau (**4c**).

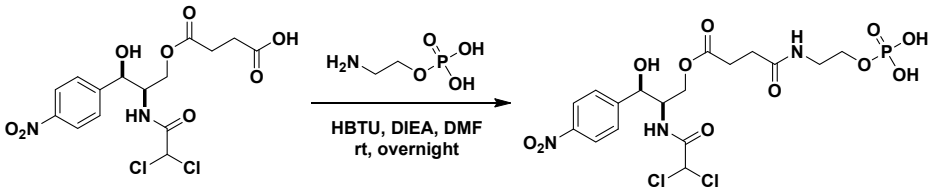

Scheme S4. Synthesis of CLsu-ep (**4d**).

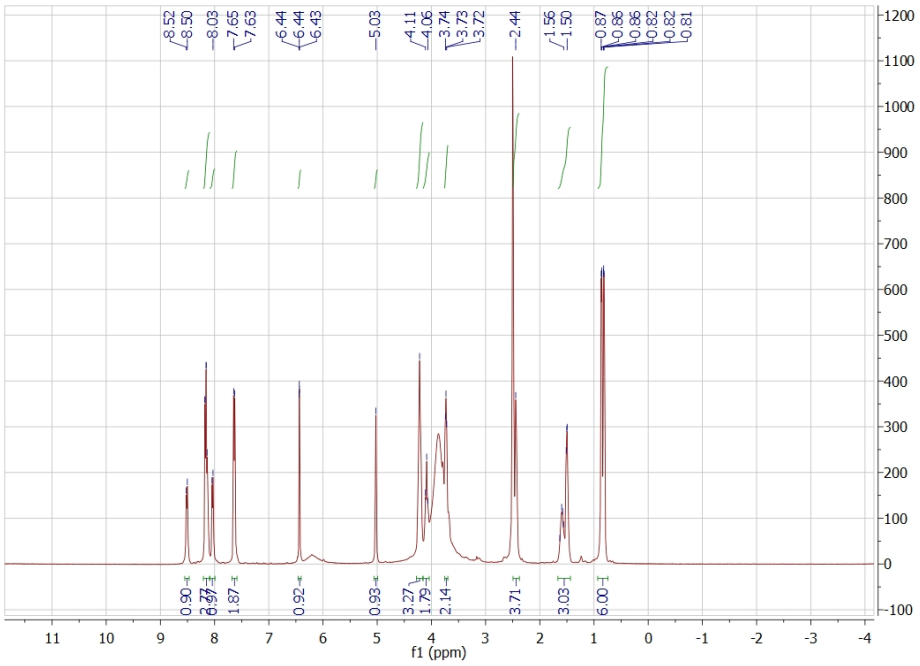

Figure S1. ^{1}H NMR of **1a** in DMSO-*d*$_6$.

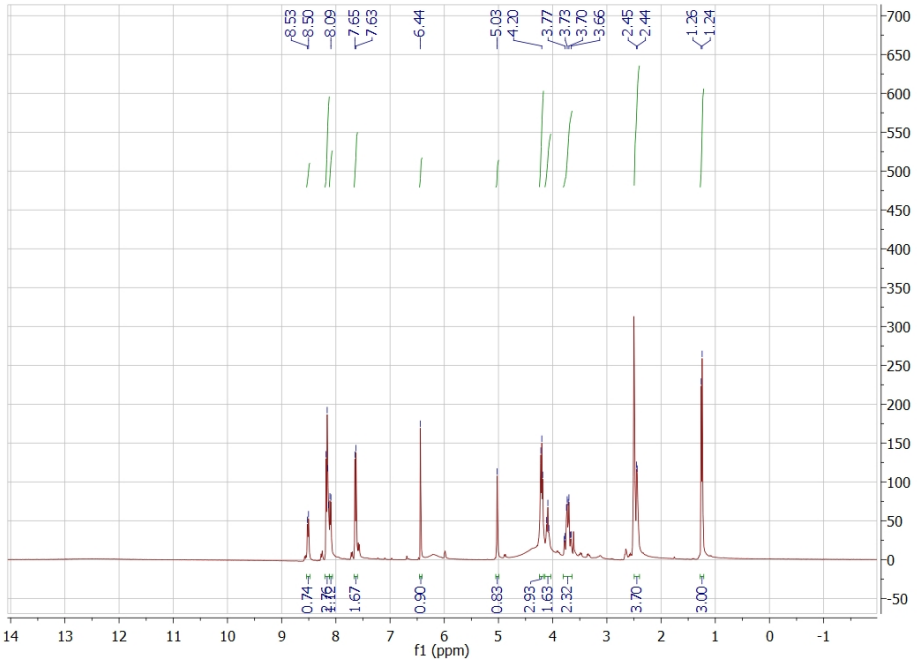

Figure S2. ^{1}H NMR of **1b** in DMSO-*d*$_6$.

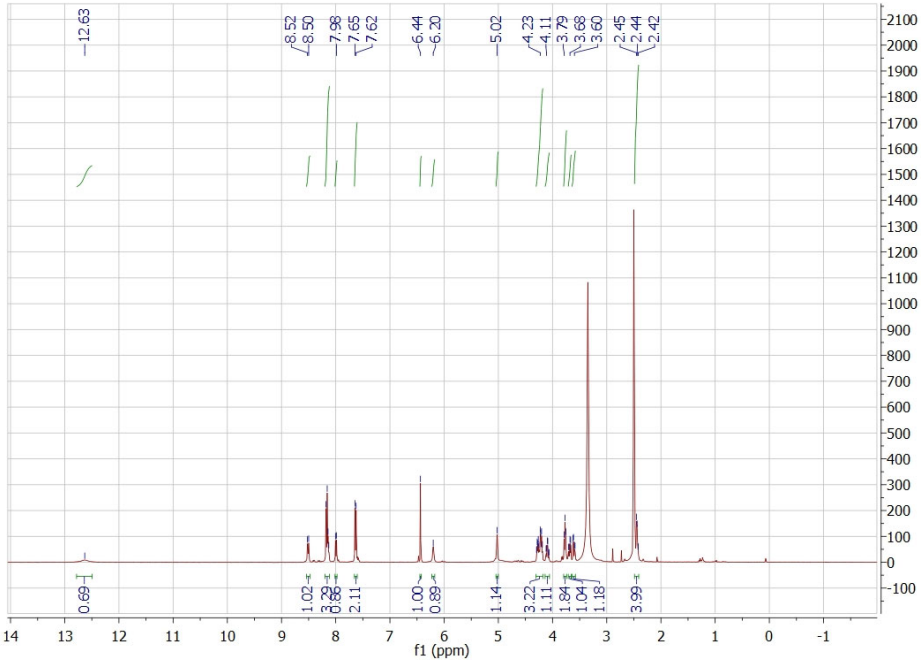

Figure S3. ^{1}H NMR of **1c** in DMSO-*d*$_6$.

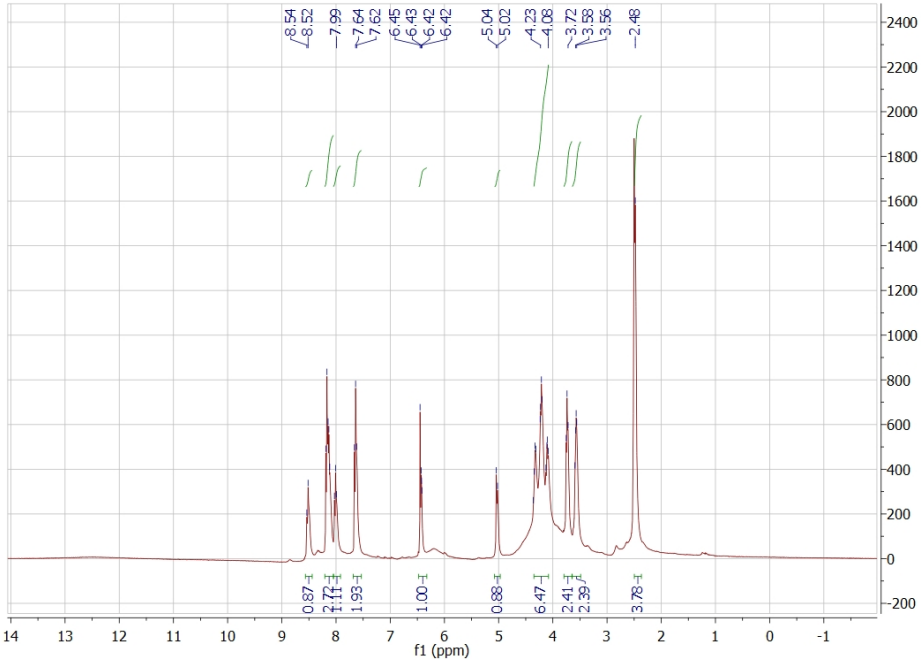

Figure S4. ^{1}H NMR of **1d** in DMSO-*d*$_6$.

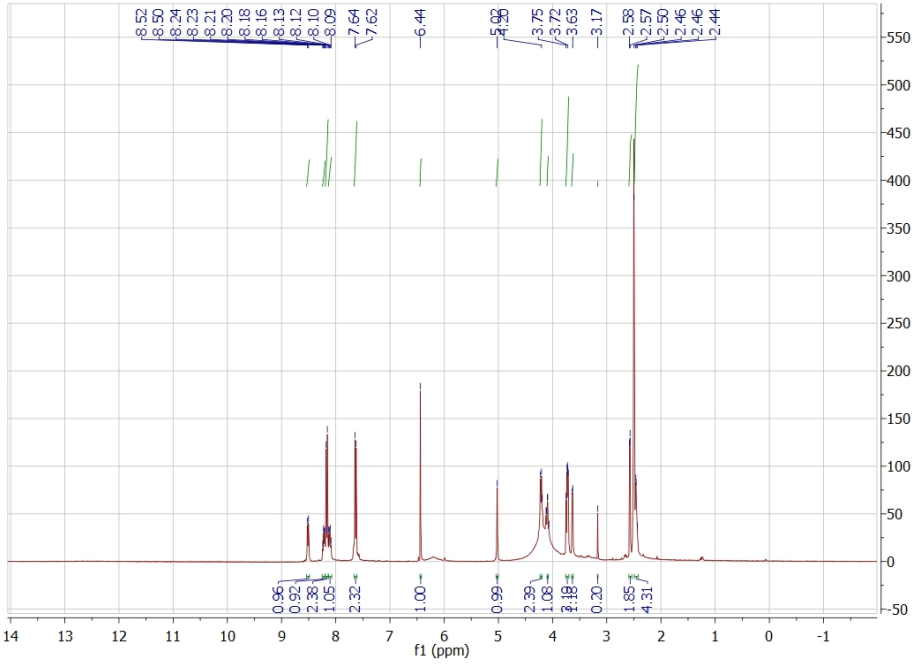

Figure S5. ^{1}H NMR of **1e** in DMSO-*d*$_6$.

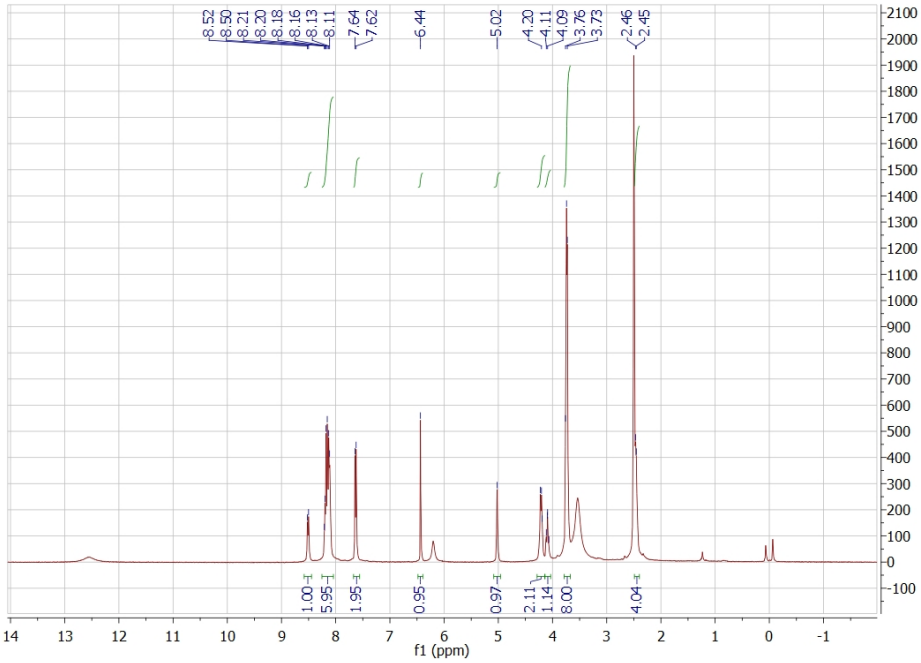

Figure S6. ^{1}H NMR of **1f** in DMSO-*d*$_6$.

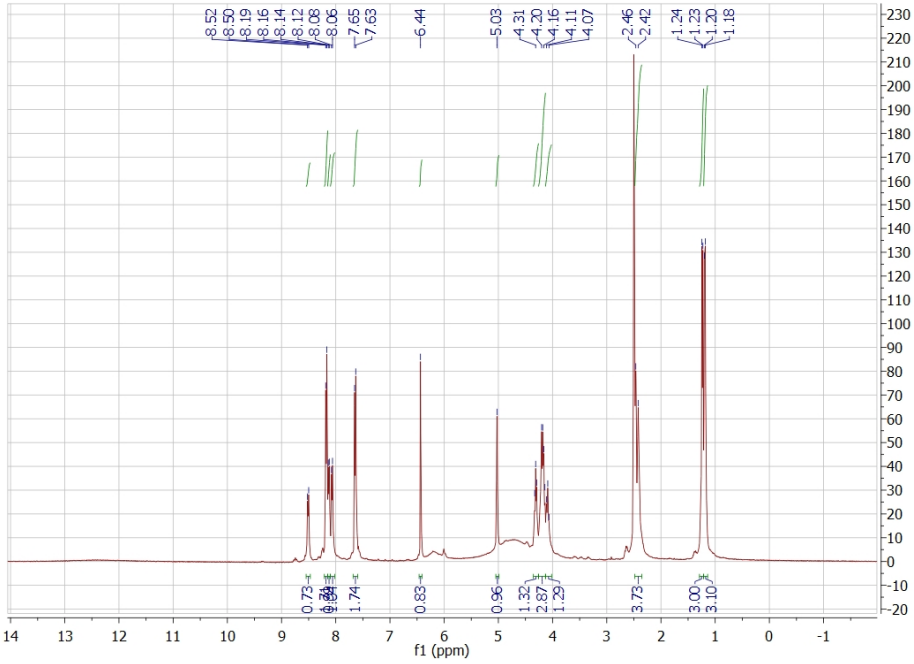

Figure S7. ^{1}H NMR of **1g** in DMSO-*d*$_6$.

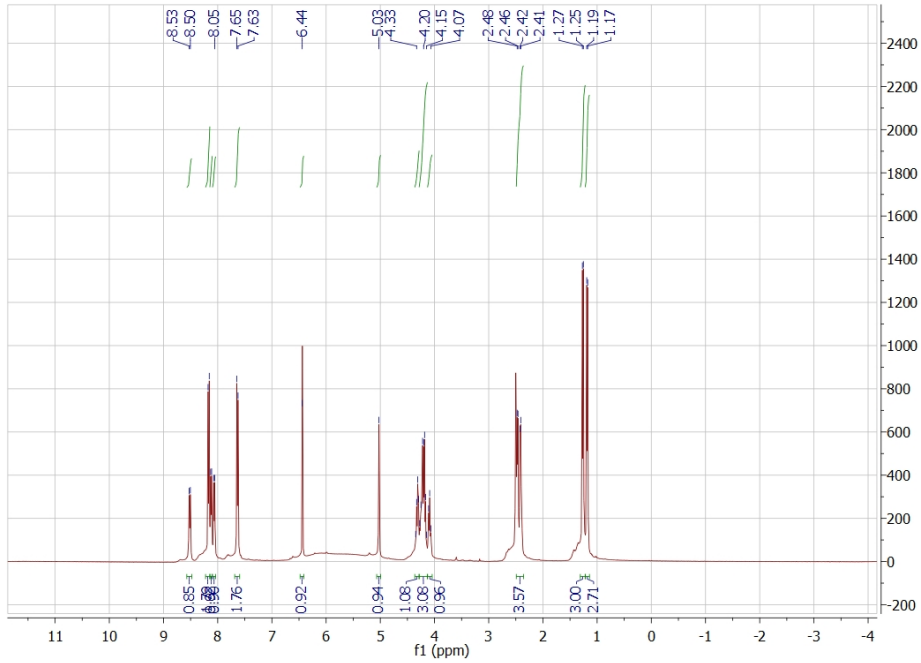

Figure S8. ^{1}H NMR of **1h** in DMSO-*d*$_6$.

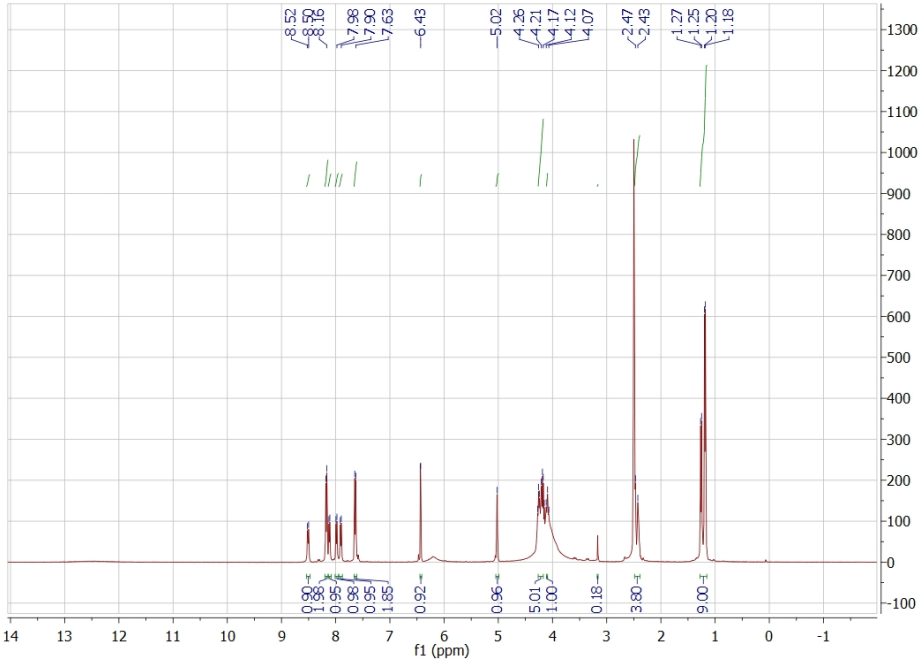

Figure S9. ^{1}H NMR of **1i** in DMSO-*d*$_6$.

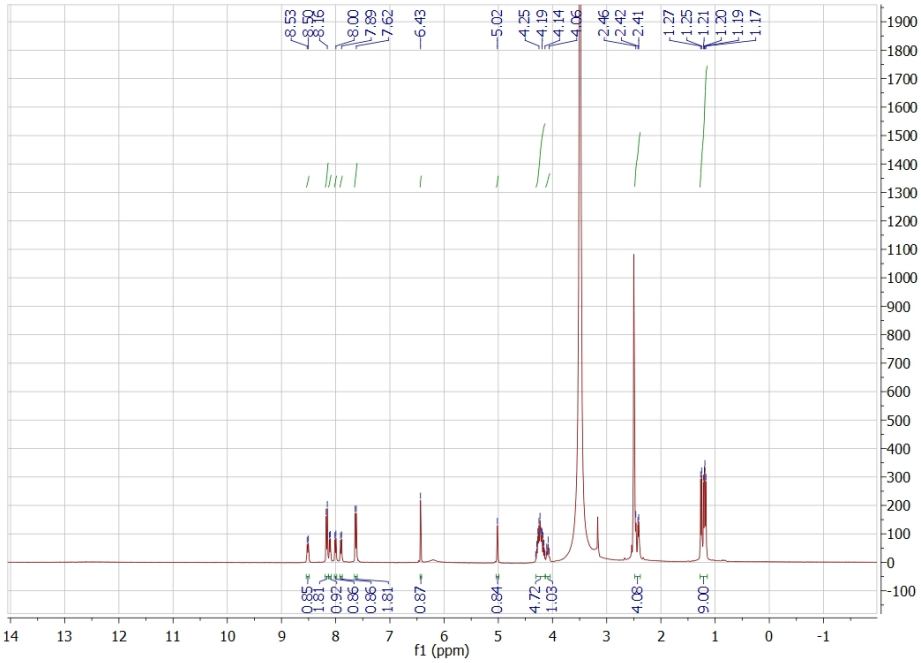

Figure S10. ^{1}H NMR of **1j** in DMSO-*d*$_6$.

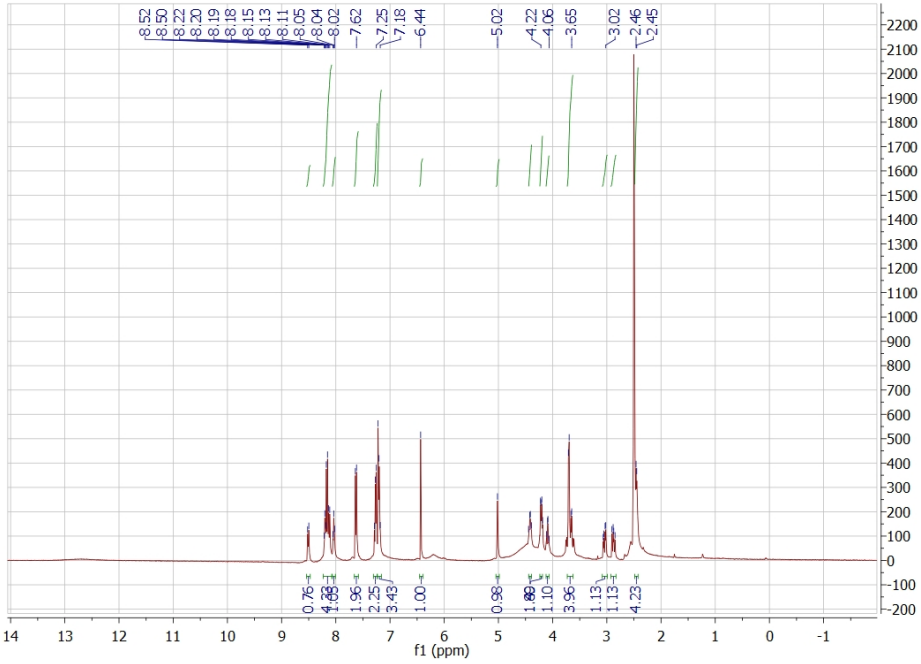

Figure S11. ^{1}H NMR of **1k** in DMSO-*d*$_6$.

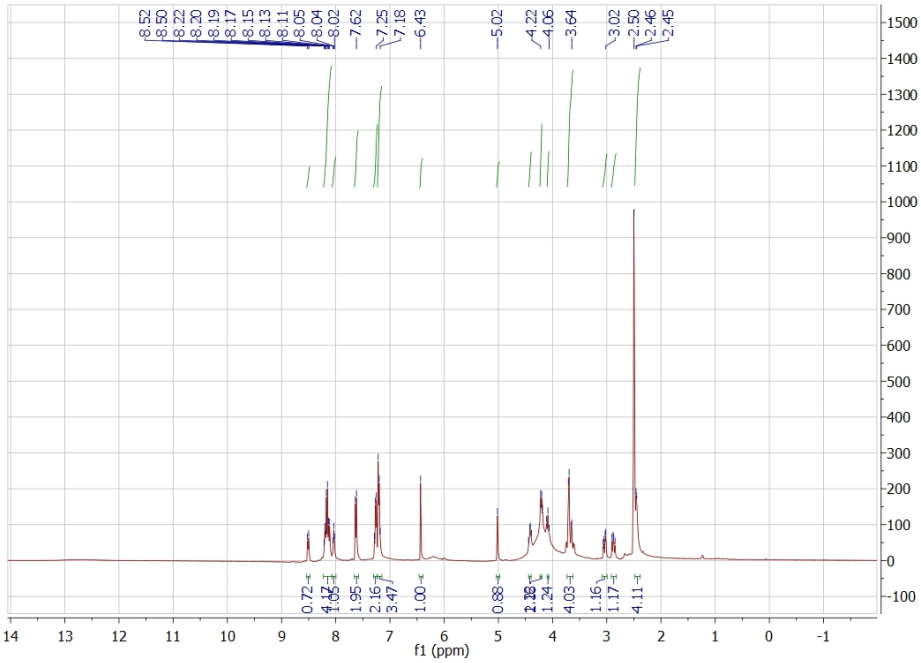

Figure S12. ^{1}H NMR of **1l** in DMSO-*d*$_6$.

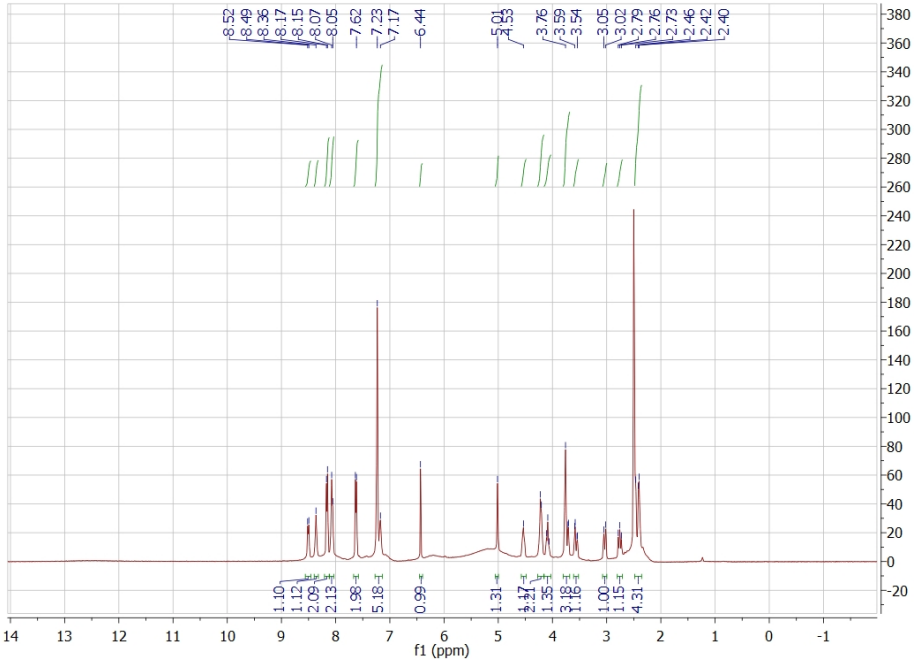

Figure S13. ^{1}H NMR of **1m** in DMSO-*d*$_6$.

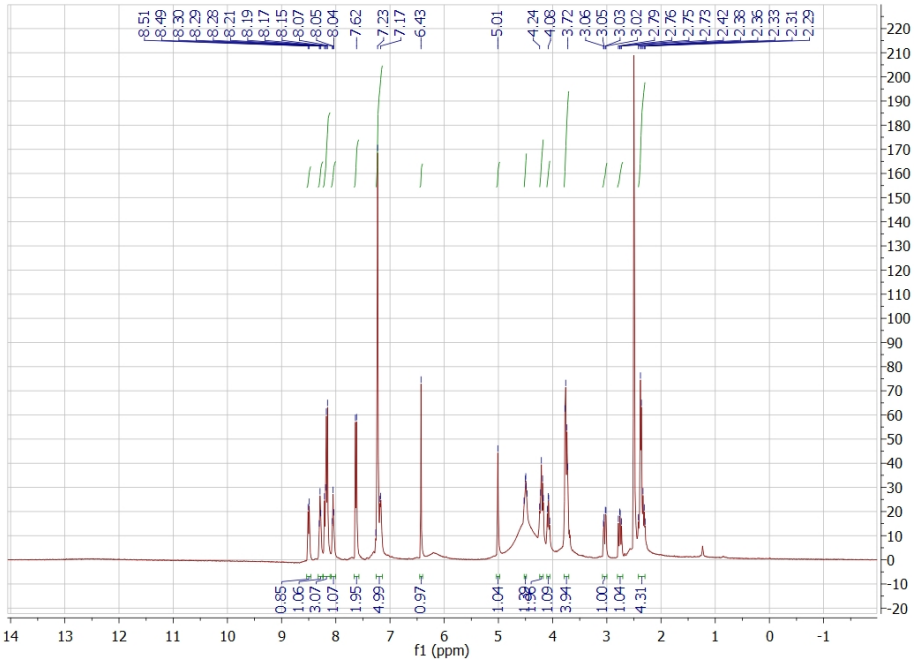

Figure S14. ^{1}H NMR of **1n** in DMSO-*d*$_6$.

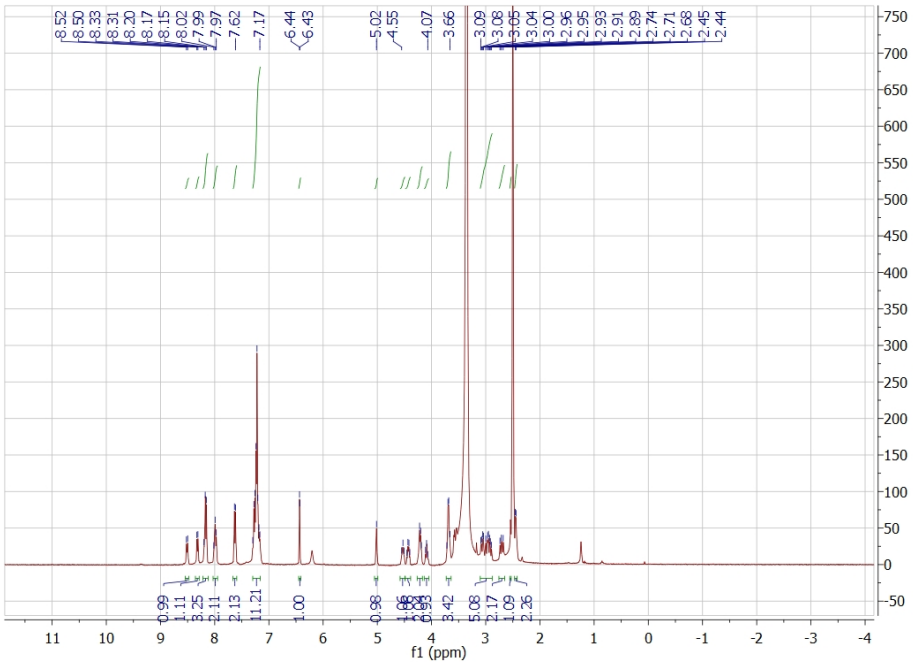

Figure S15. ^{1}H NMR of **1o** in DMSO-*d*$_6$.

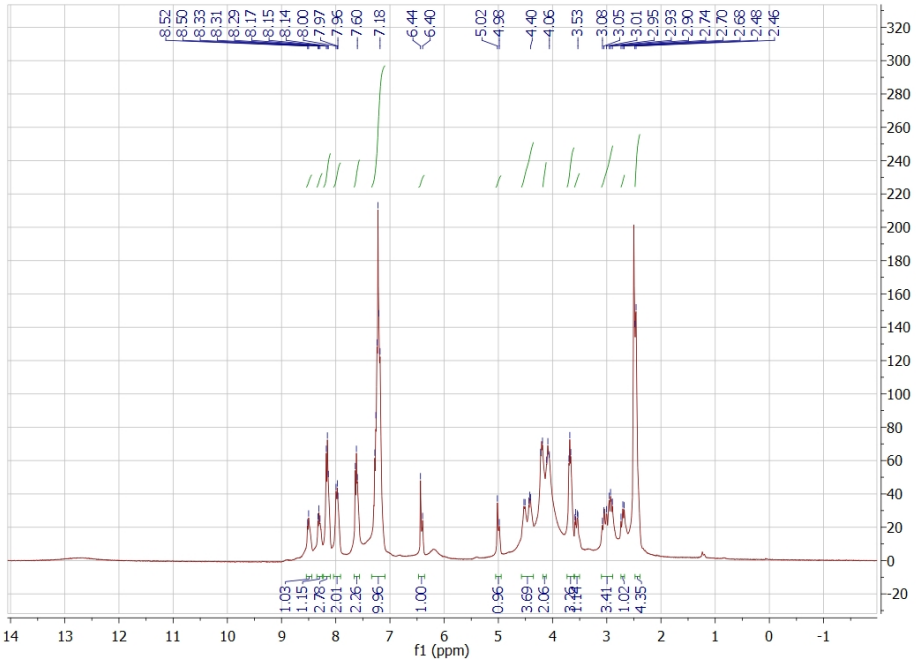

Figure S16. ^{1}H NMR of **1p** in DMSO-*d*$_6$.

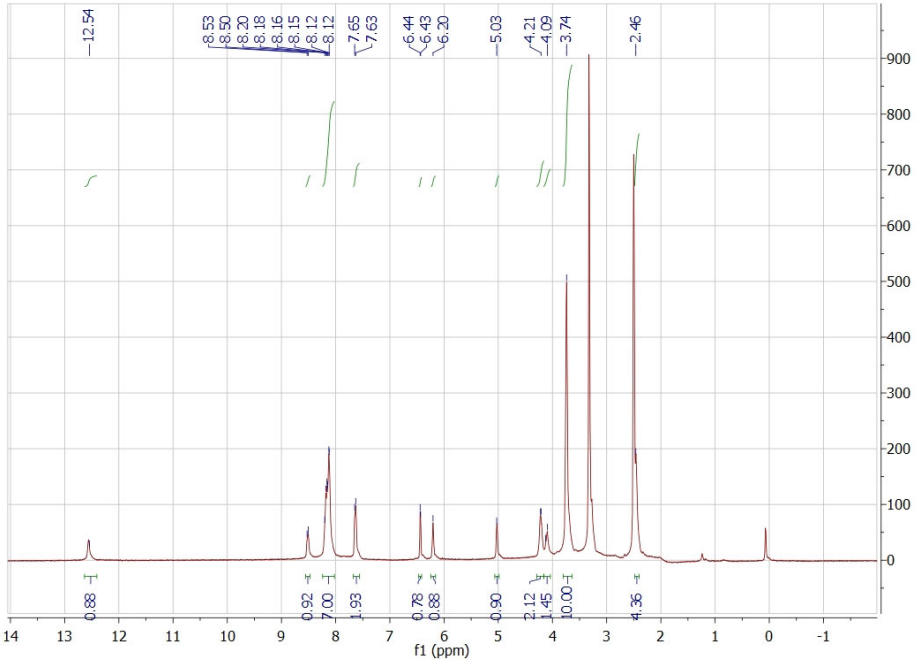

Figure S17. ^{1}H NMR of **1q** in DMSO-*d*$_6$.

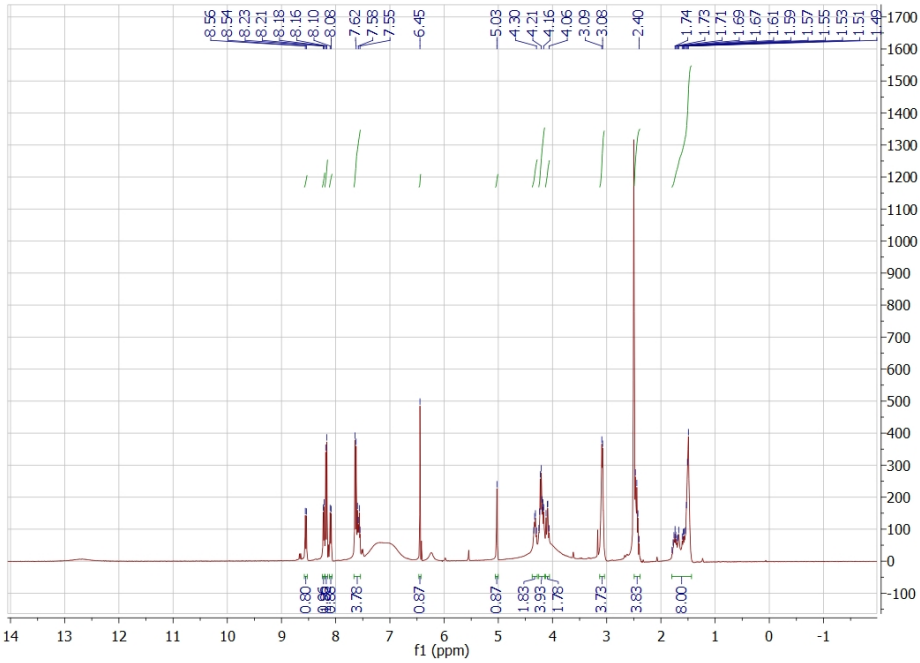

Figure S18. ^{1}H NMR of **2a** in DMSO-*d*$_6$.

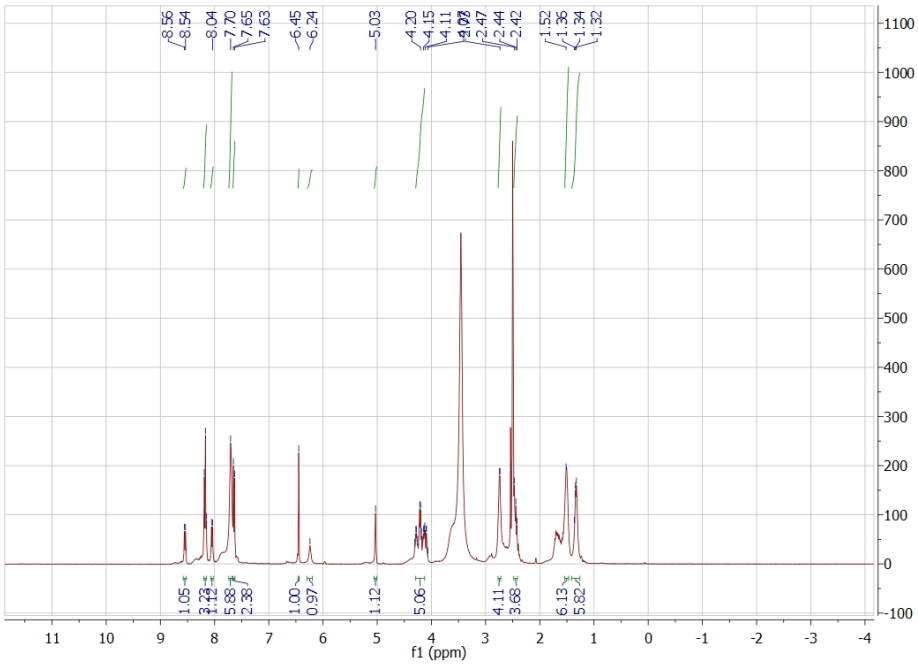

Figure S19. ^{1}H NMR of **2b** in DMSO-*d*$_6$.

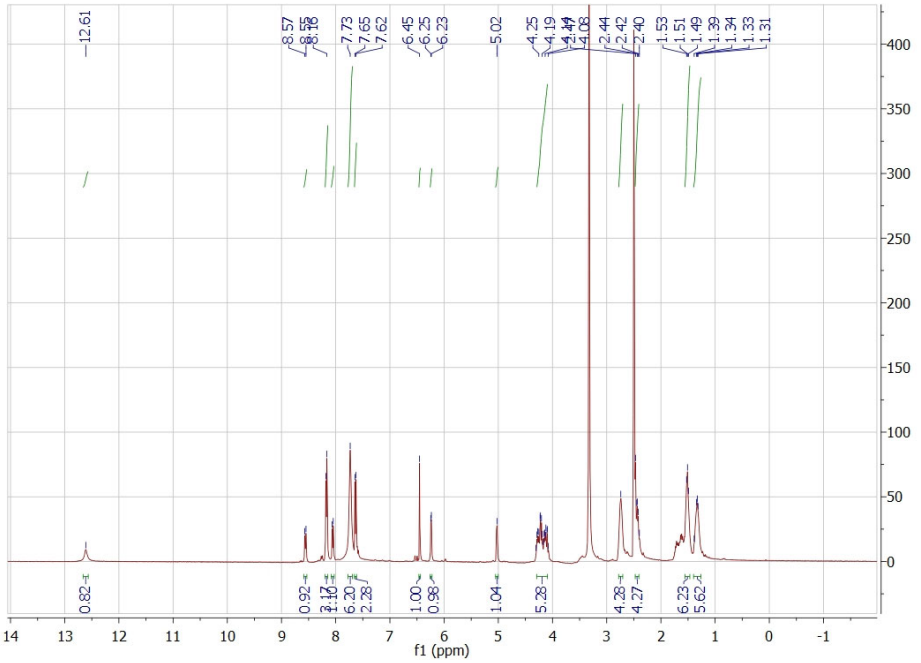

Figure S20. ^{1}H NMR of **2c** in DMSO-*d*$_6$.

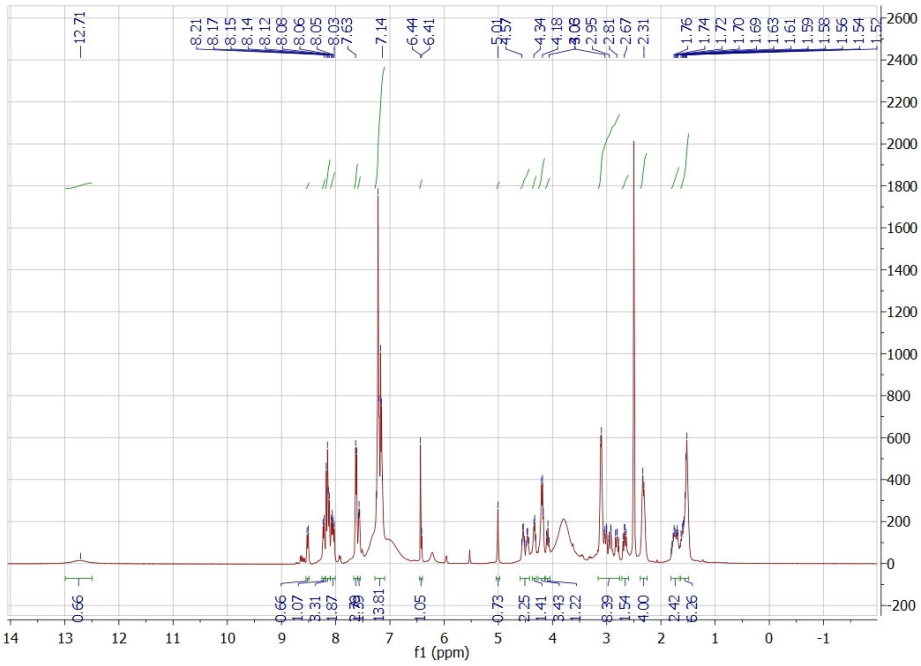

Figure S21. [1]H NMR of **2d** in DMSO-*d*$_6$.

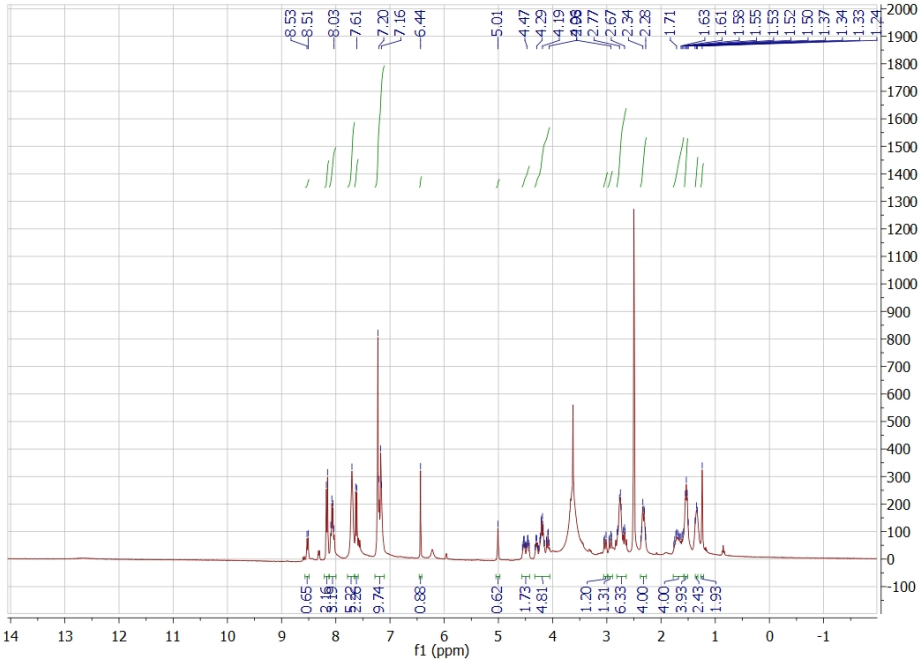

Figure S22. [1]H NMR of **2e** in DMSO-*d*$_6$.

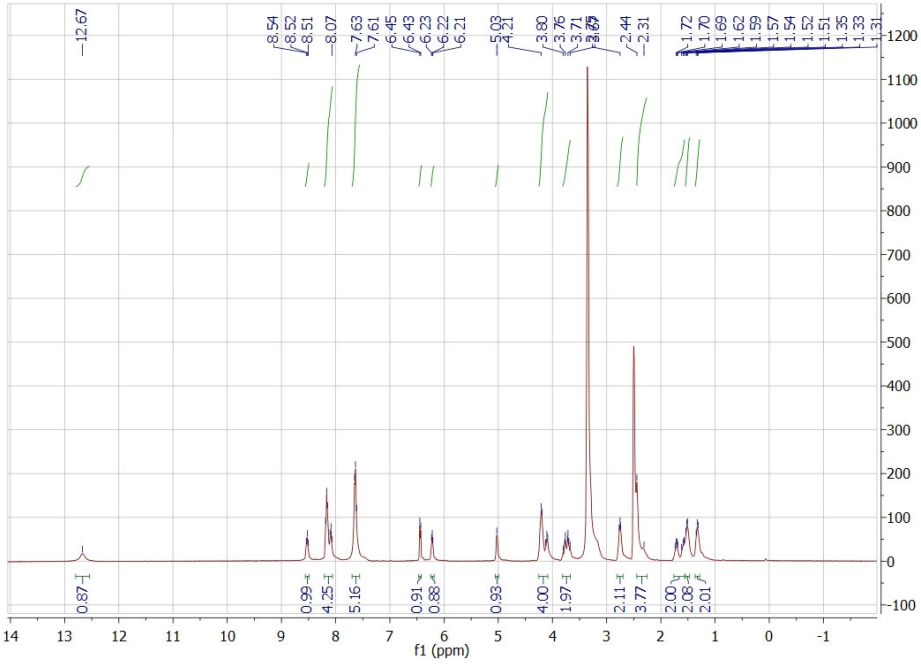

Figure S23. ^{1}H NMR of **2f** in DMSO-*d*$_6$.

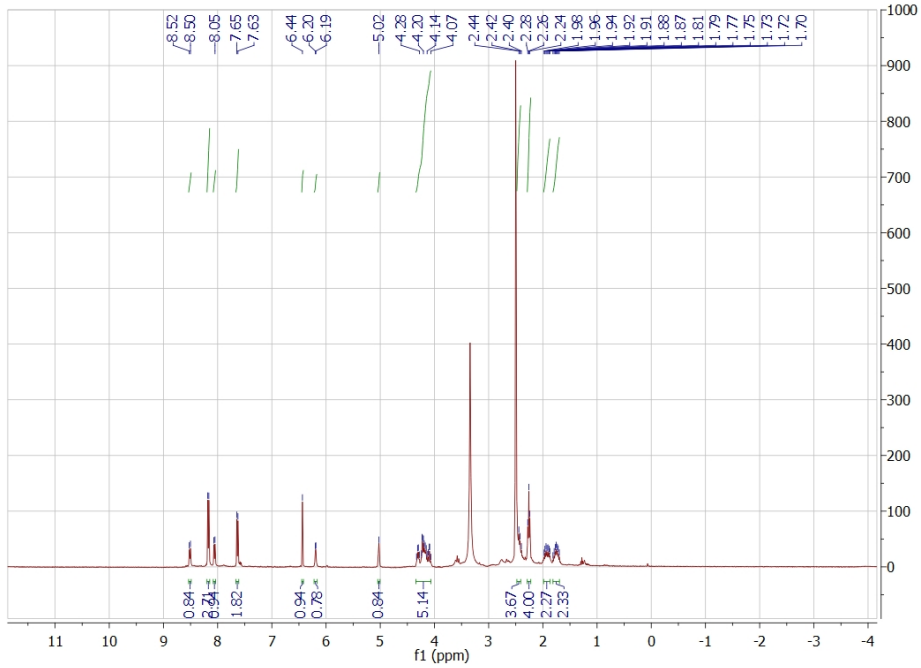

Figure S24. ^{1}H NMR of **2g** in DMSO-*d*$_6$.

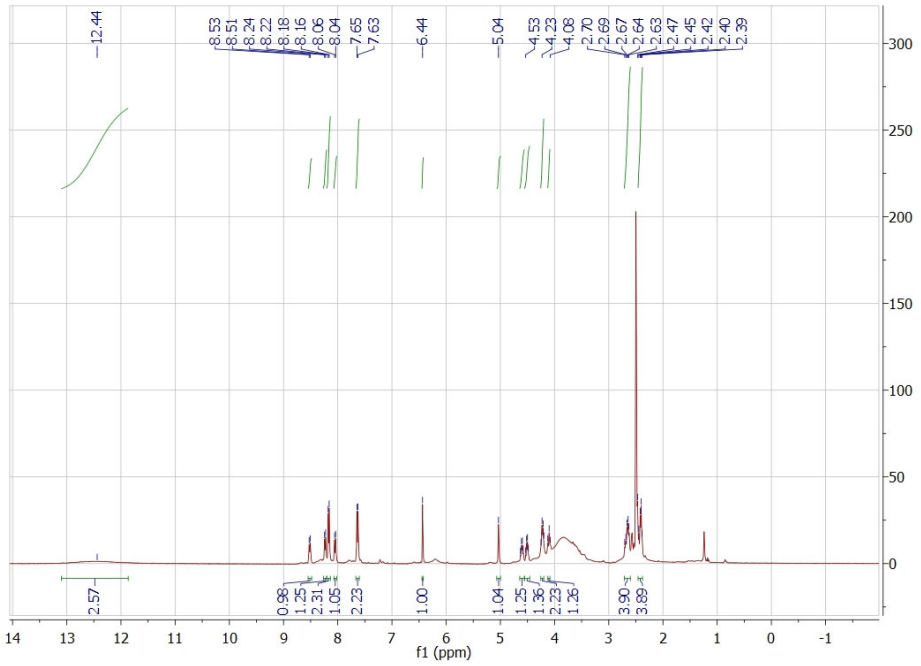

Figure S25. ^{1}H NMR of **2h** in DMSO-*d*$_6$.

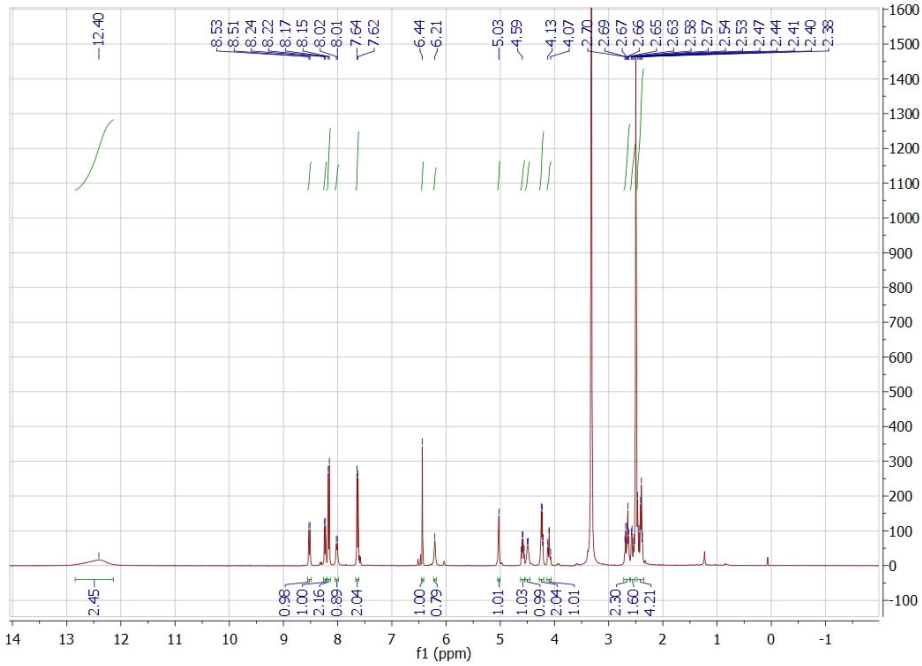

Figure S26. ^{1}H NMR of **2i** in DMSO-*d*$_6$.

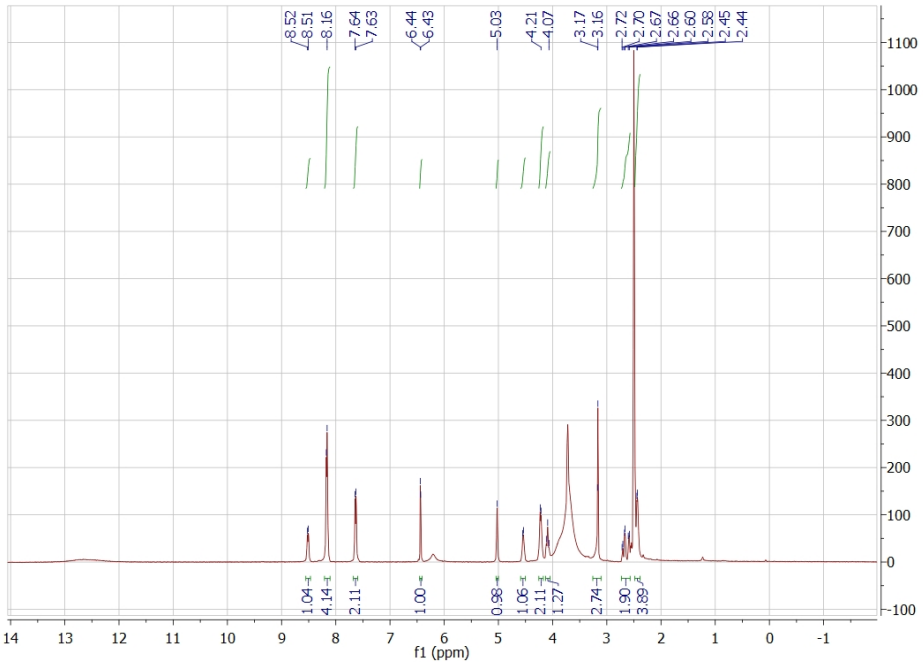

Figure S27. ^{1}H NMR of **2j** in DMSO-*d*$_6$.

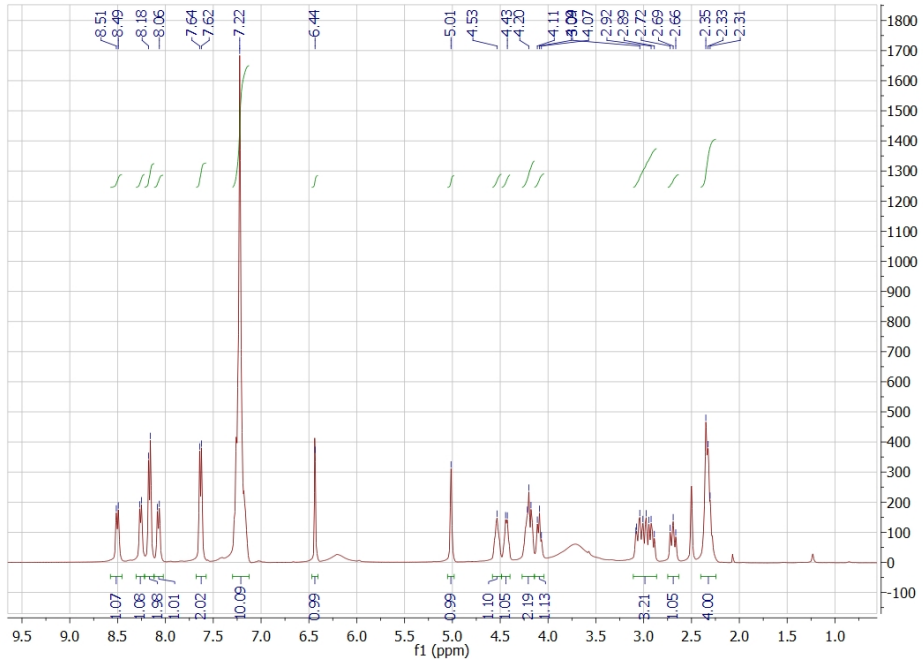

Figure S28. ^{1}H NMR of **3a** in DMSO-*d*$_6$.

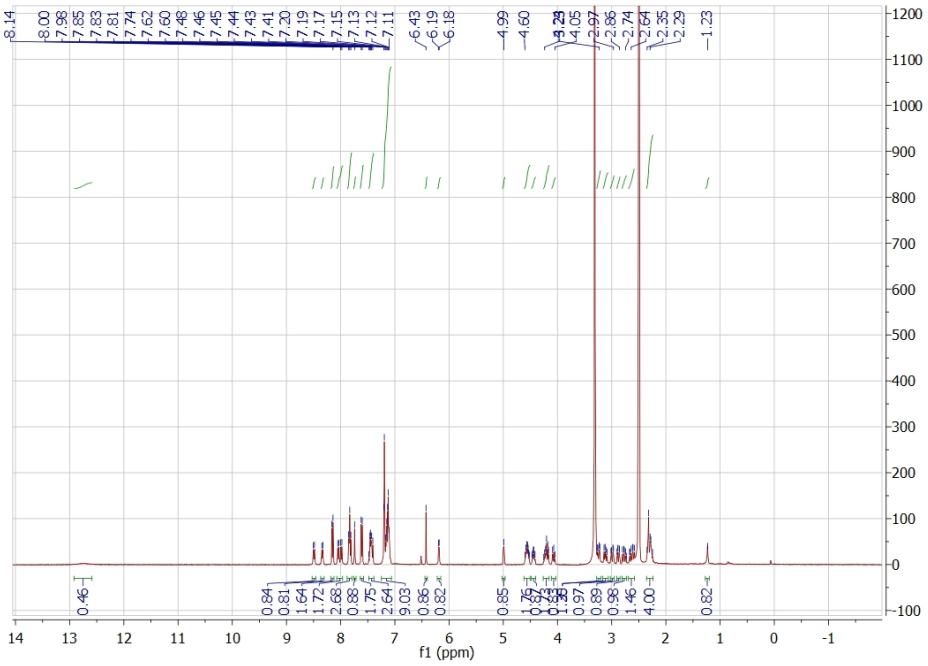

Figure S29. ^{1}H NMR of **3b** in DMSO-*d*$_6$.

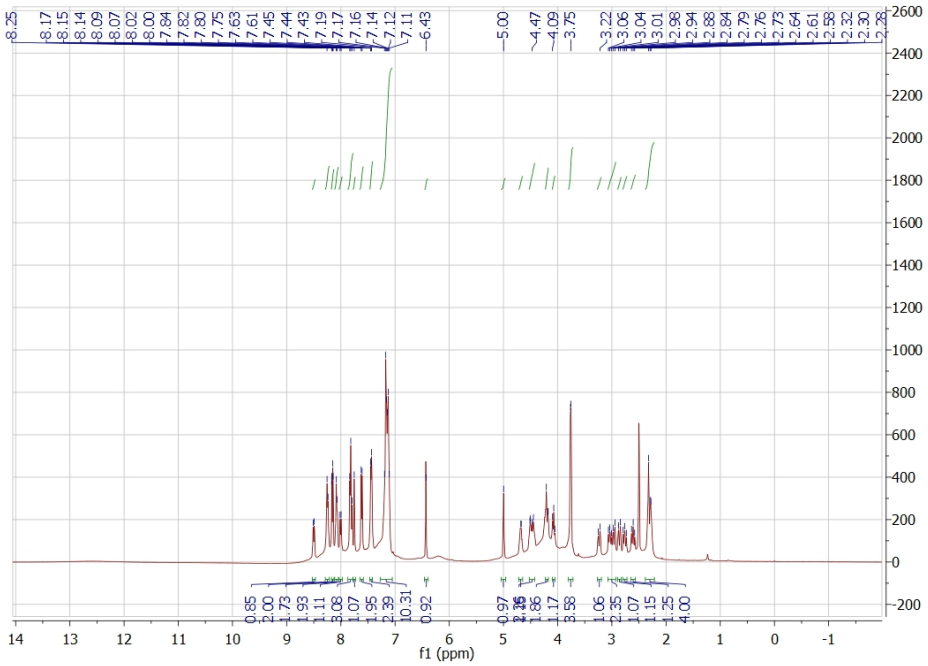

Figure S30. ^{1}H NMR of **3c** in DMSO-*d*$_6$.

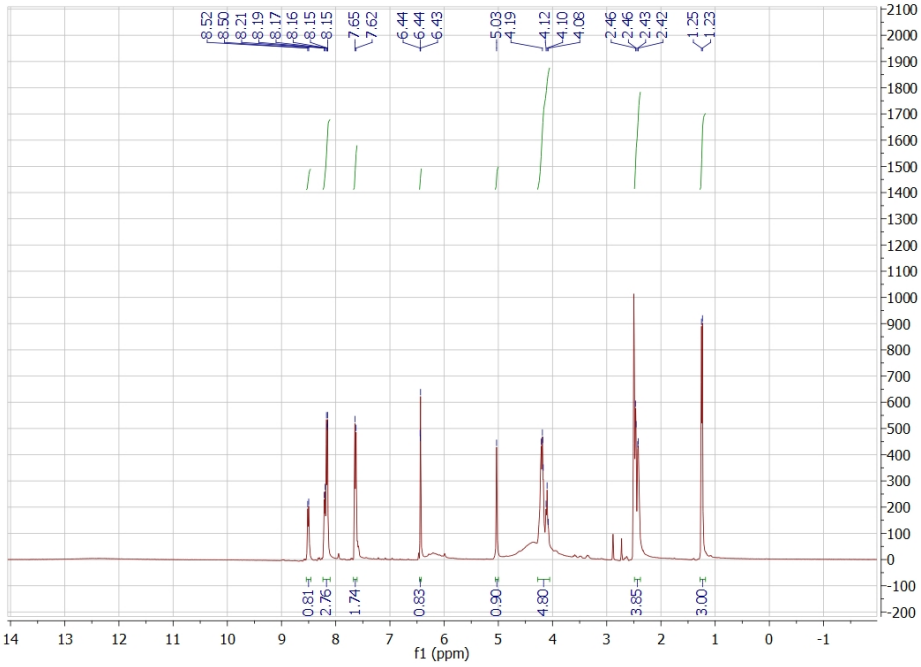

Figure S31. [1]H NMR of **4a** in DMSO-*d*$_6$.

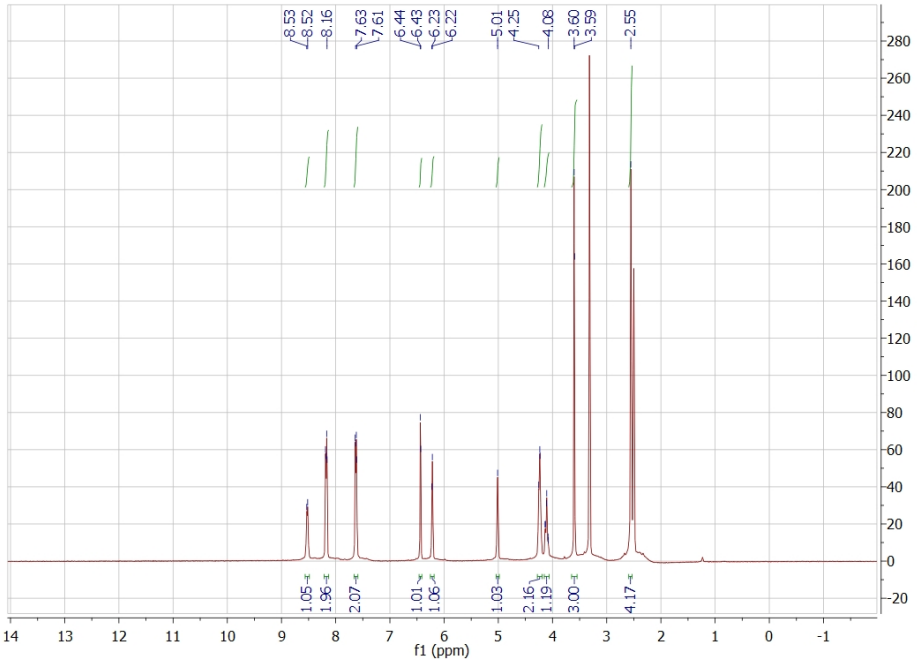

Figure S32. [1]H NMR of **4b** in DMSO-*d*$_6$.

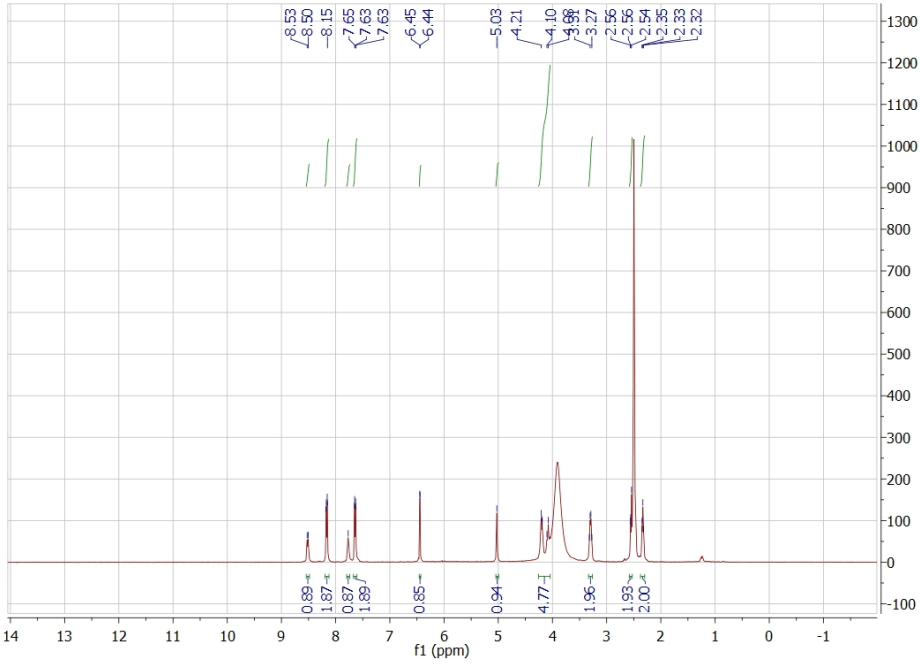

Figure S33. ^{1}H NMR of **4c** in DMSO-*d*$_6$.

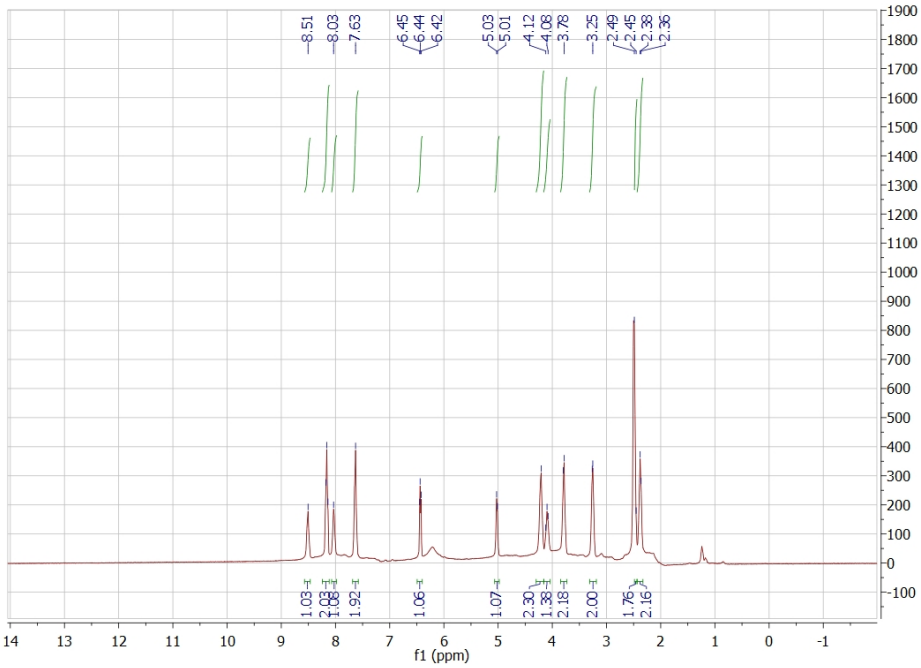

Figure S34. ^{1}H NMR of **4d** in DMSO-*d*$_6$.

Table S1. LC-MS purities of compound **1a-4d**.

Compound	Purity (based on LC-MS) (%)	Retention time (min)	Calculated mass	Observed mass
1a	95.33	2.02	592.13	591.27
1b	98.80	1.74	550.09	549.28
1c	95.21	1.64	566.08	565.27
1d	97.16	1.60	566.08	565.27
1e	95.86	1.60	549.10	548.20
1f	99.29	1.77	650.11	649.20
1g	97.86	1.80	564.10	563.35
1h	98.64	1.77	564.10	563.06
1i	98.41	1.77	635.14	634.30
1j	96.19	1.74	635.14	634.30
1k	95.45	2.10	683.14	682.30
1l	94.90	2.01	683.14	682.39
1m	96.89	2.01	683.14	682.17
1n	97.54	2.08	683.14	682.30
1o	97.62	2.25	830.21	829.29
1p	98.76	2.27	830.21	829.29
1q	99.70	1.63	707.14	706.22
2a	94.89	1.18	736.25	733.43
2b	97.50	1.06	680.23	677.27
2c	95.91	1.11	680.23	677.42
2d	97.60	1.87	1030.38	1027.59
2e	99.50	1.64	974.37	971.37
2f	97.60	1.38	608.15	606.33
2g	97.74	1.66	680.11	679.23
2h	99.26	1.63	652.08	651.15
2i	99.60	1.62	652.08	651.25
2j	97.22	1.66	594.08	593.32
3a	98.28	2.47	716.17	715.39
3b	98.33	2.82	913.25	912.45
3c	97.26	2.60	1027.29	1026.49
4a	97.64	1.84	493.07	492.29
4b	98.94	2.18	436.04	435.15
4c	95.79	1.50, 1.57, 1.62	529.03	528.25
4d	97.21	1.47	545.04	544.24

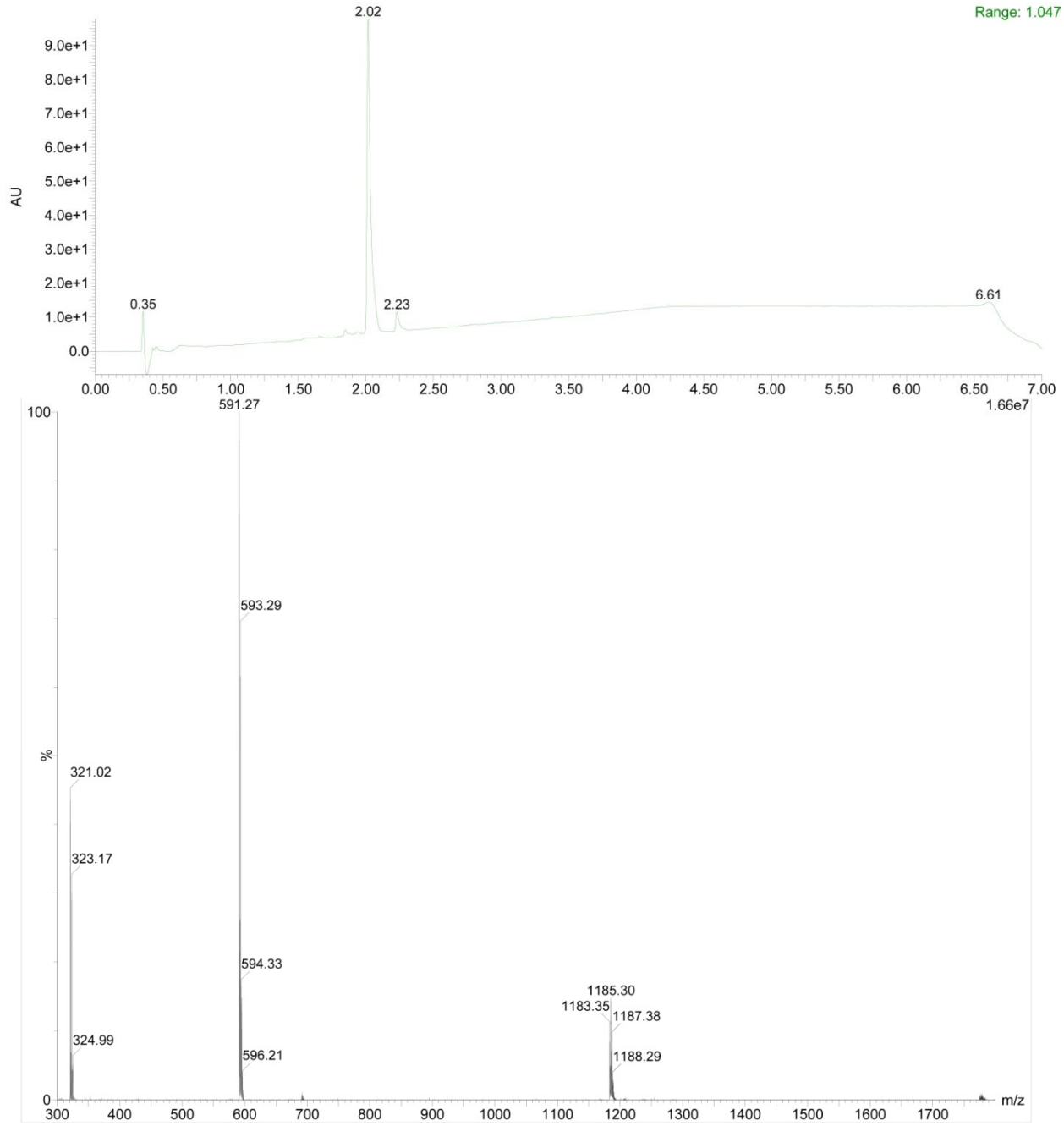

Figure S35. The ultra-performance LC (top) and Mass (bottom) spectrum of **1a**, $[M-H]^-$ at m/z 591.27.

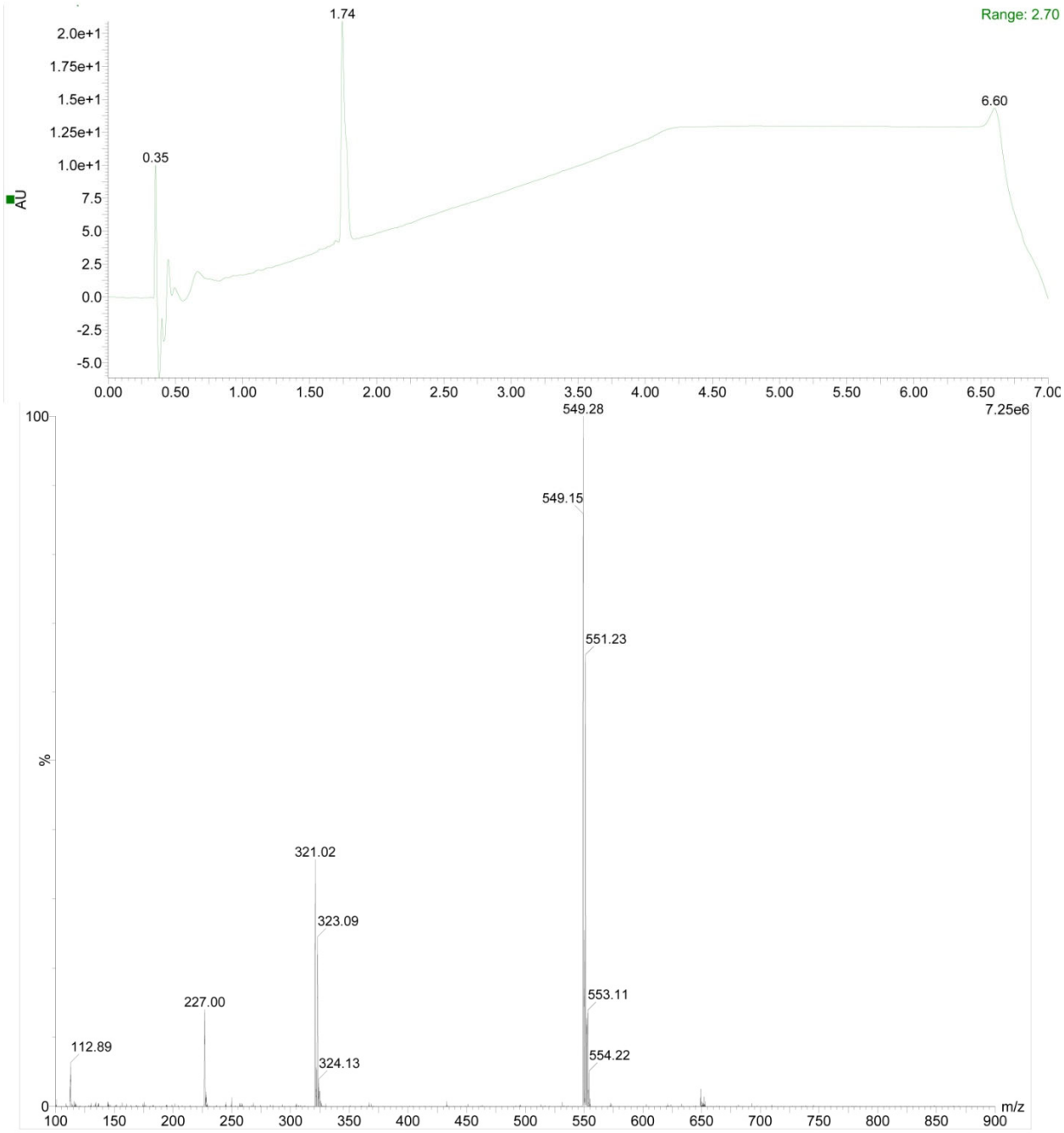

Figure S36. The ultra-performance LC (top) and Mass (bottom) spectrum of **1b**, $[M-H]^-$ at m/z 549.28.

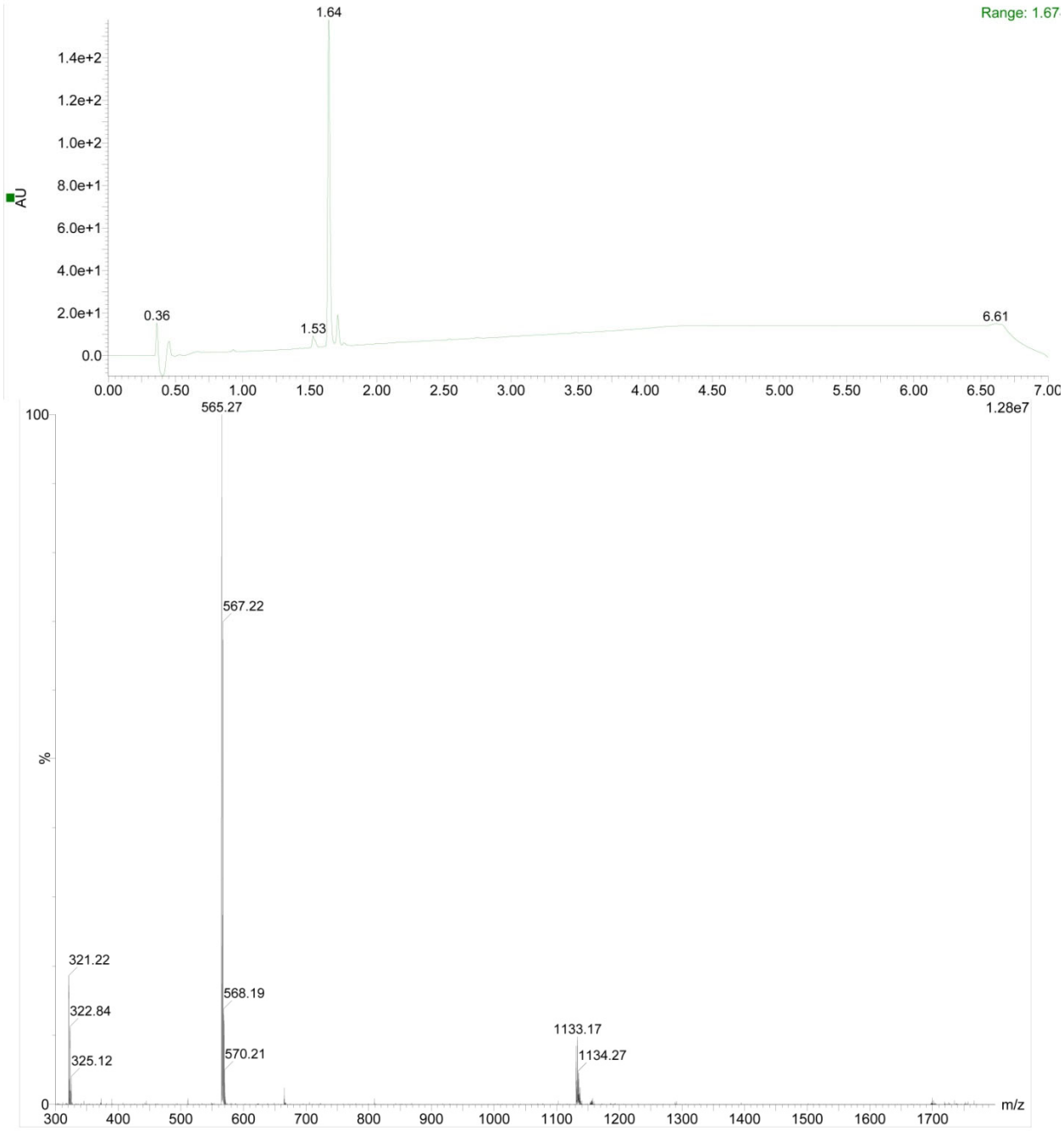

Figure S37. The ultra-performance LC (top) and Mass (bottom) spectrum of **1c**, $[M-H]^-$ at m/z 565.27.

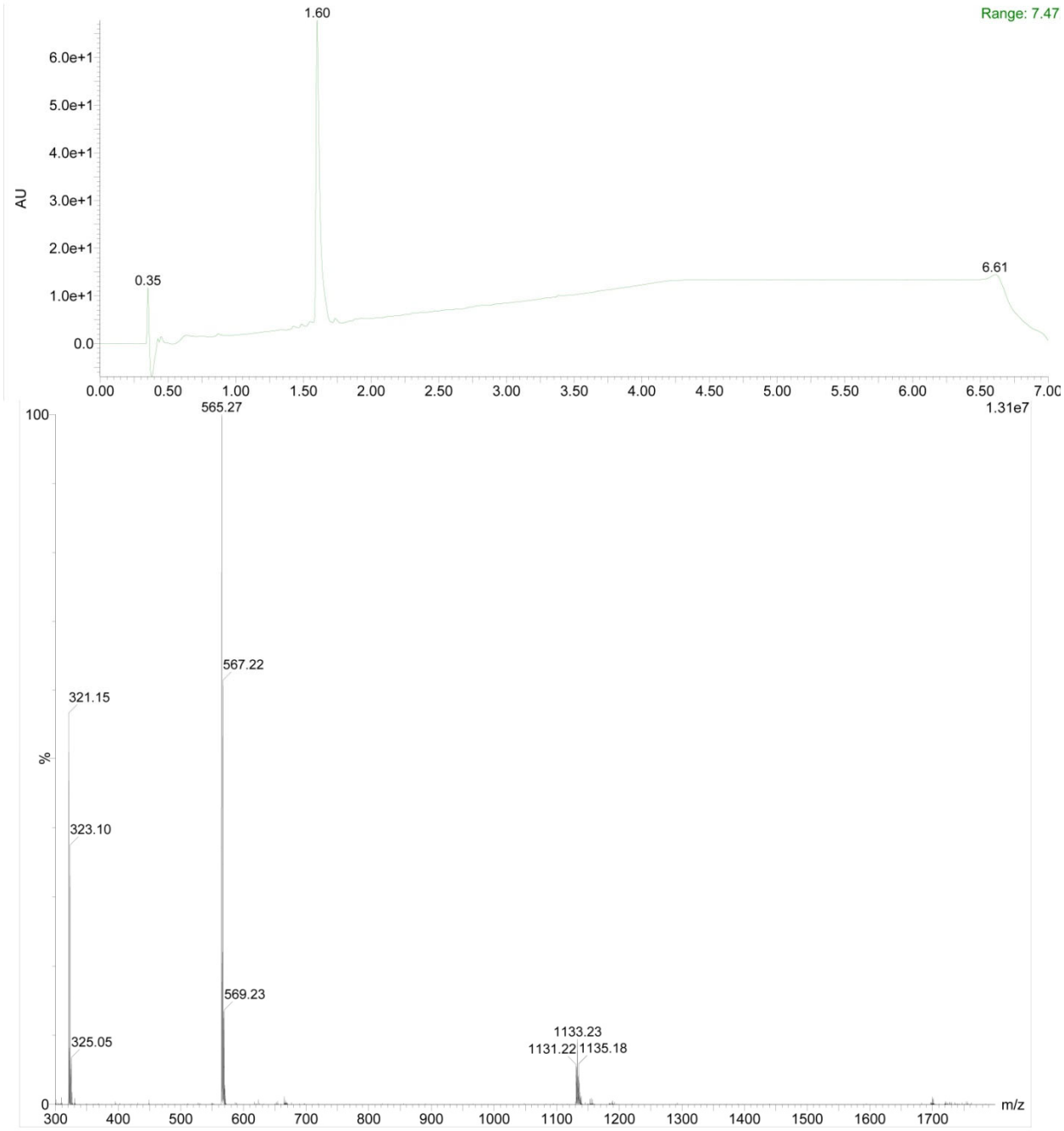

Figure S38. The ultra-performance LC (top) and Mass (bottom) spectrum of **1d**, $[M-H]^-$ at m/z 565.27.

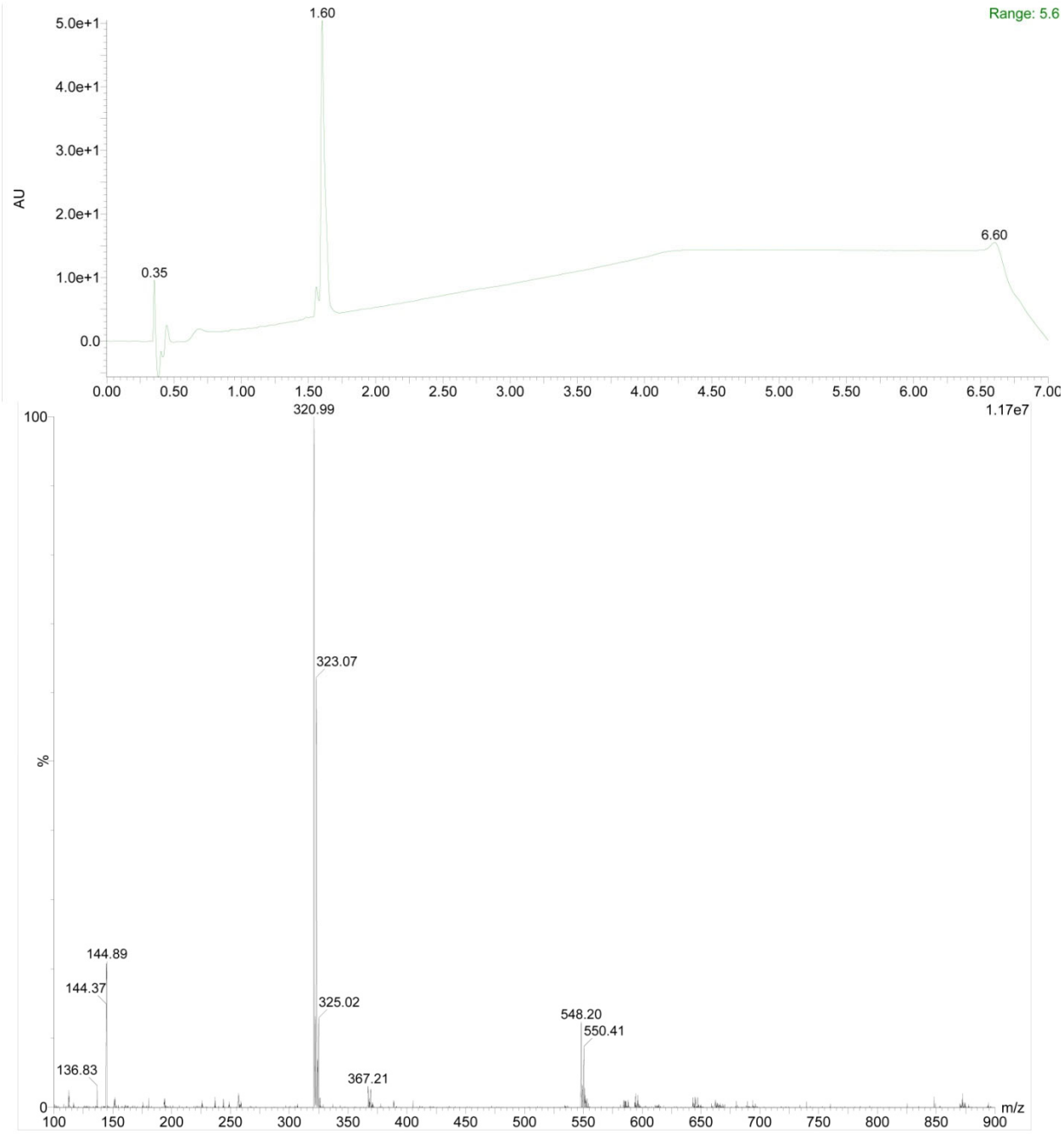

Figure S39. The ultra-performance LC (top) and Mass (bottom) spectrum of **1e**, $[M-H]^-$ at m/z 548.20.

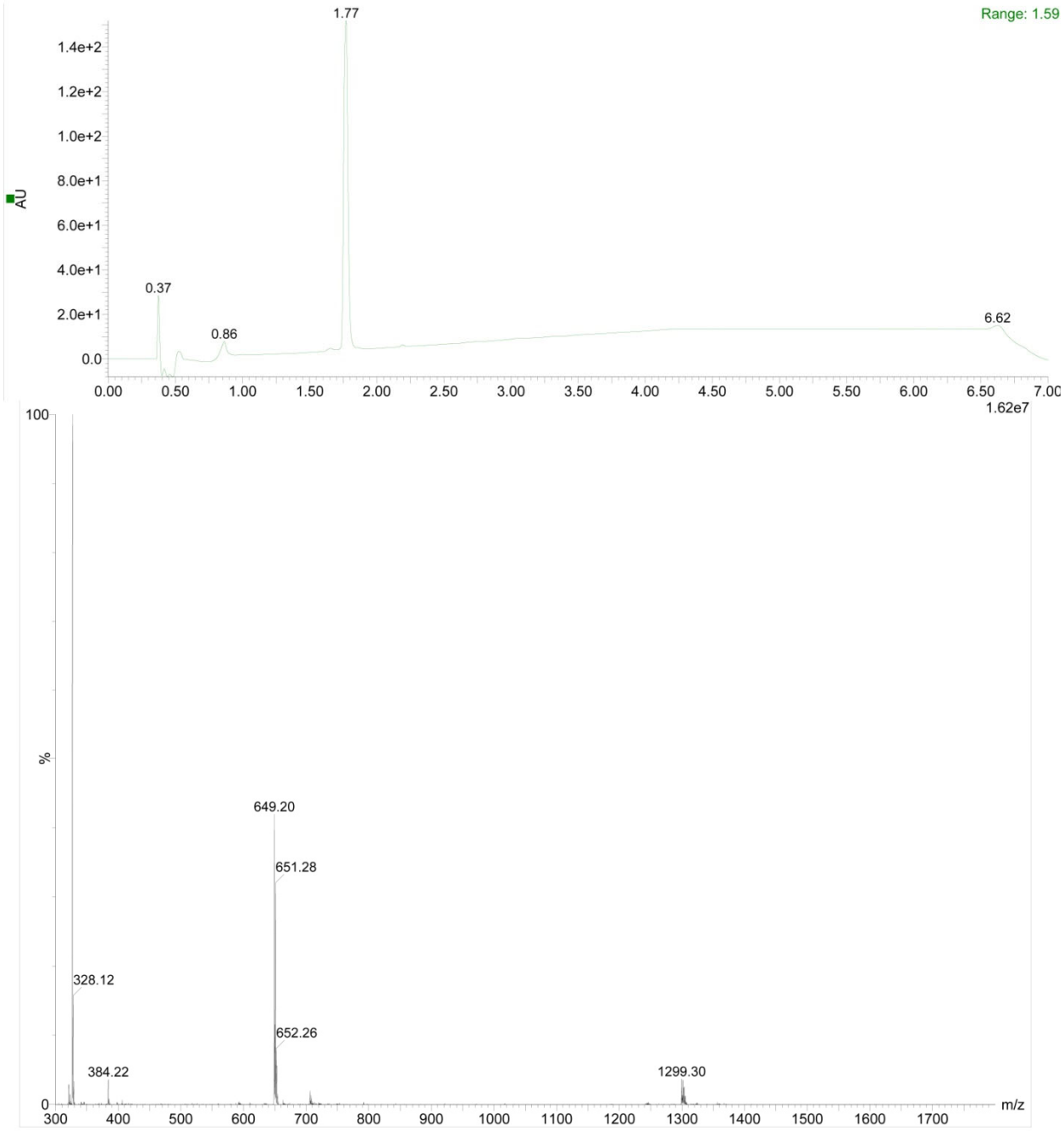

Figure S40. The ultra-performance LC (top) and Mass (bottom) spectrum of **1f**, $[M-H]^-$ at m/z 649.20.

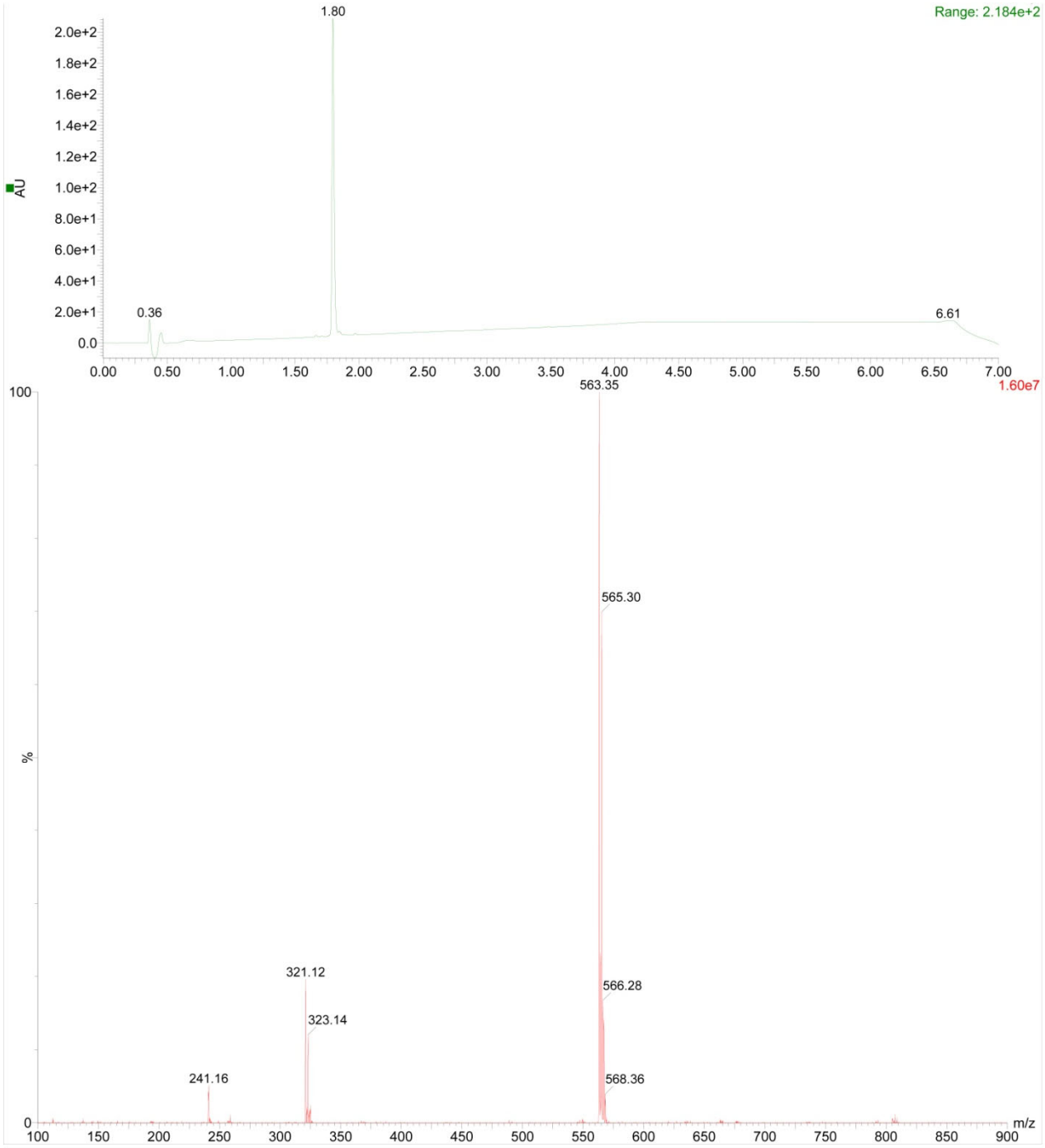

Figure S41. The ultra-performance LC (top) and Mass (bottom) spectrum of **1g**, $[M-H]^-$ at m/z 563.35.

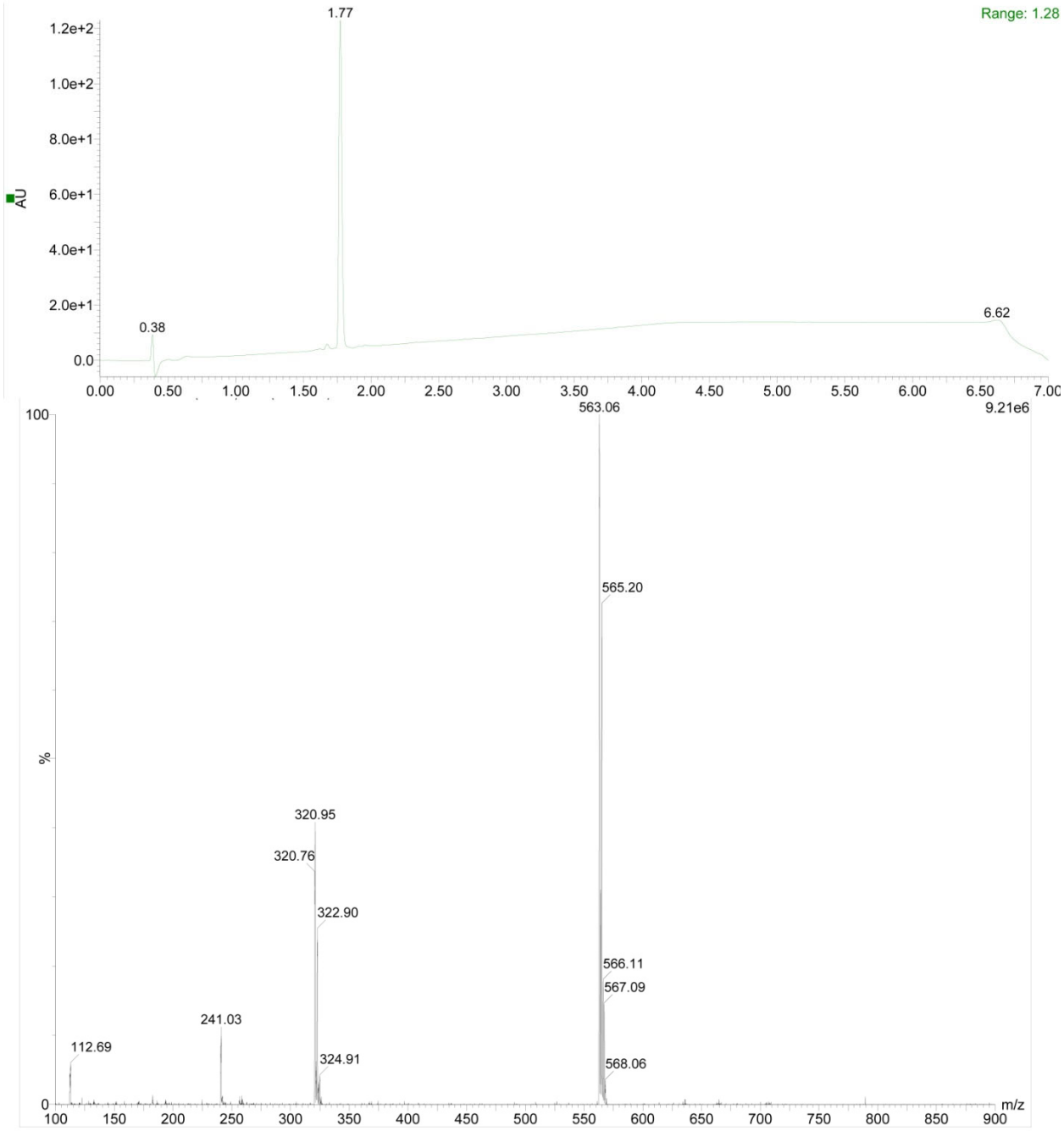

Figure S42. The ultra-performance LC (top) and Mass (bottom) spectrum of **1h**, $[M-H]^-$ at m/z 563.06.

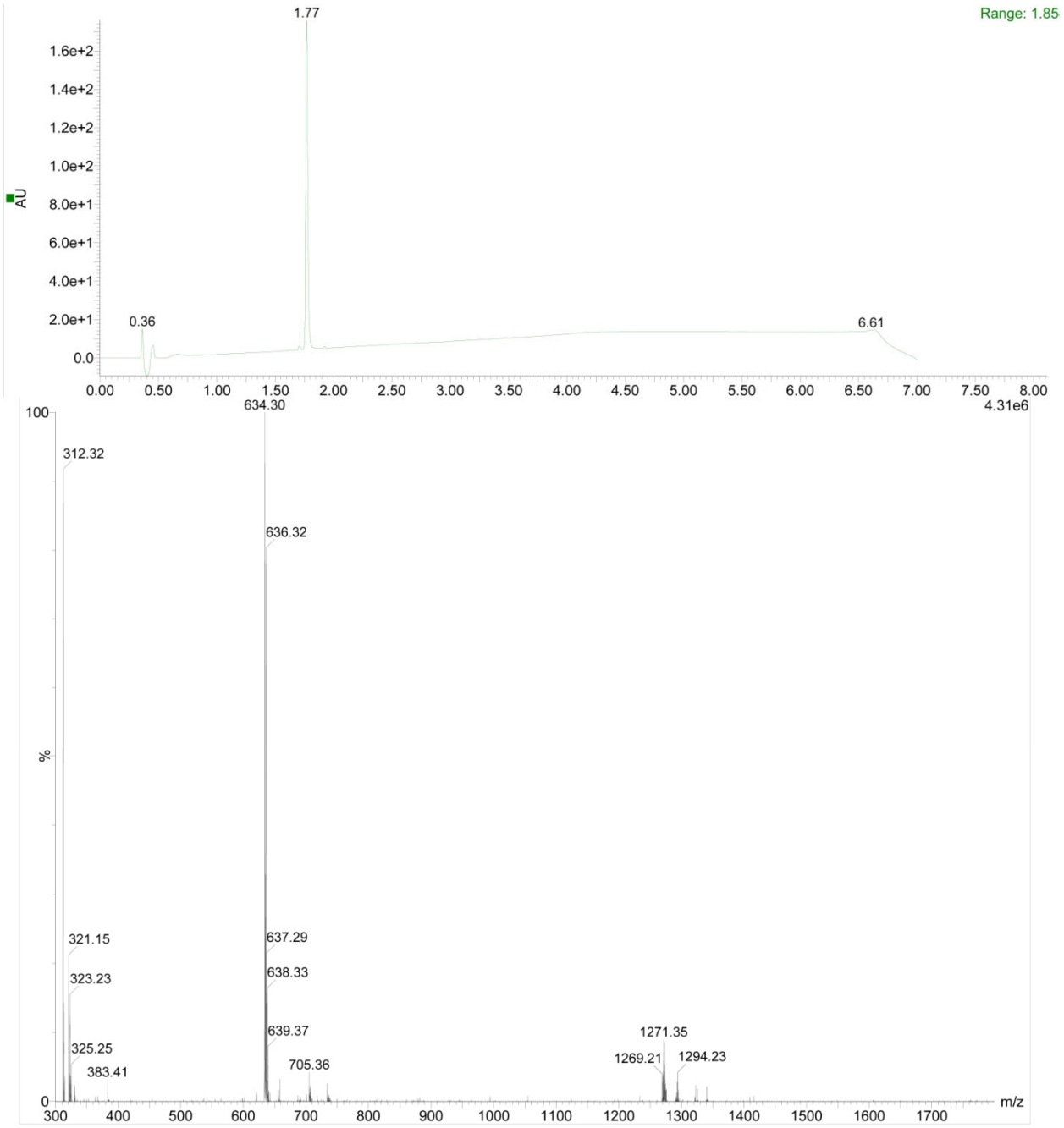

Figure S43. The ultra-performance LC (top) and Mass (bottom) spectrum of **1i**, $[M-H]^-$ at m/z 634.30.

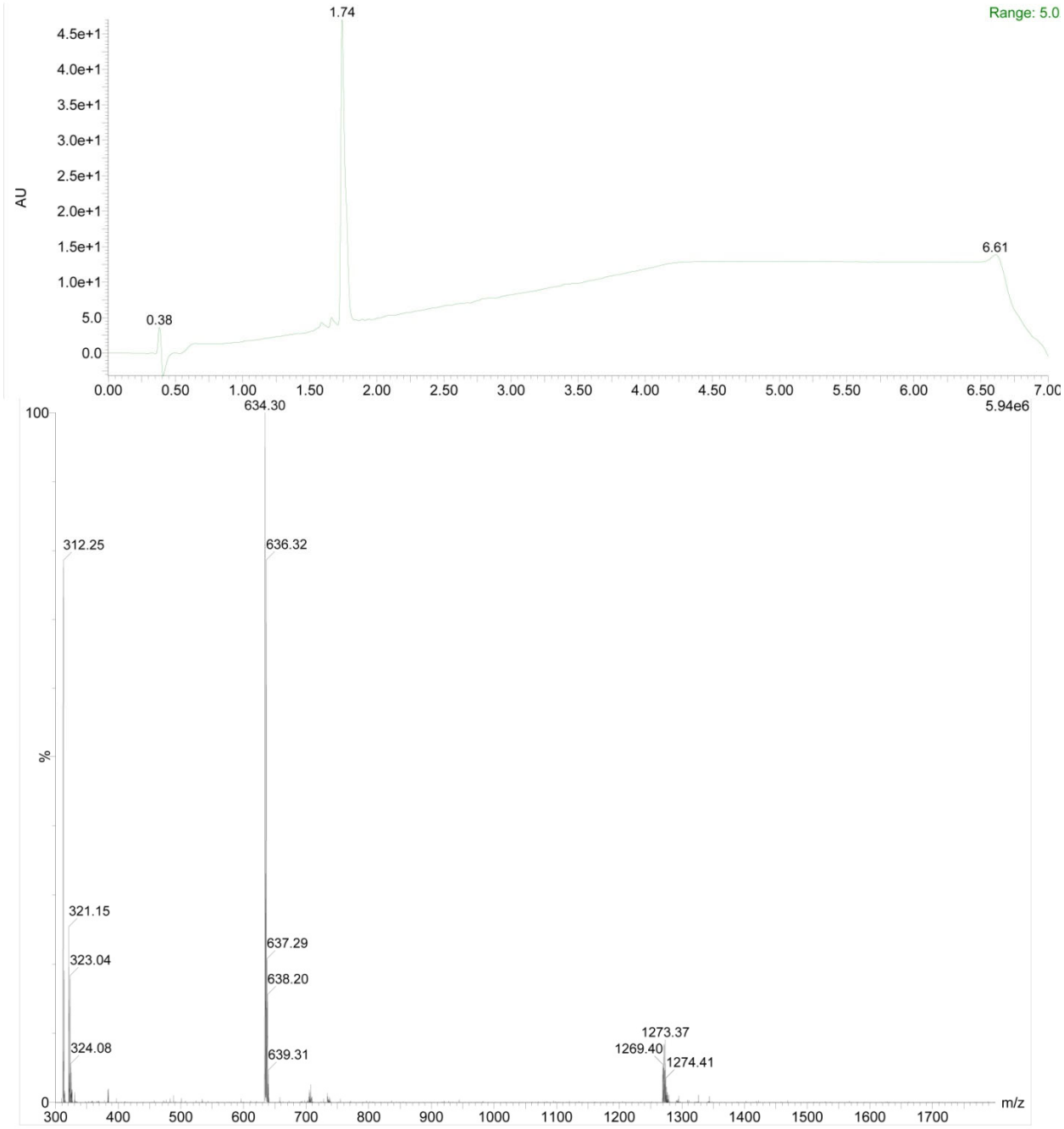

Figure S44. The ultra-performance LC (top) and Mass (bottom) spectrum of **1j**, $[M-H]^-$ at m/z 634.30.

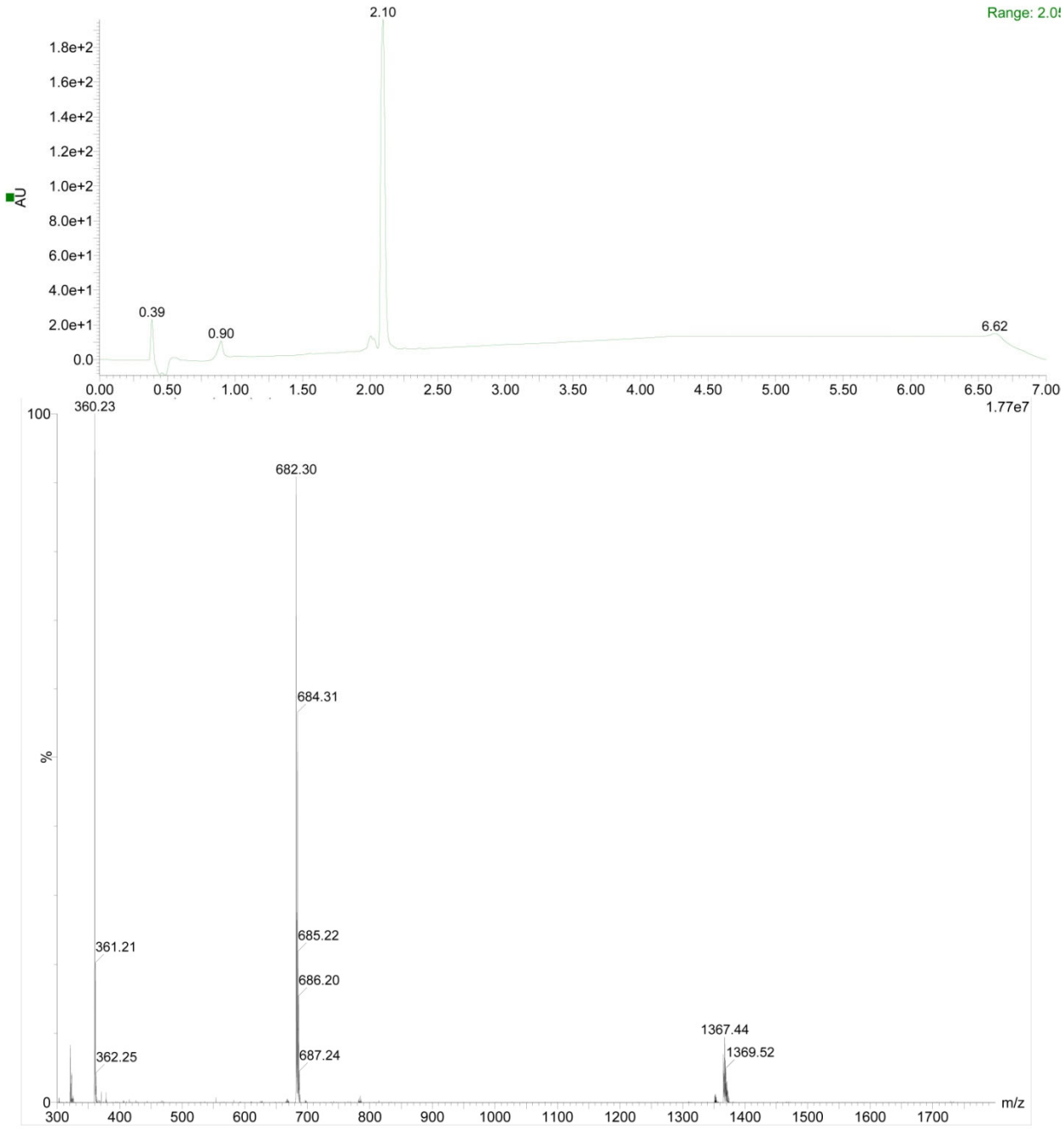

Figure S45. The ultra-performance LC (top) and Mass (bottom) spectrum of **1k**, $[M-H]^-$ at m/z 682.30.

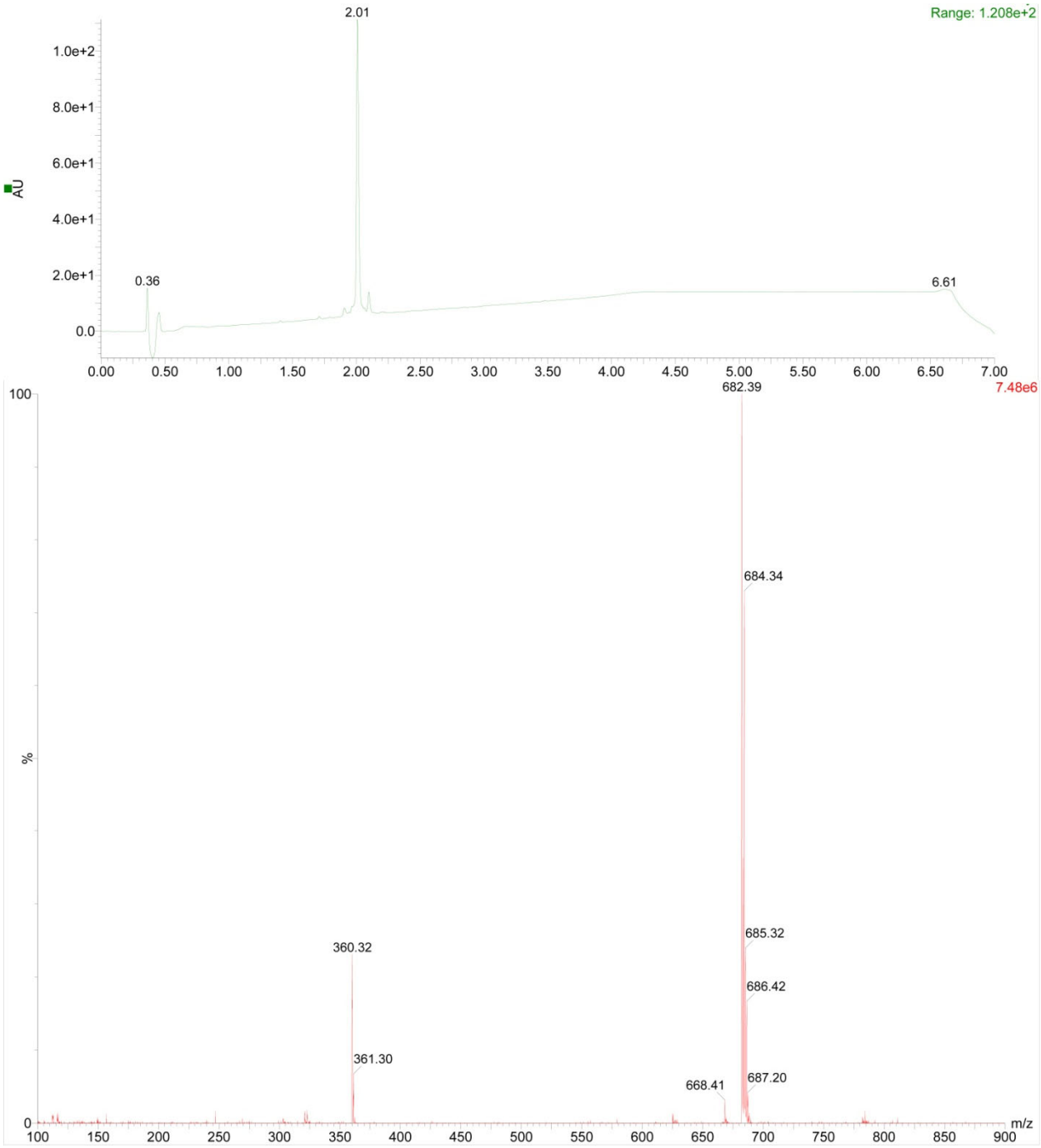

Figure S46. The ultra-performance LC (top) and Mass (bottom) spectrum of **1l**, $[M-H]^-$ at m/z 682.39.

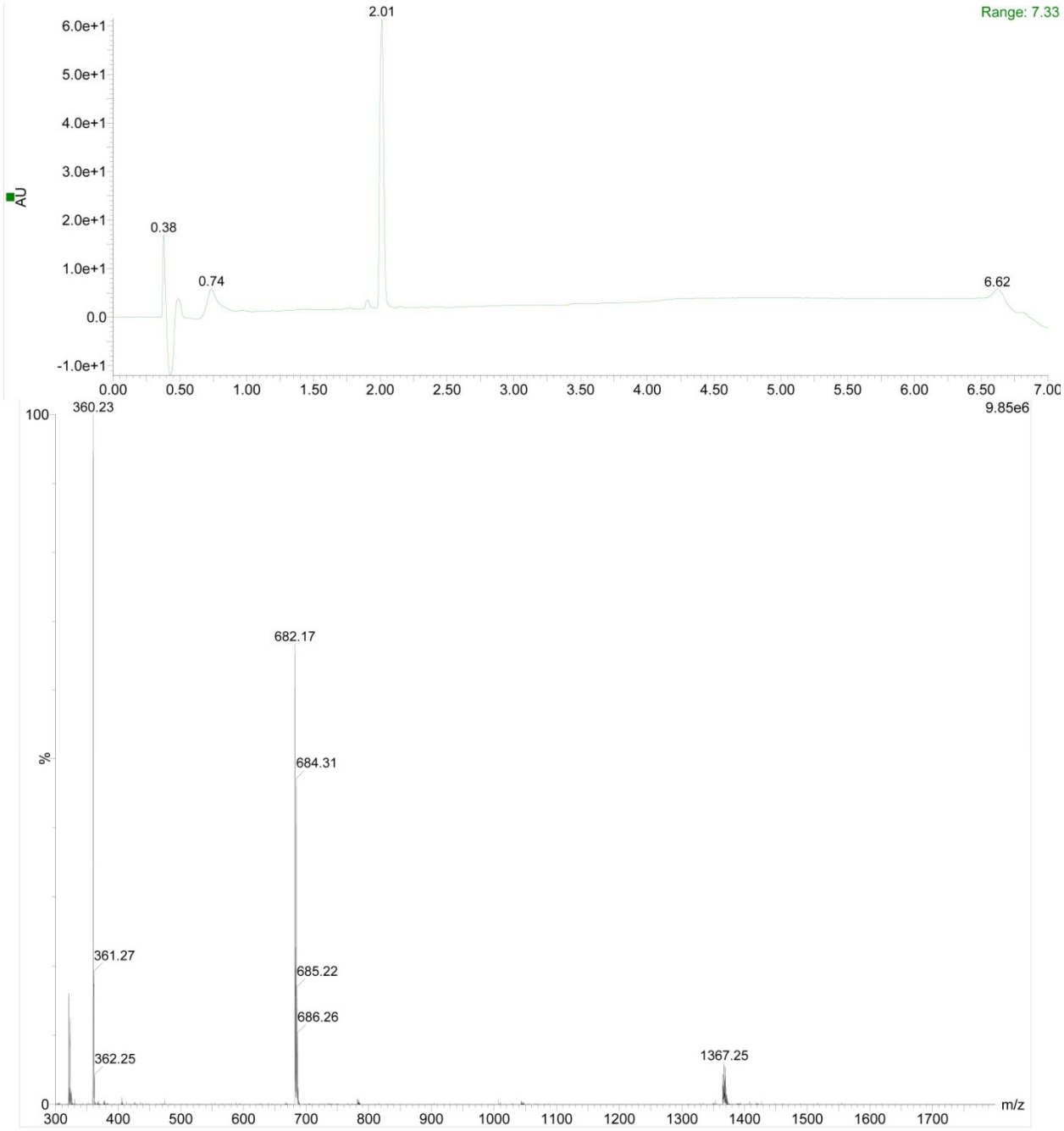

Figure S47. The ultra-performance LC (top) and Mass (bottom) spectrum of **1m**, $[M-H]^-$ at m/z 682.17.

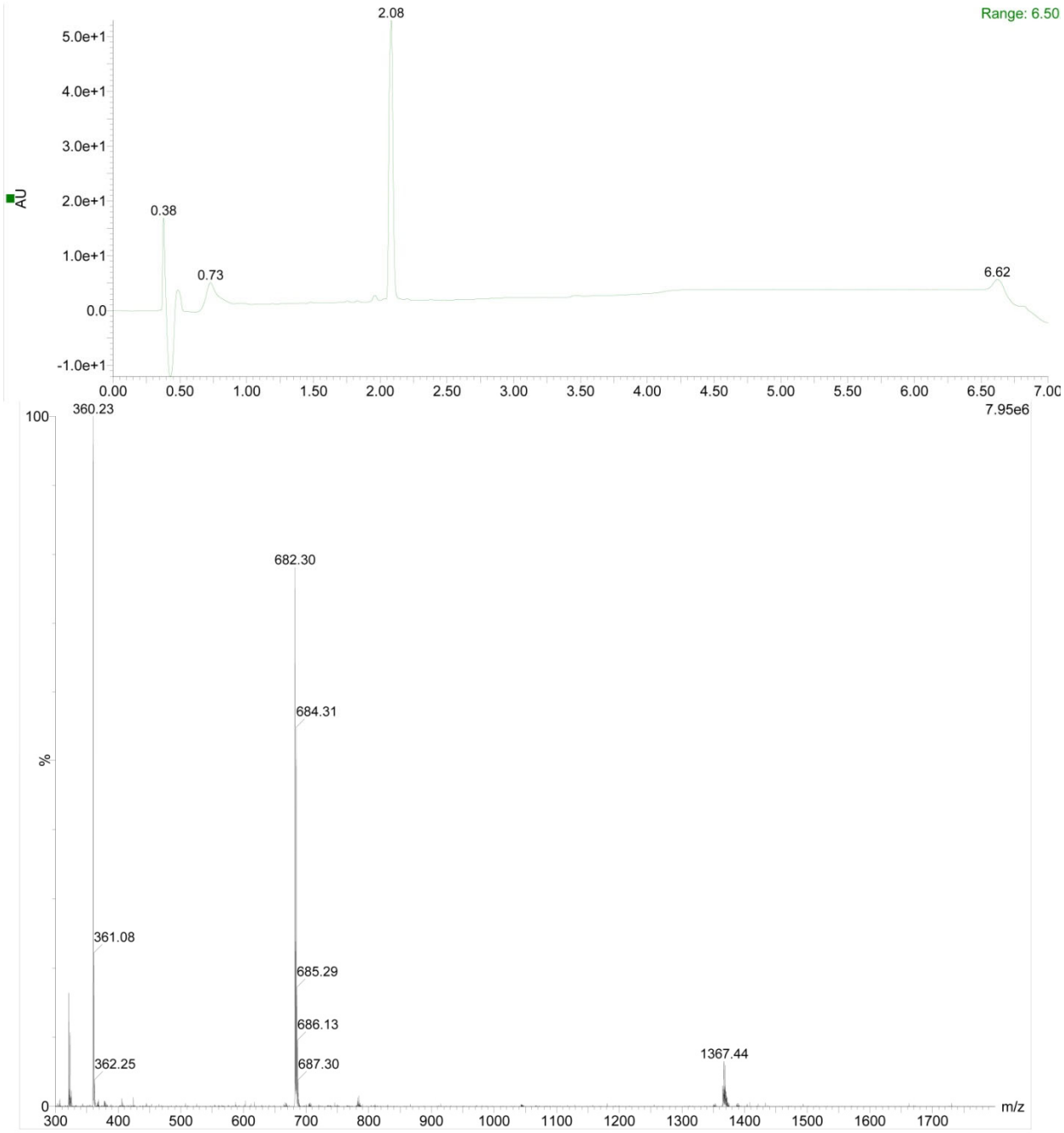

Figure S48. The ultra-performance LC (top) and Mass (bottom) spectrum of **1n**, $[M-H]^-$ at m/z 682.30.

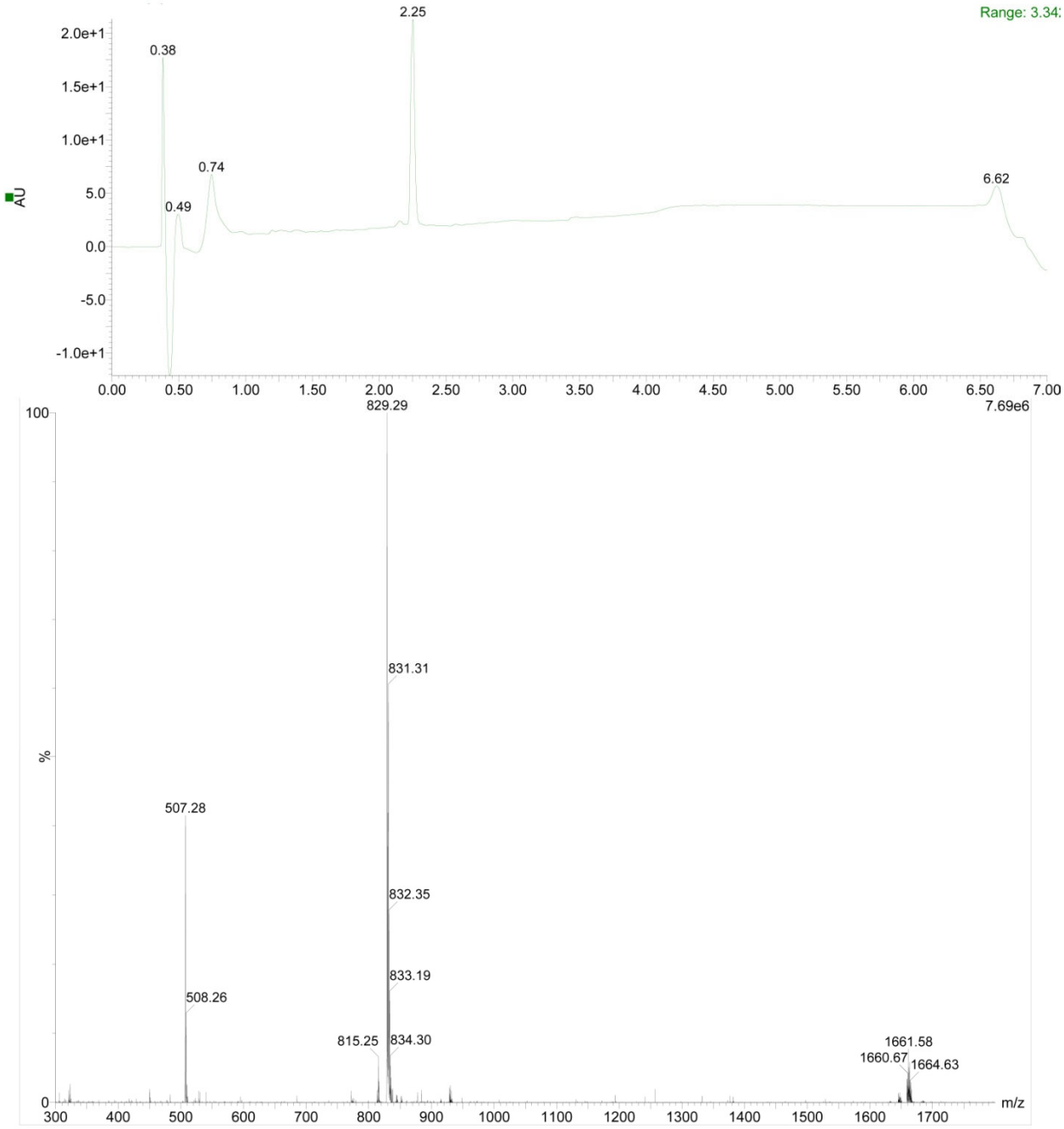

Figure S49. The ultra-performance LC (top) and Mass (bottom) spectrum of **1o**, $[M-H]^-$ at m/z 829.29.

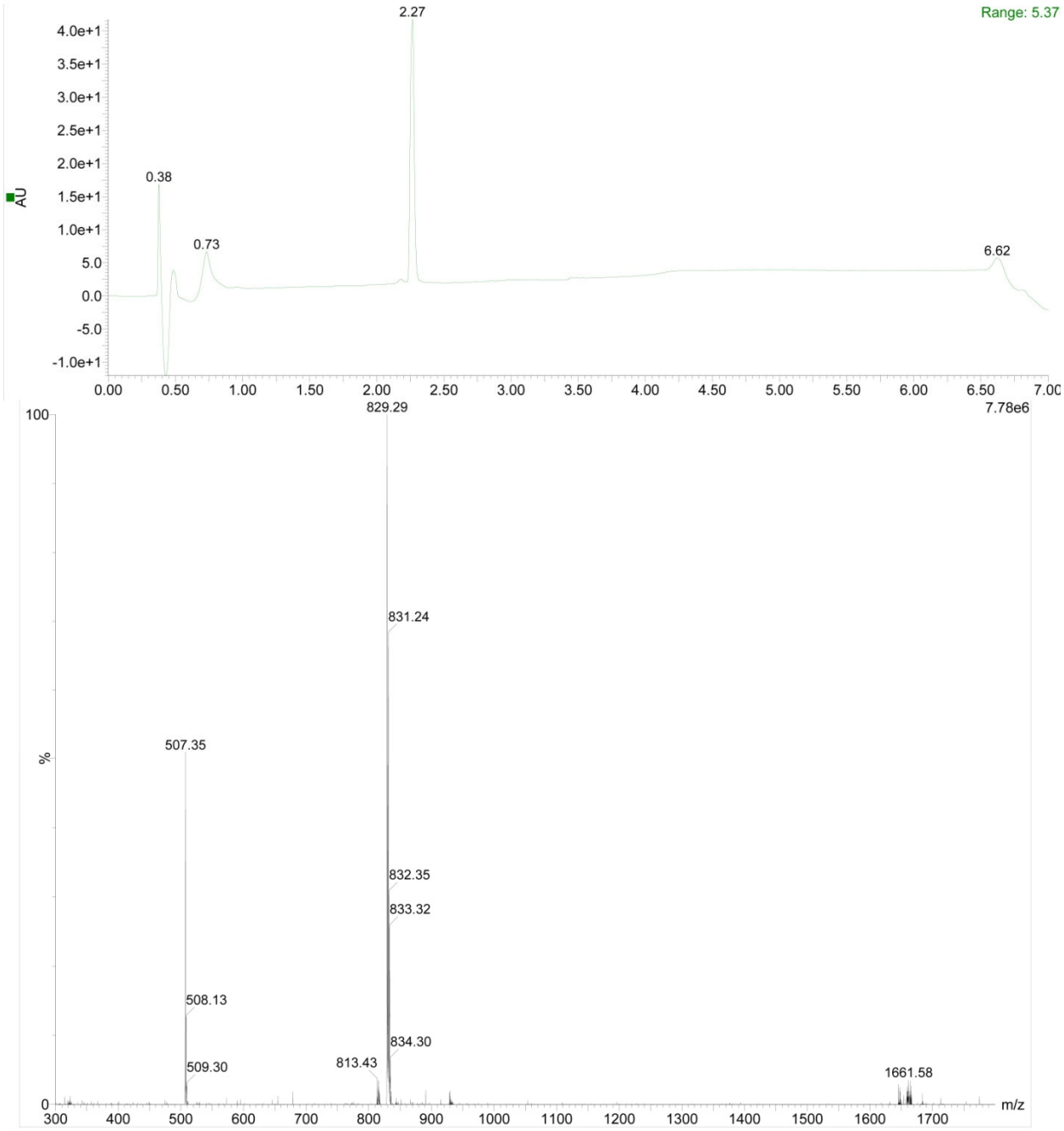

Figure S50. The ultra-performance LC (top) and Mass (bottom) spectrum of **1p**, $[M-H]^-$ at m/z 829.29.

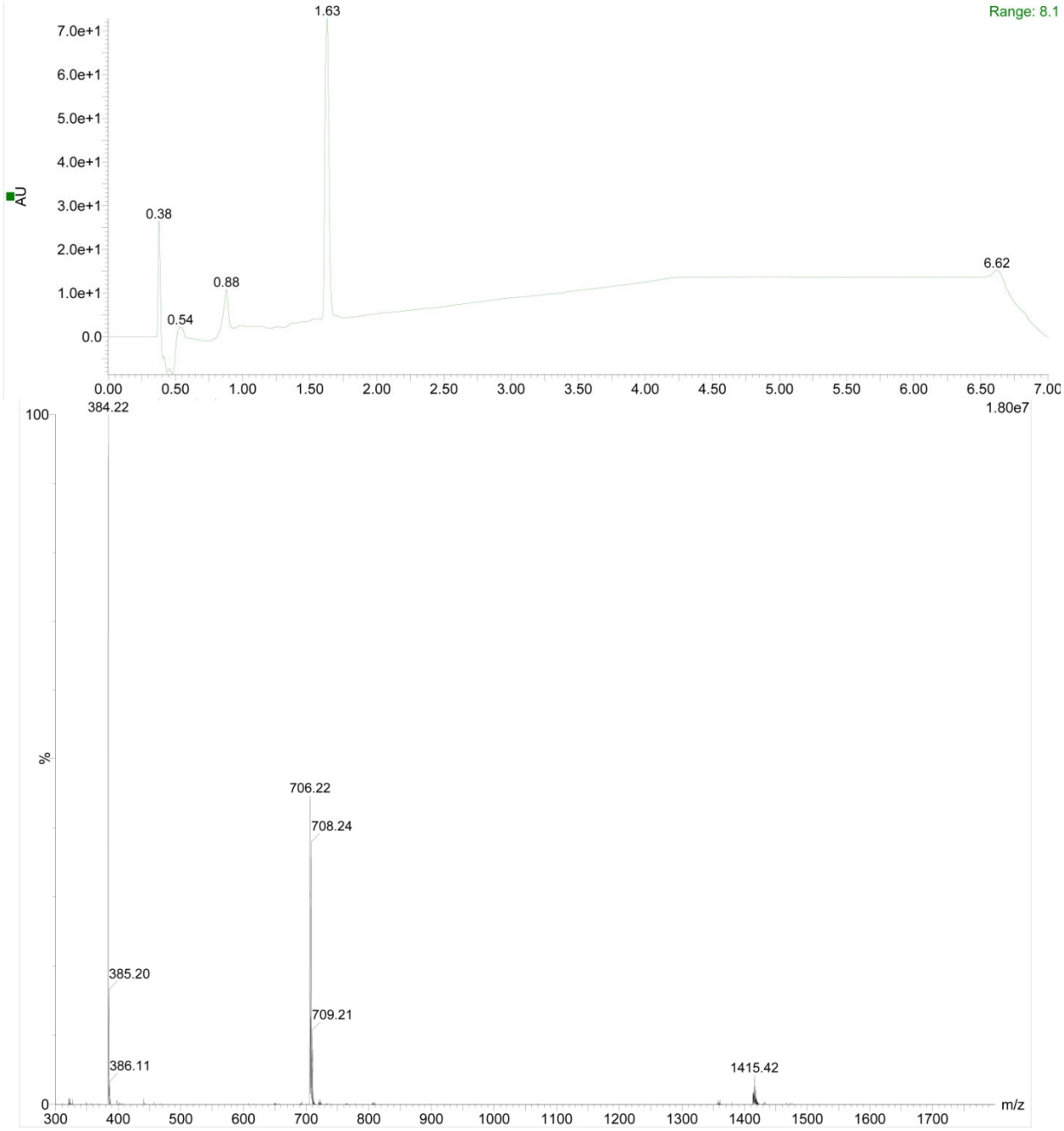

Figure S51. The ultra-performance LC (top) and Mass (bottom) spectrum of **1q**, $[M-H]^-$ at m/z 706.22.

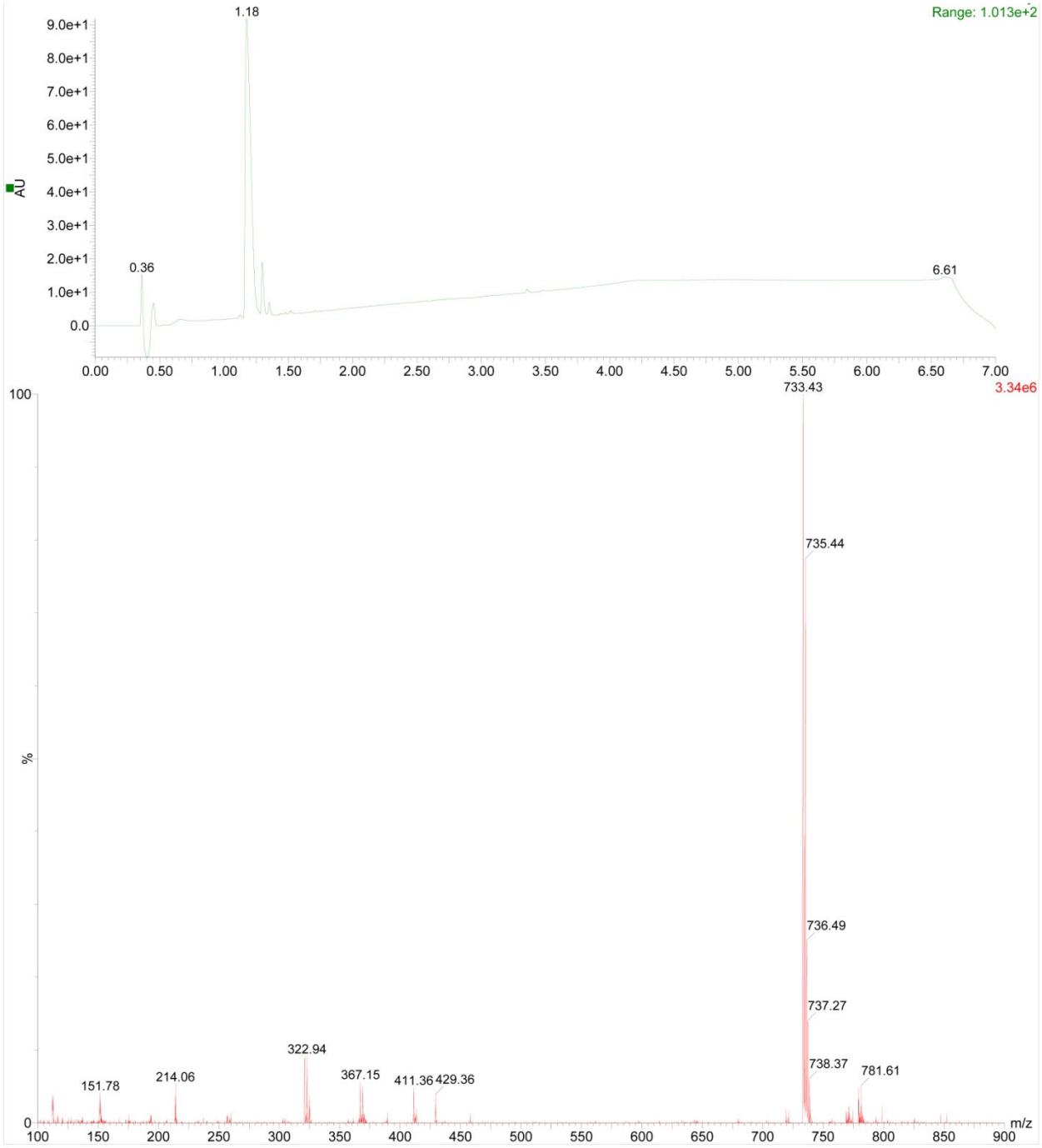

Figure S52. The ultra-performance LC (top) and Mass (bottom) spectrum of **2a**, $[M-H]^-$ at m/z 733.43.

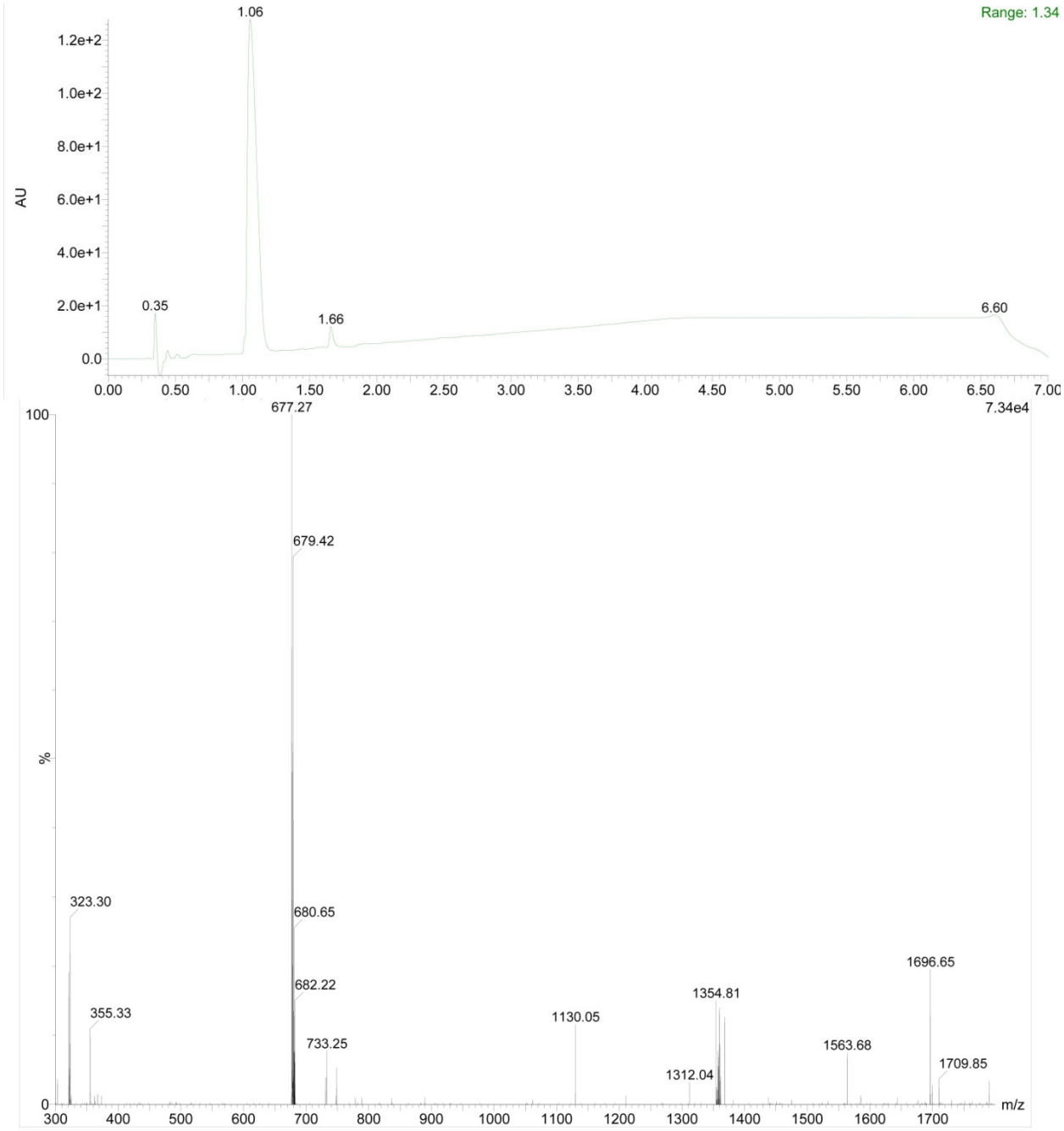

Figure S53. The ultra-performance LC (top) and Mass (bottom) spectrum of **2b**, $[M-H]^-$ at m/z 677.27.

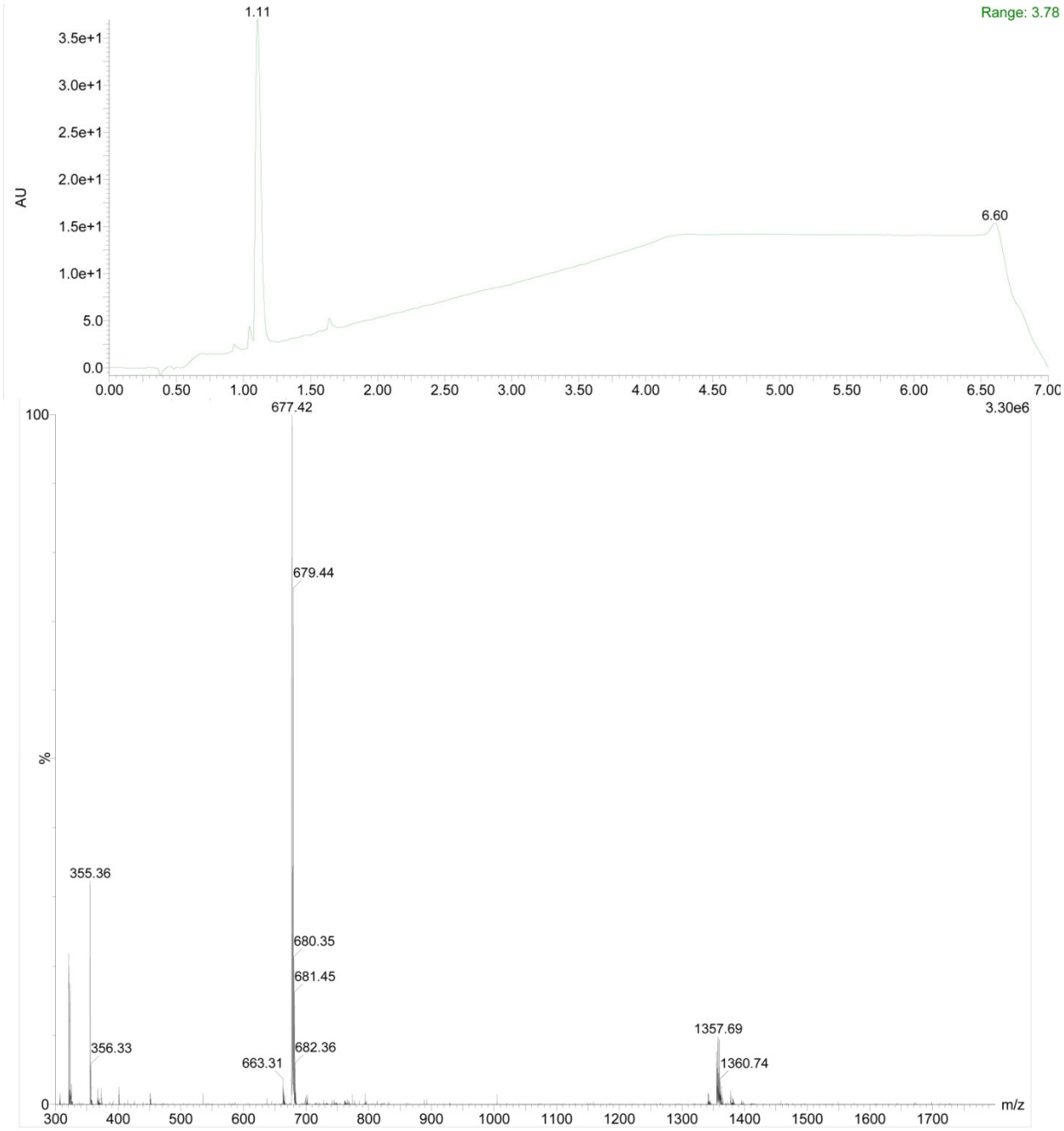

Figure S54. The ultra-performance LC (top) and Mass (bottom) spectrum of **2c**, $[M-H]^-$ at m/z 677.42.

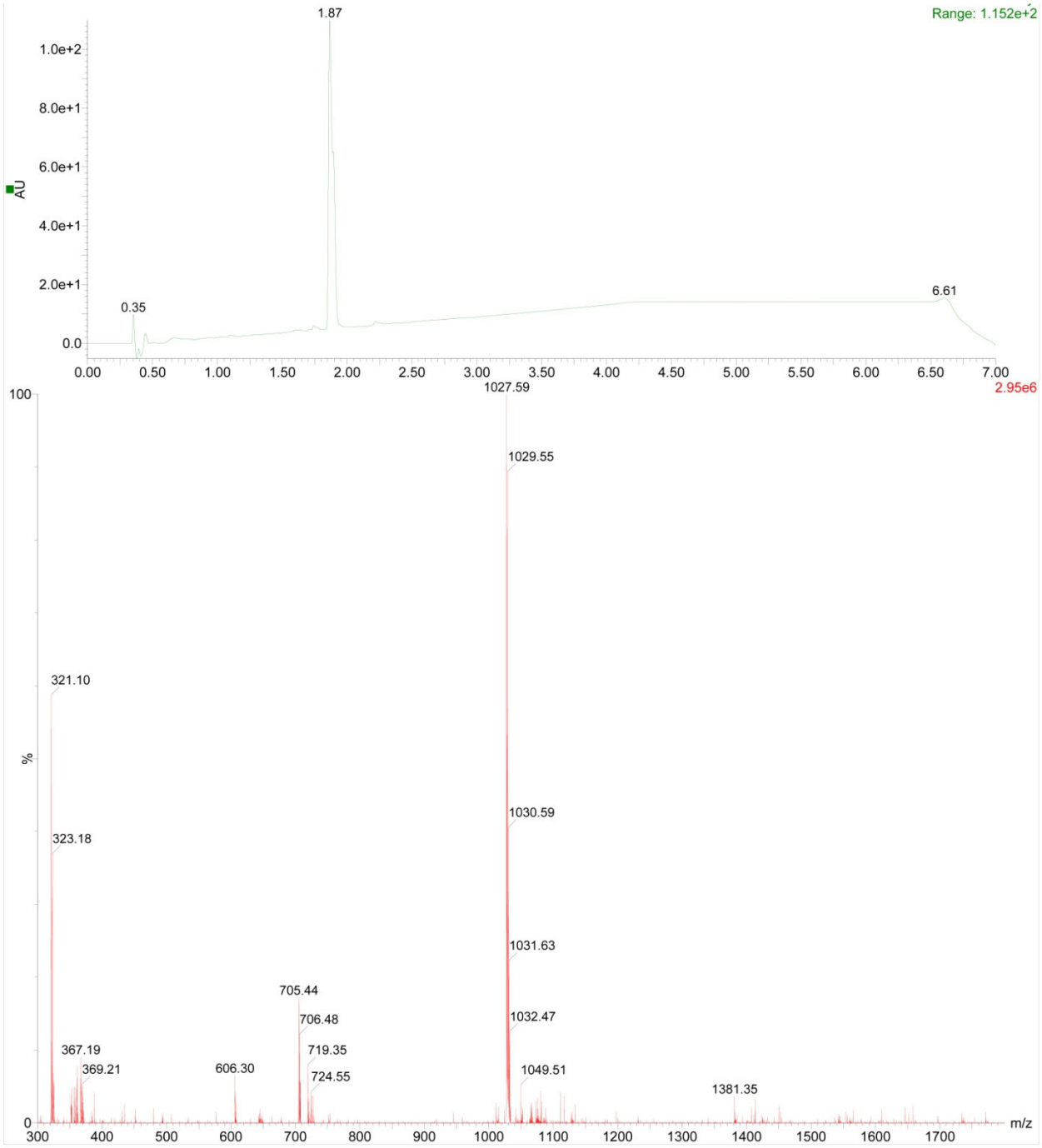

Figure S55. The ultra-performance LC (top) and Mass (bottom) spectrum of **2d**, $[M-H]^-$ at m/z 1027.59.

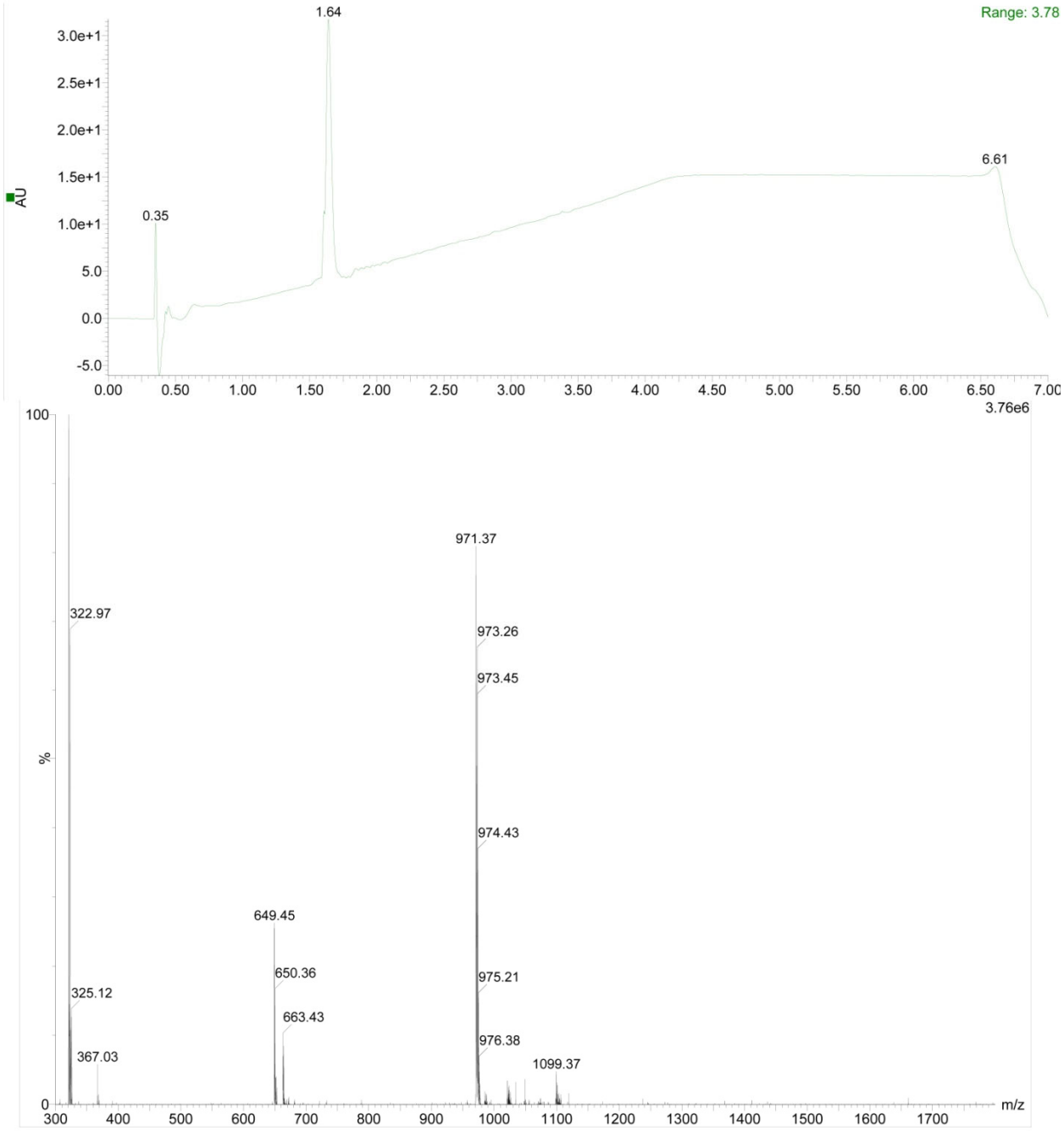

Figure S56. The ultra-performance LC (top) and Mass (bottom) spectrum of **2e**, $[M-H]^-$ at m/z 971.37.

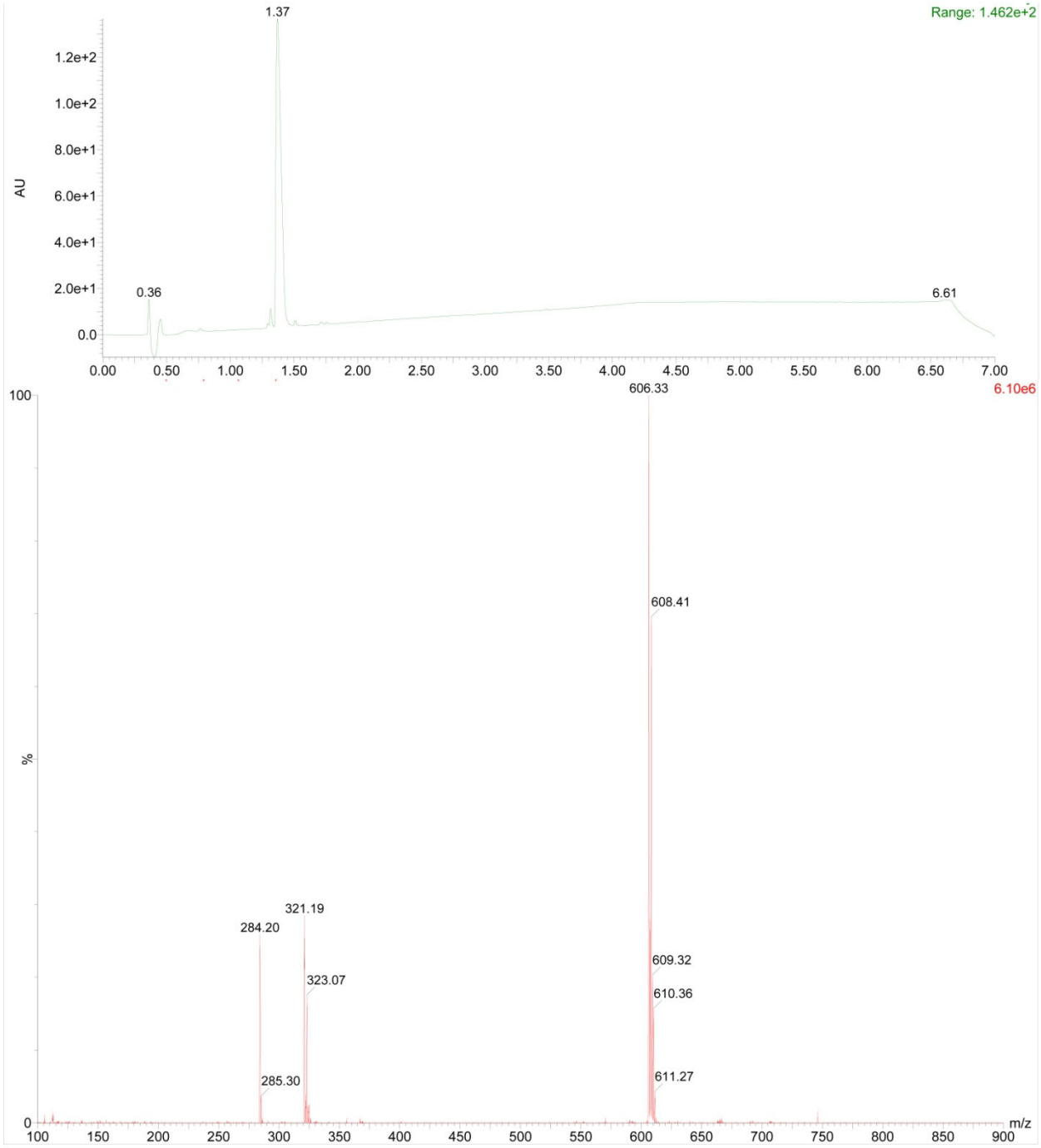

Figure S57. The ultra-performance LC (top) and Mass (bottom) spectrum of **2f**, $[M-H]^-$ at m/z 606.33.

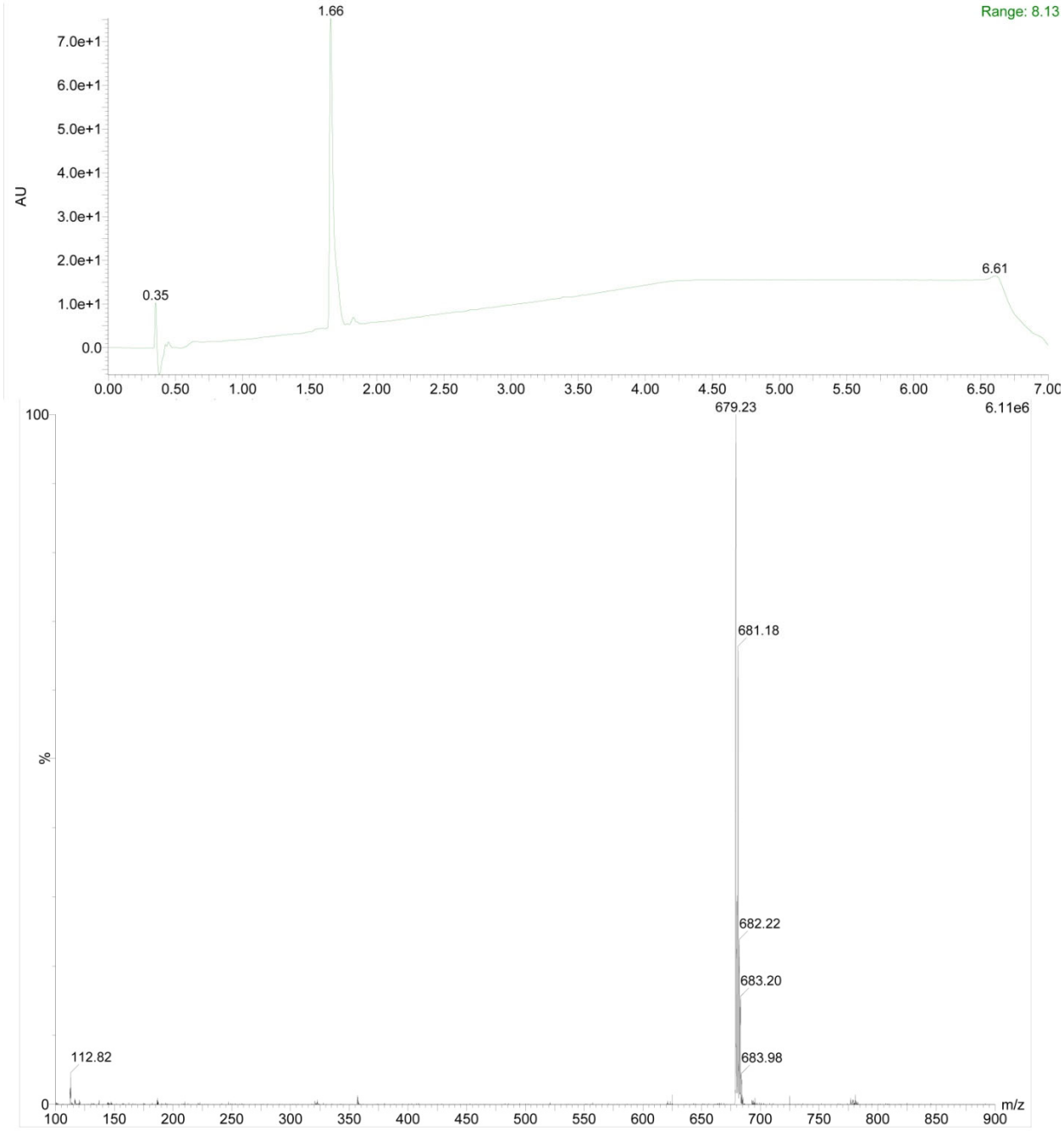

Figure S58. The ultra-performance LC (top) and Mass (bottom) spectrum of **2g**, $[M-H]^-$ at m/z 679.23.

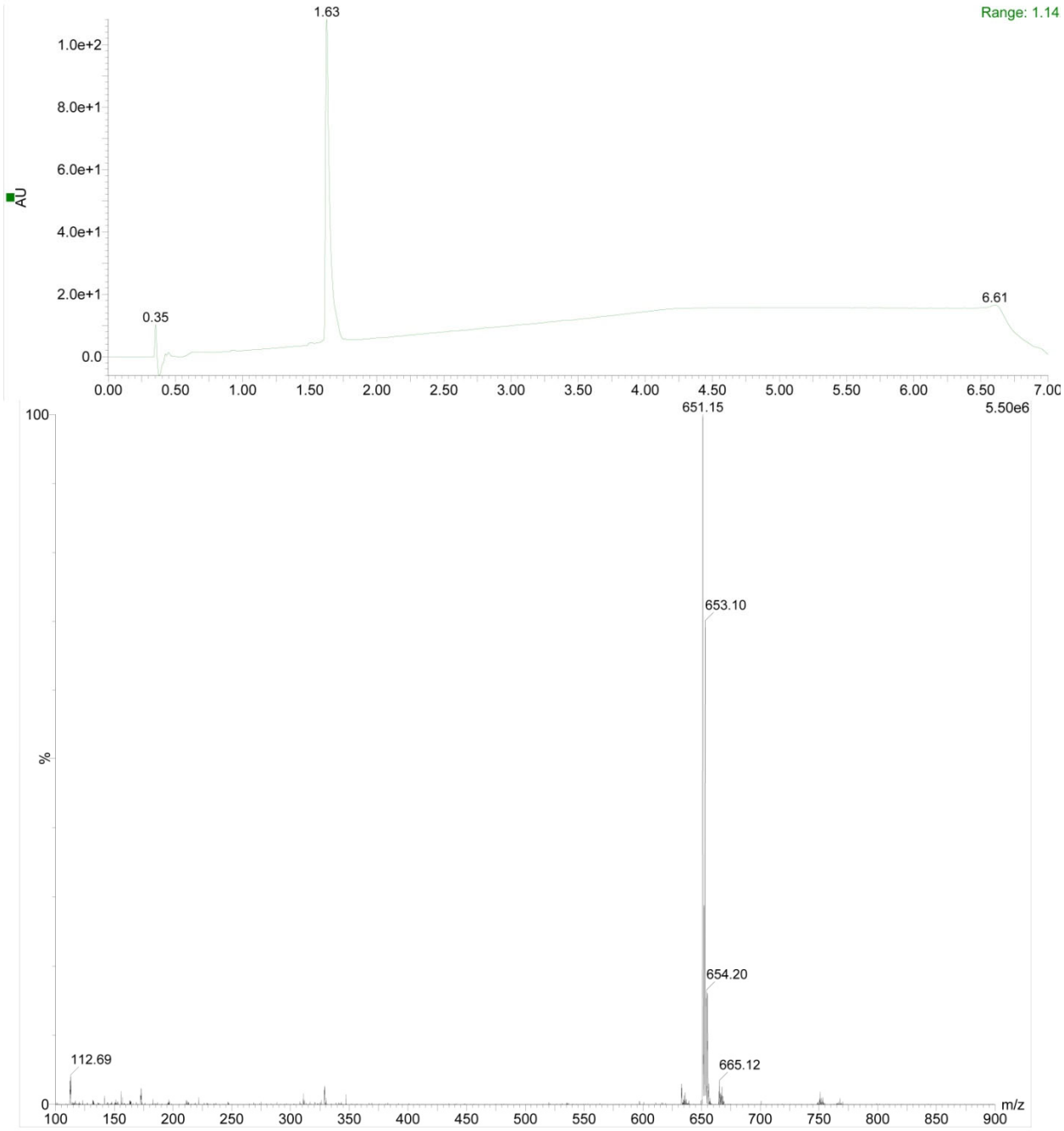

Figure S59. The ultra-performance LC (top) and Mass (bottom) spectrum of **2h**, $[M-H]^-$ at m/z 651.15.

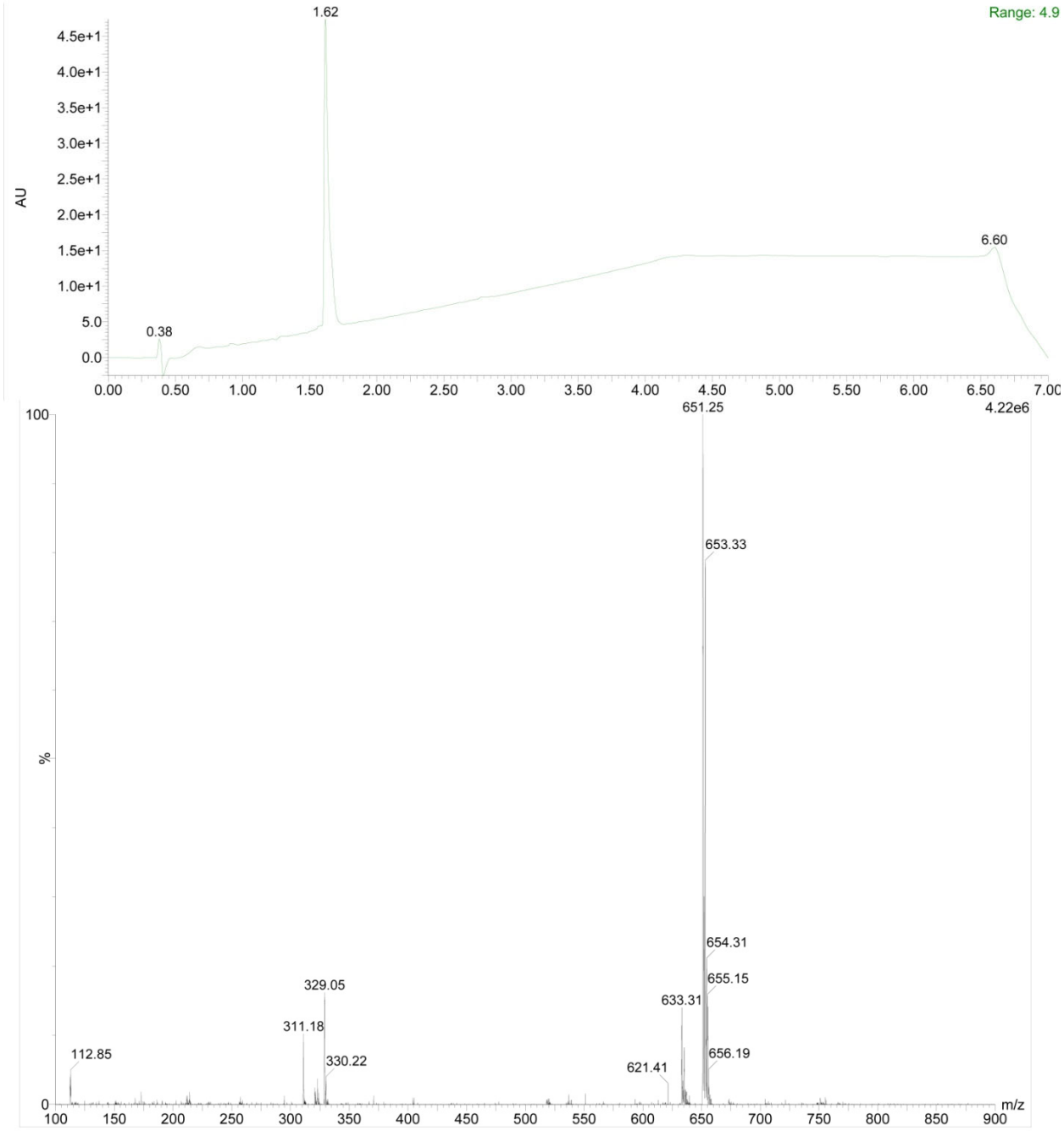

Figure S60. The ultra-performance LC (top) and Mass (bottom) spectrum of **2i**, $[M-H]^-$ at m/z 651.25.

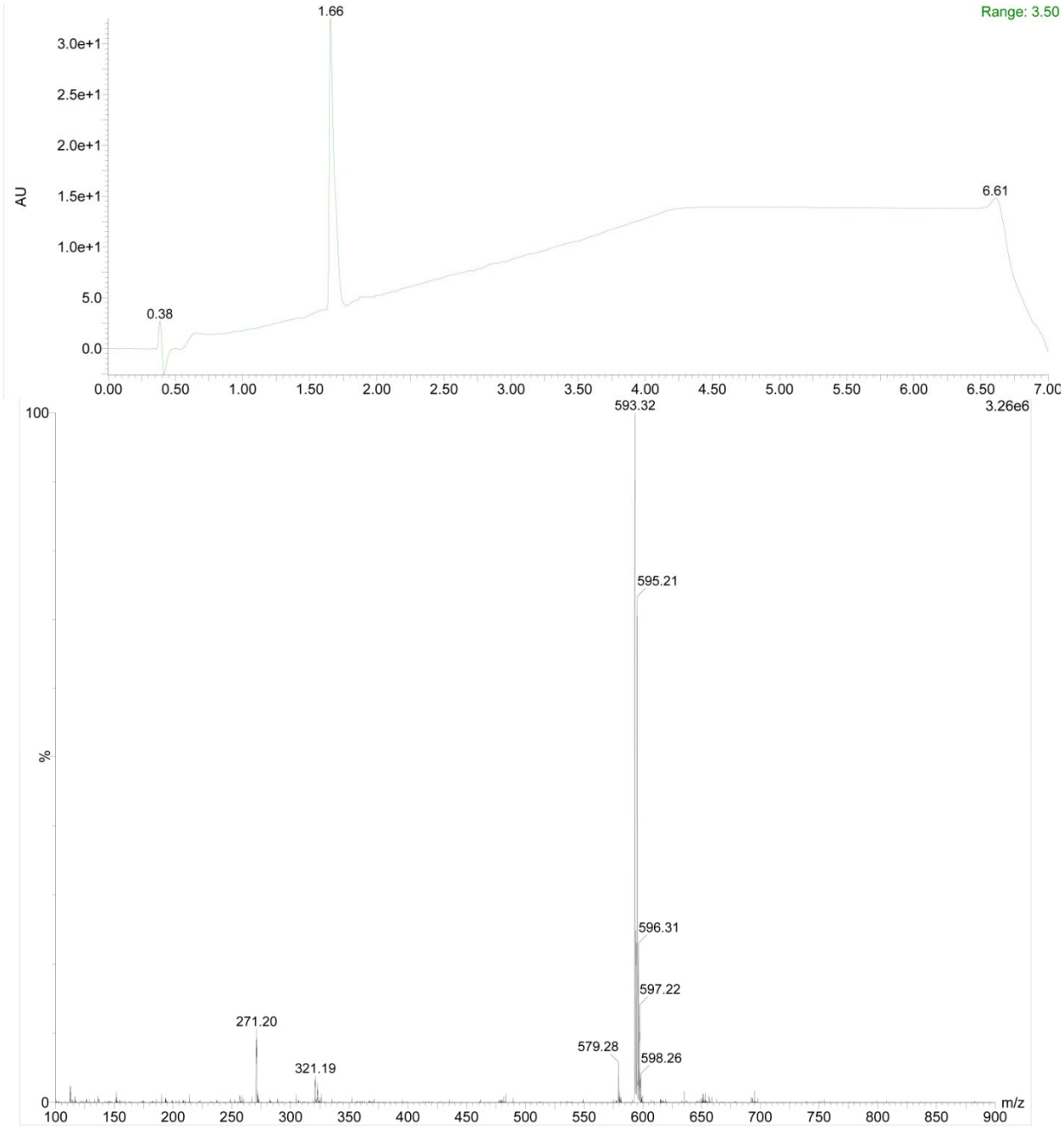

Figure S61. The ultra-performance LC (top) and Mass (bottom) spectrum of **2j**, $[M-H]^-$ at m/z 593.32.

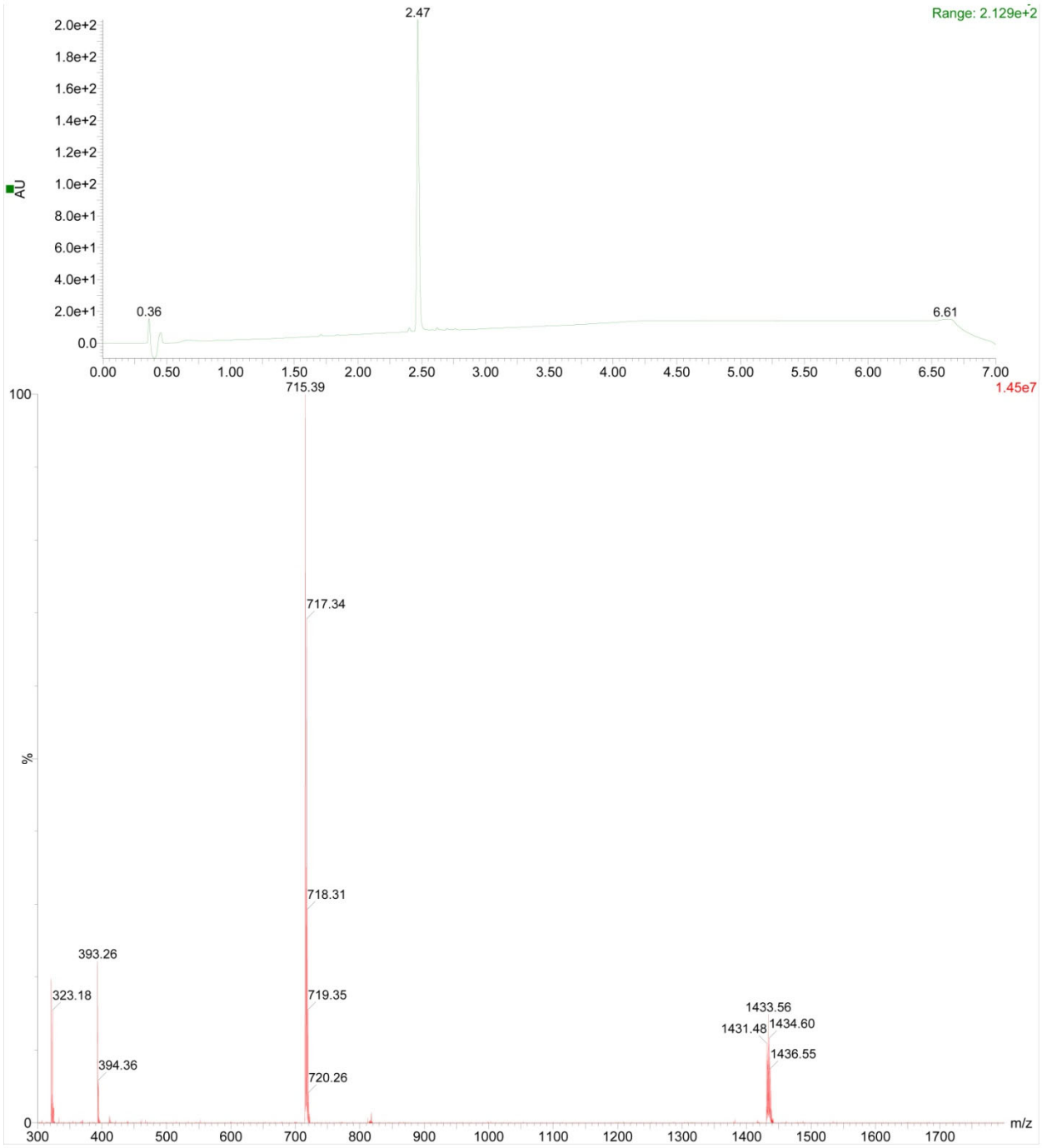

Figure S62. The ultra-performance LC (top) and Mass (bottom) spectrum of **3a**, $[M-H]^-$ at m/z 715.39.

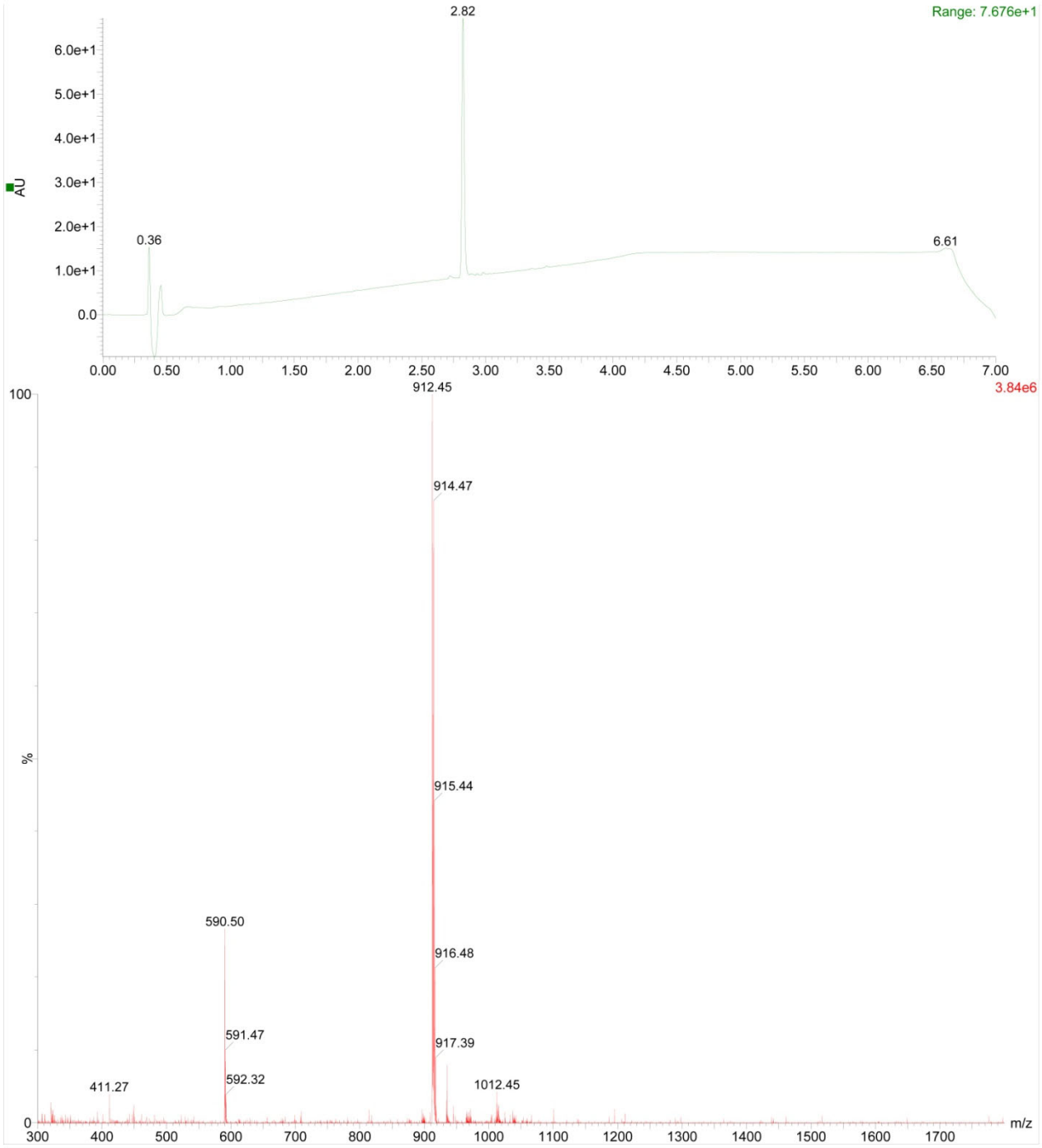

Figure S63. The ultra-performance LC (top) and Mass (bottom) spectrum of **3b**, $[M-H]^-$ at m/z 912.45.

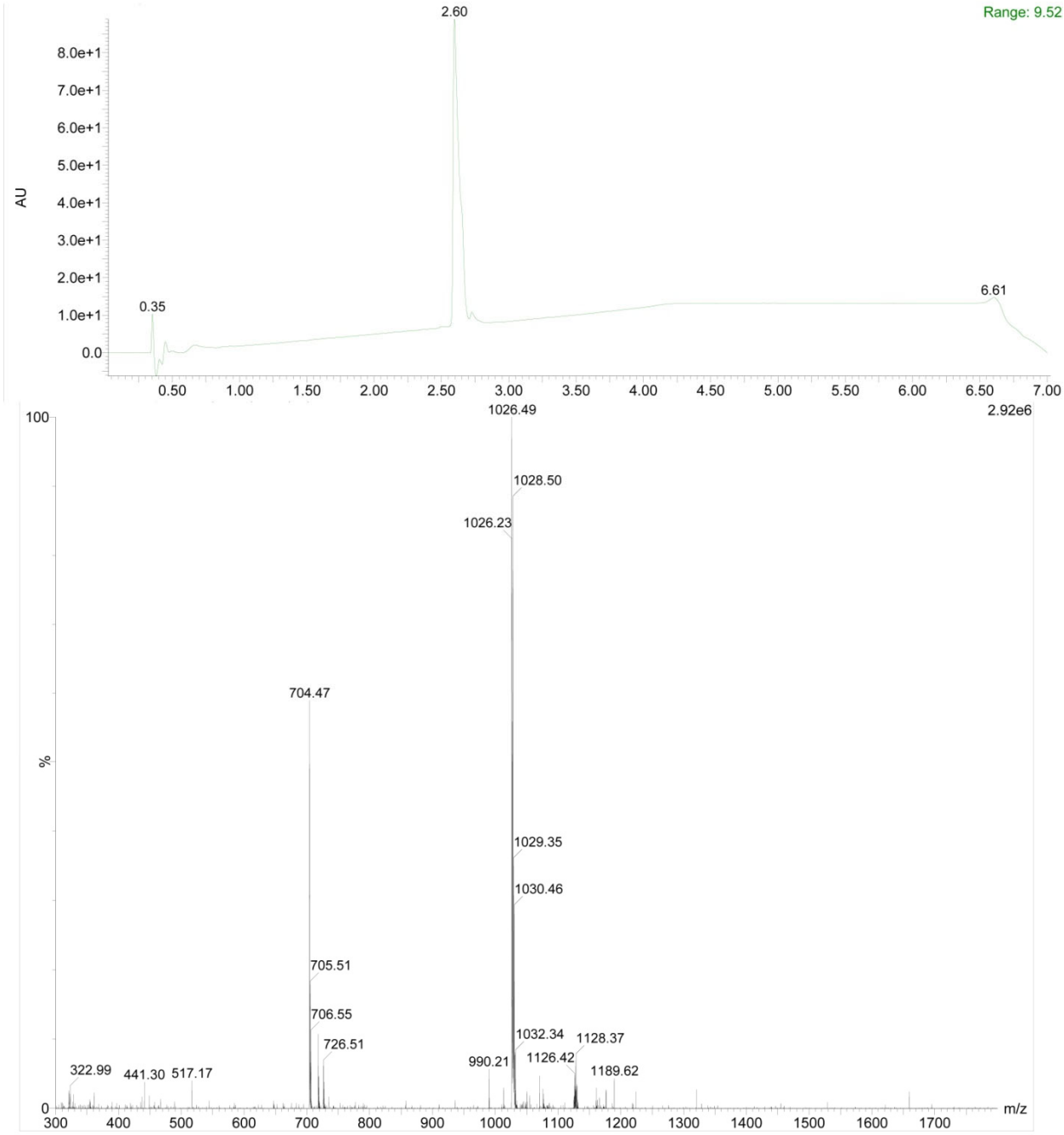

Figure S64. The ultra-performance LC (top) and Mass (bottom) spectrum of **3c**, $[M-H]^-$ at m/z 1026.49.

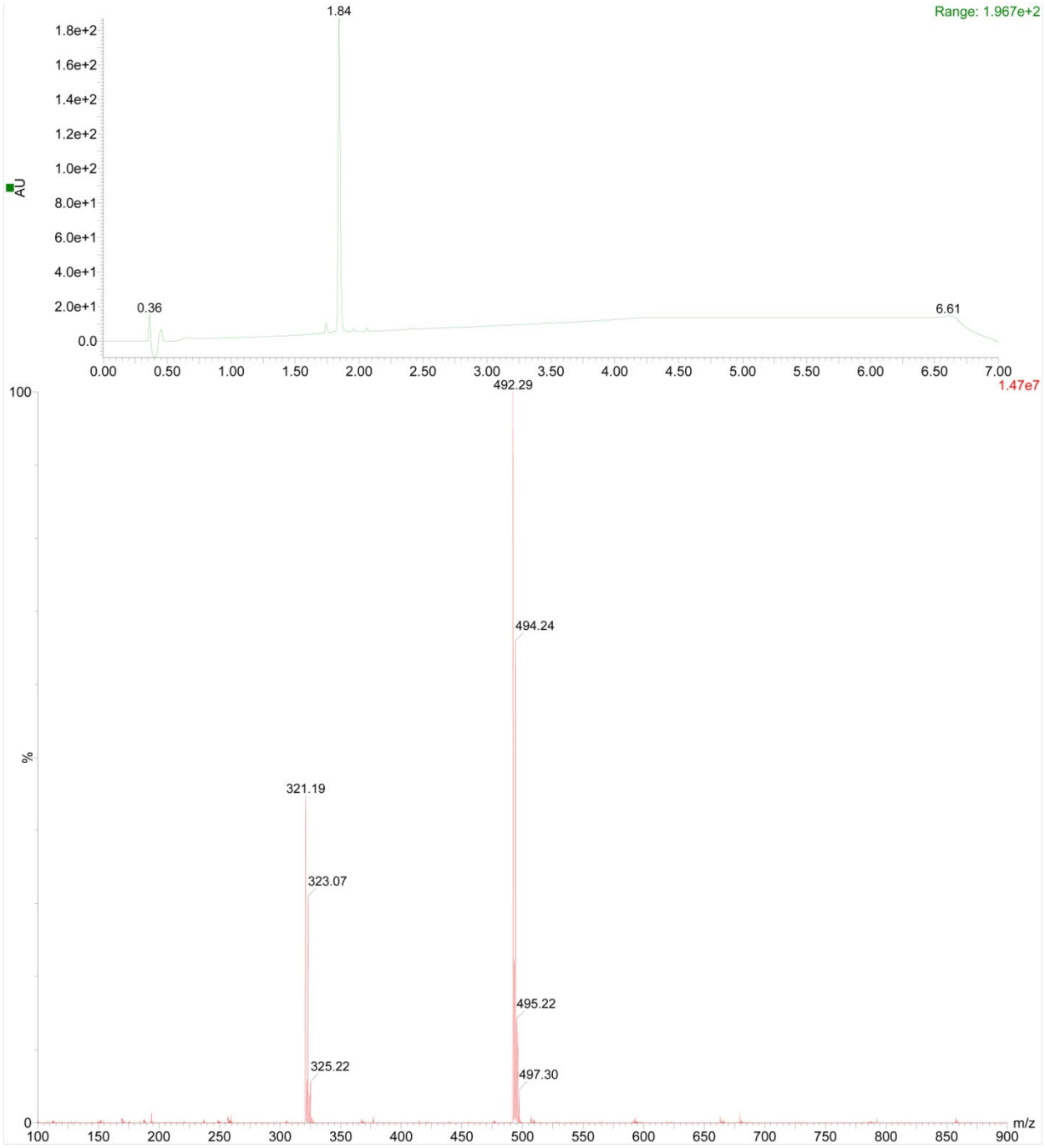

Figure S65. The ultra-performance LC (top) and Mass (bottom) spectrum of **4a**, $[M-H]^-$ at m/z 492.29.

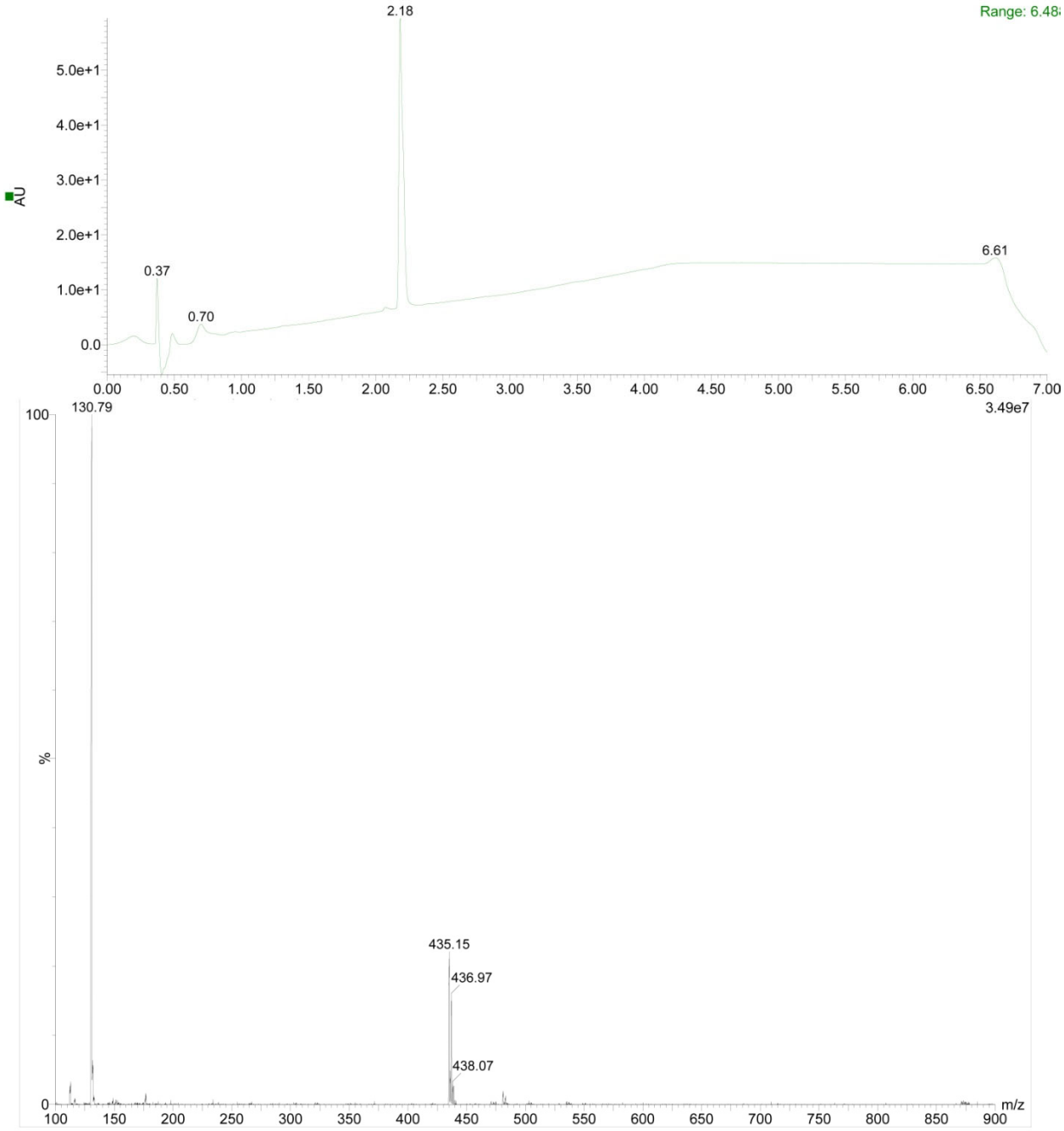

Figure S66. The ultra-performance LC (top) and Mass (bottom) spectrum of **4b**, $[M-H]^-$ at m/z 435.15.

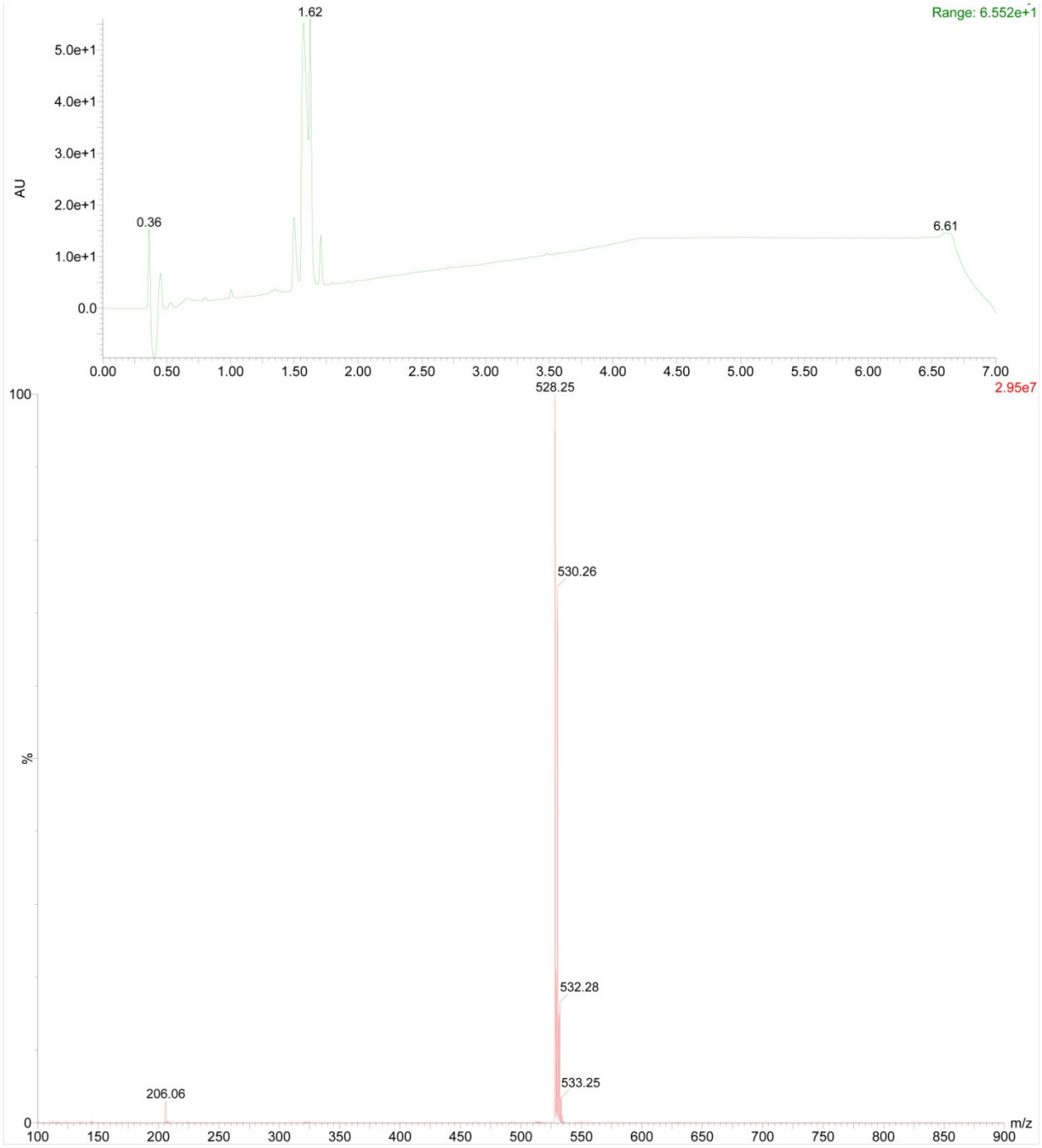

Figure S67. The ultra-performance LC (top) and Mass (bottom) spectrum of **4c**, $[M-H]^-$ at m/z 528.25.

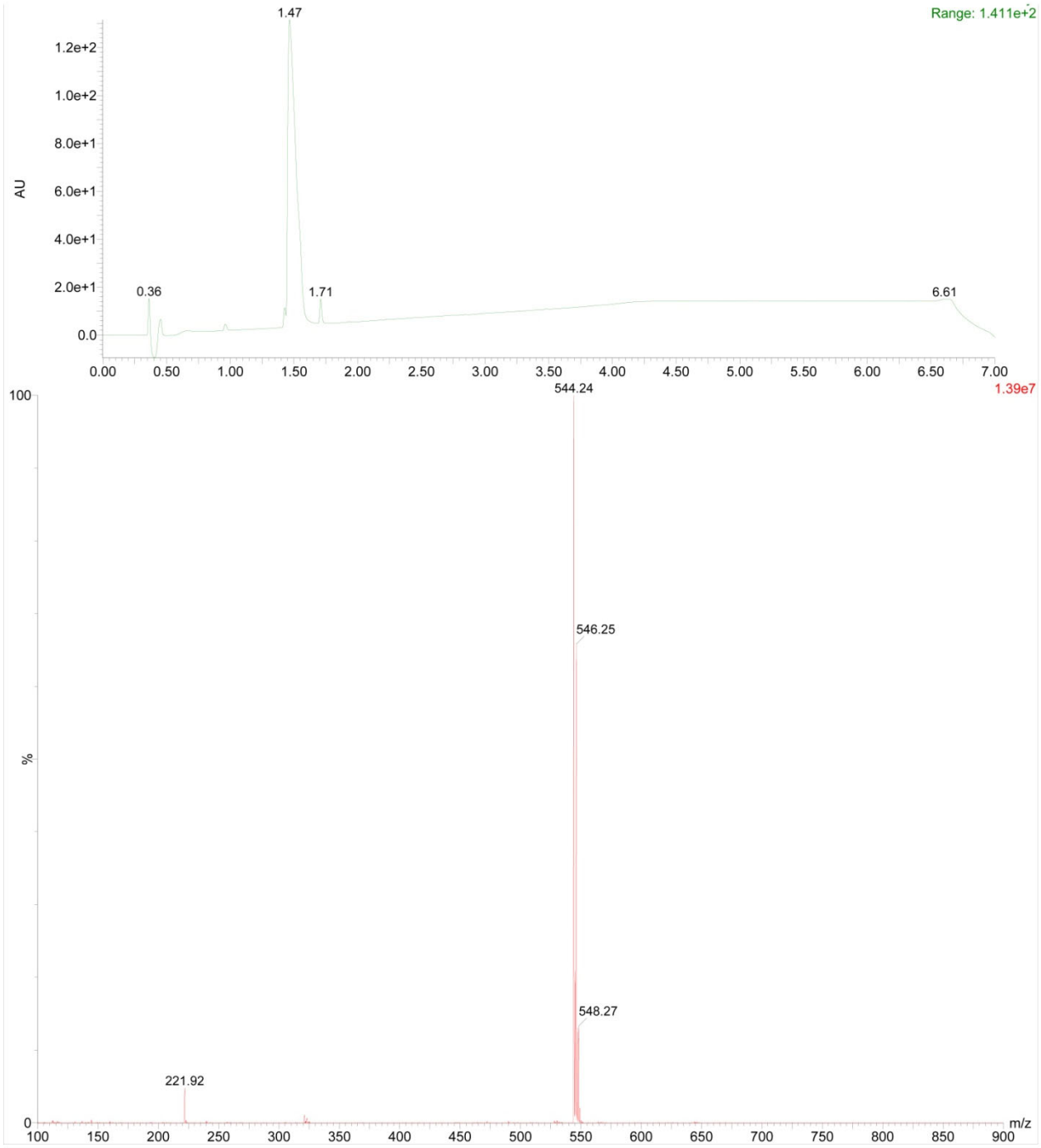

Figure S68. The ultra-performance LC (top) and Mass (bottom) spectrum of **4d**, $[M-H]^-$ at m/z 544.24.

Table S2. The stability of CLsu, **1c**, **1d**, **1k**, **1o**, **2b**, **2c** and **2f** in human serum.[a]

Compound	Compounds remaining (%)		
	0 h	2 h	24 h
CLsu	100	96.2	87.0
1c	100	0	0
1d	100	16.7	0
1k	100	0	0
1o	100	7.2	0
2b	100	52.9	0
2c	100	49.2	0
2f	100	0	0

[a.] All compounds were incubated in human serum (from human male AB plasma) at the concentration at 200 μM, 37 ℃ for 2 h and 24 h, respectively.

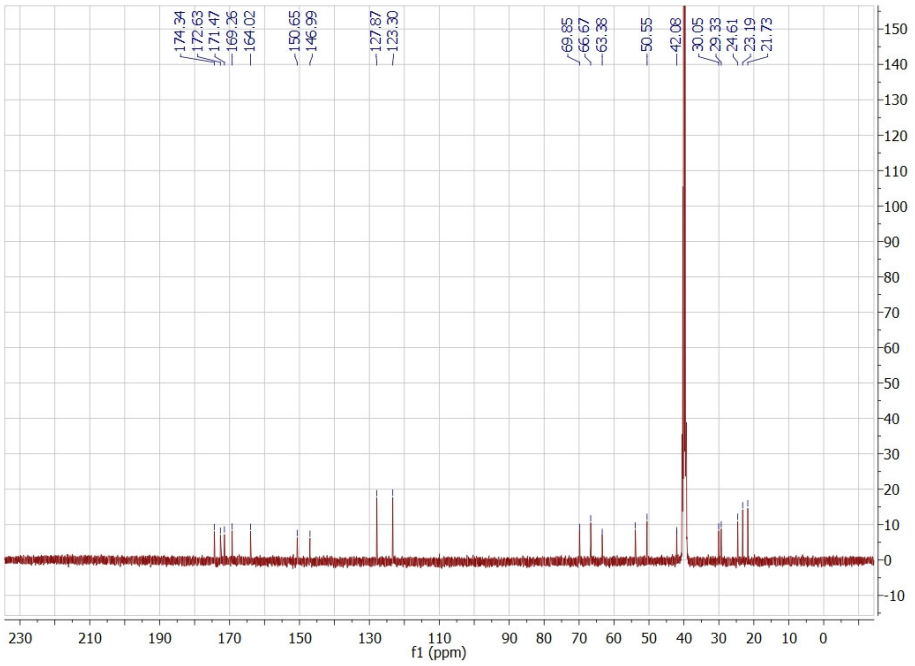

Figure S69. ^{13}C NMR of **1a** in DMSO-d_6.

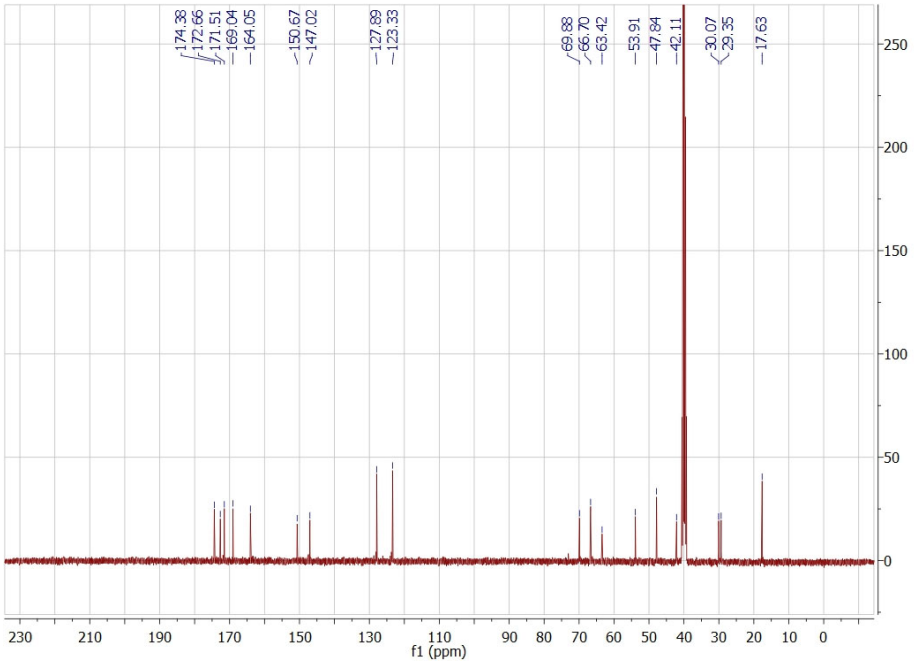

Figure S70. ^{13}C NMR of **1b** in DMSO-d_6.

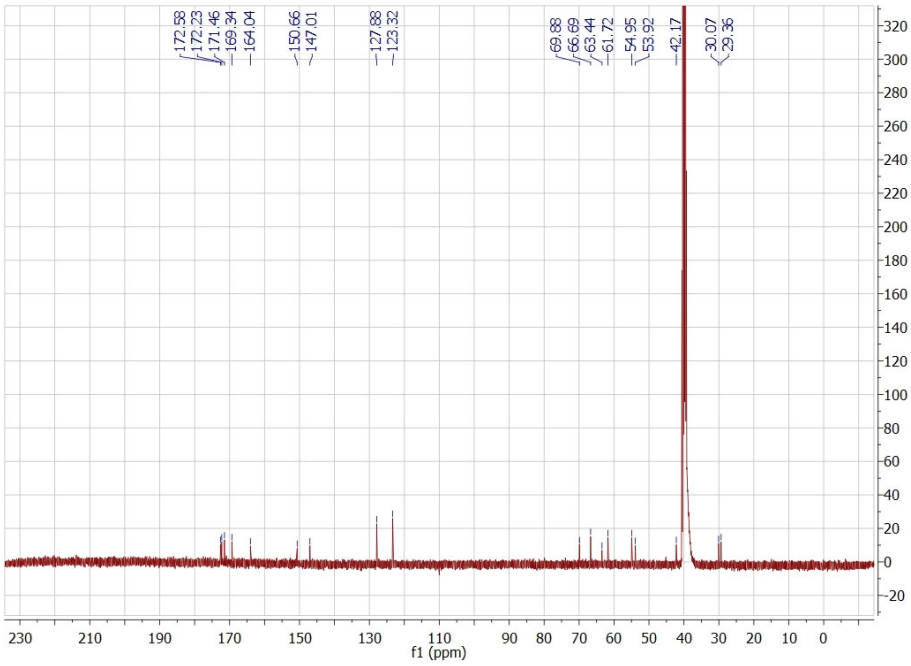

Figure S71. ^{13}C NMR of **1c** in DMSO-*d*$_6$.

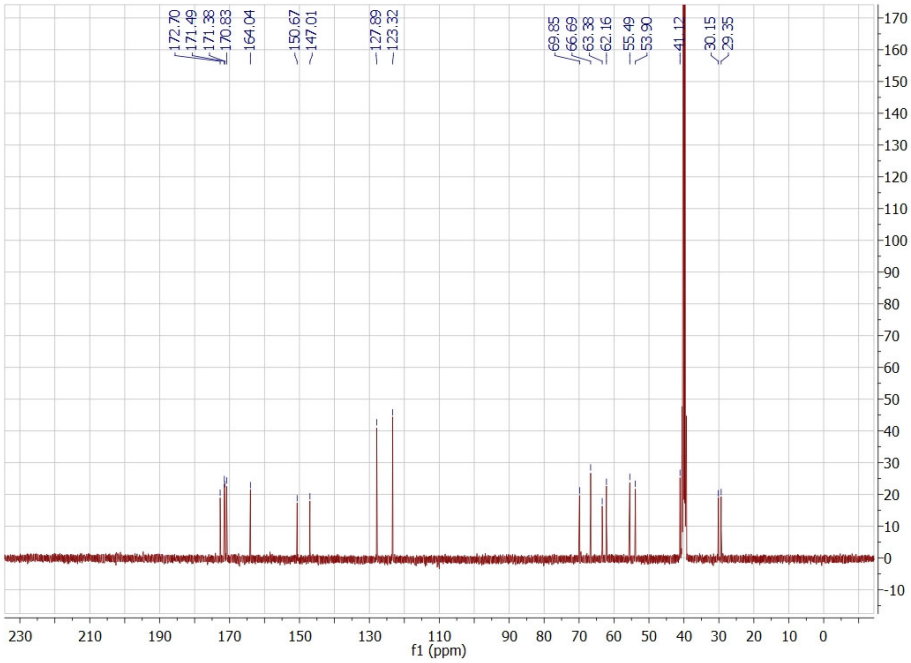

Figure S72. ^{13}C NMR of **1d** in DMSO-*d*$_6$.

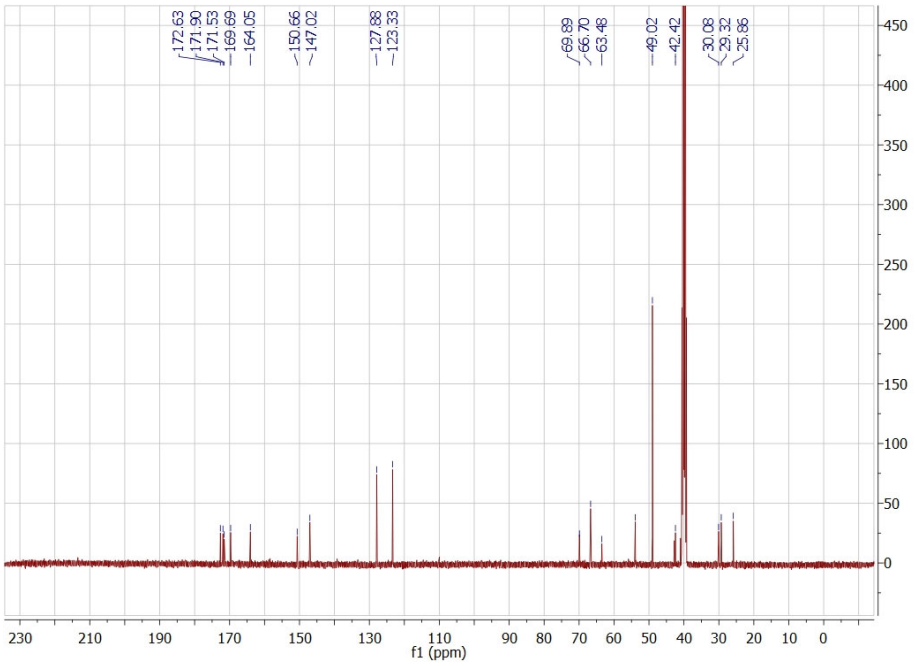

Figure S73. ^{13}C NMR of **1e** in DMSO-*d*$_6$.

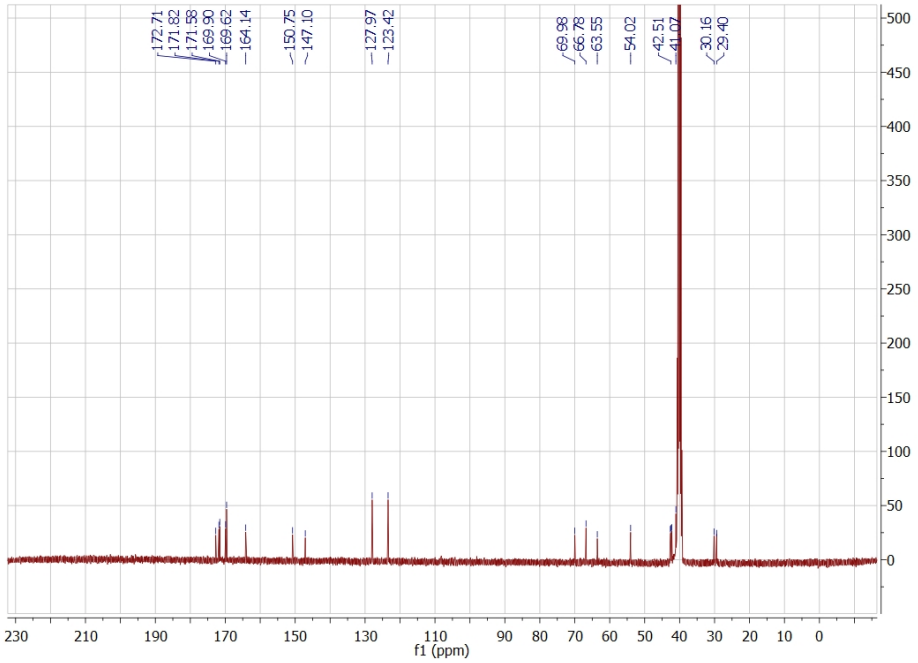

Figure S74. ^{13}C NMR of **1f** in DMSO-*d*$_6$.

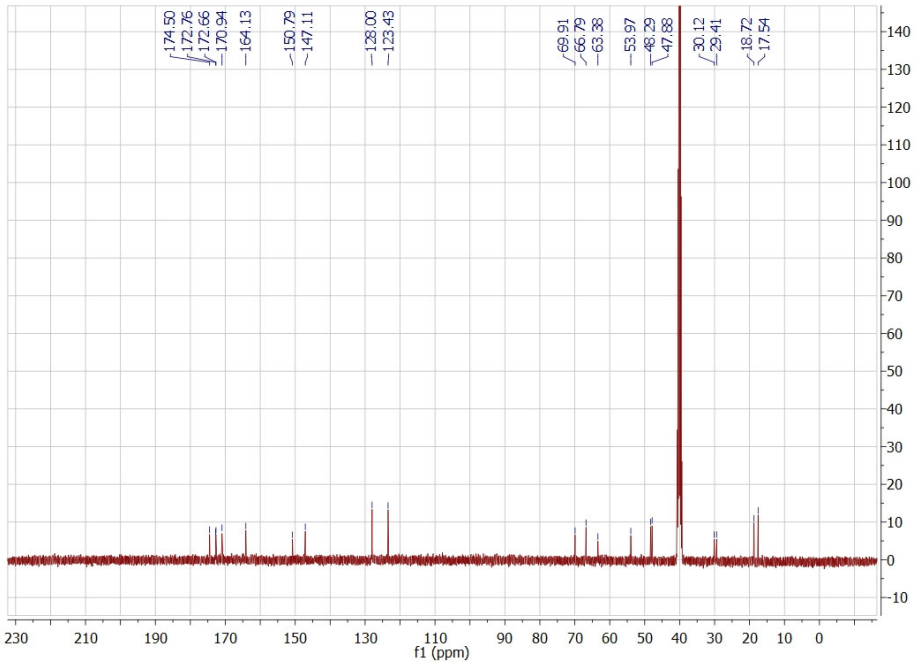

Figure S75. ^{13}C NMR of **1g** in DMSO-*d*$_6$.

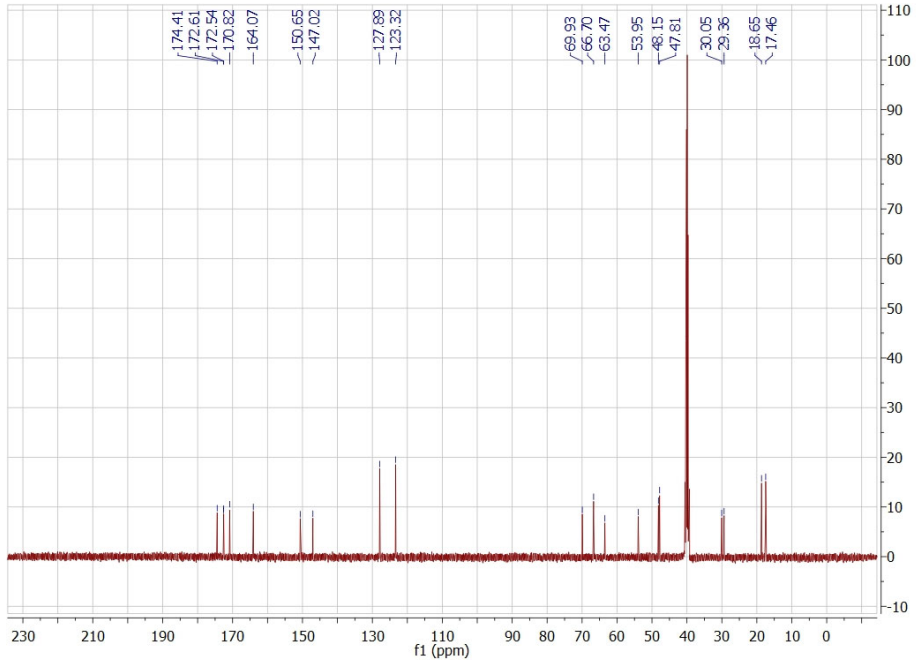

Figure S76. ^{13}C NMR of **1h** in DMSO-*d*$_6$.

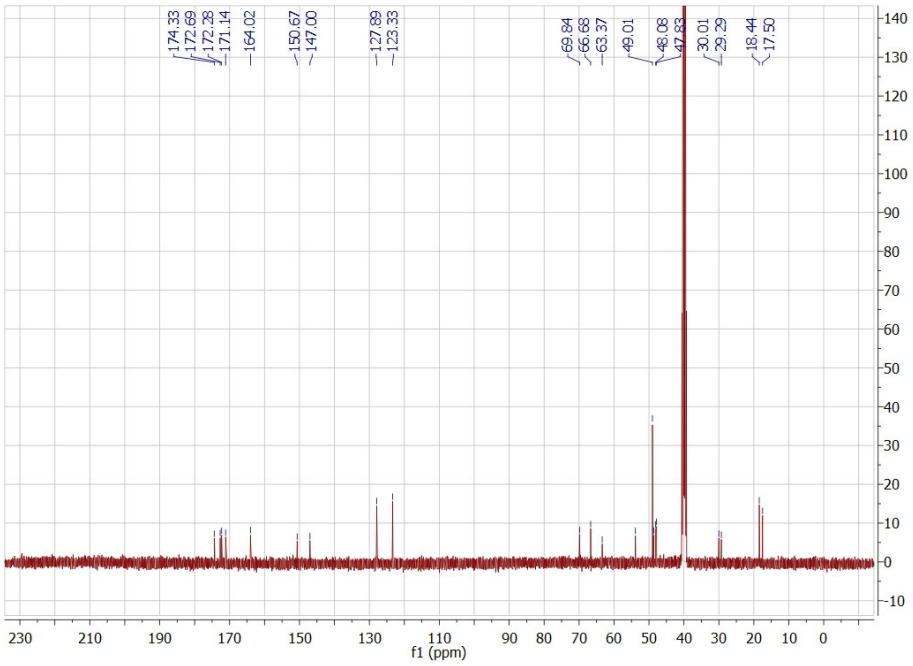

Figure S77. ^{13}C NMR of **1i** in DMSO-*d*$_6$.

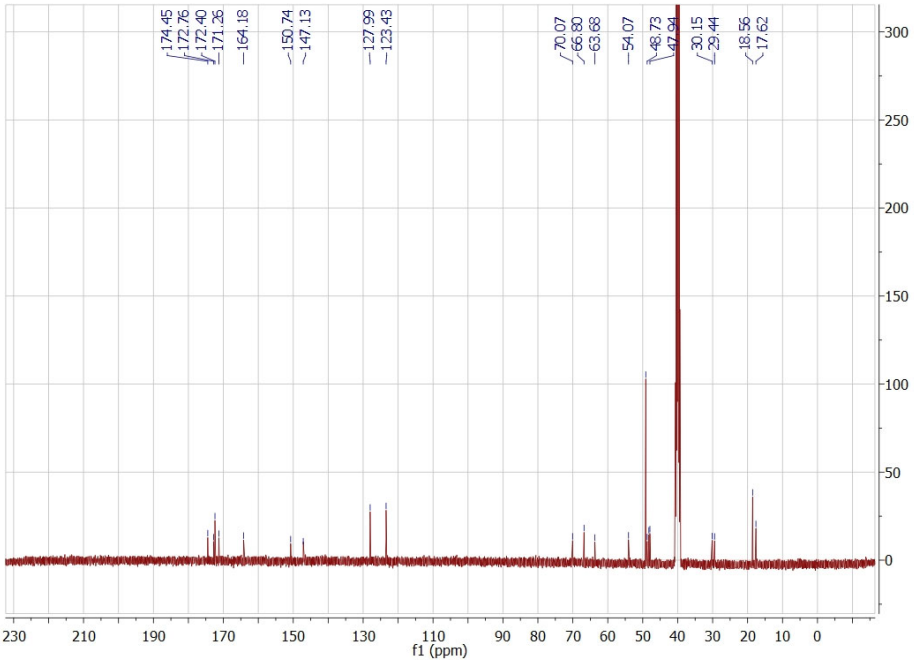

Figure S78. ^{13}C NMR of **1j** in DMSO-*d*$_6$.

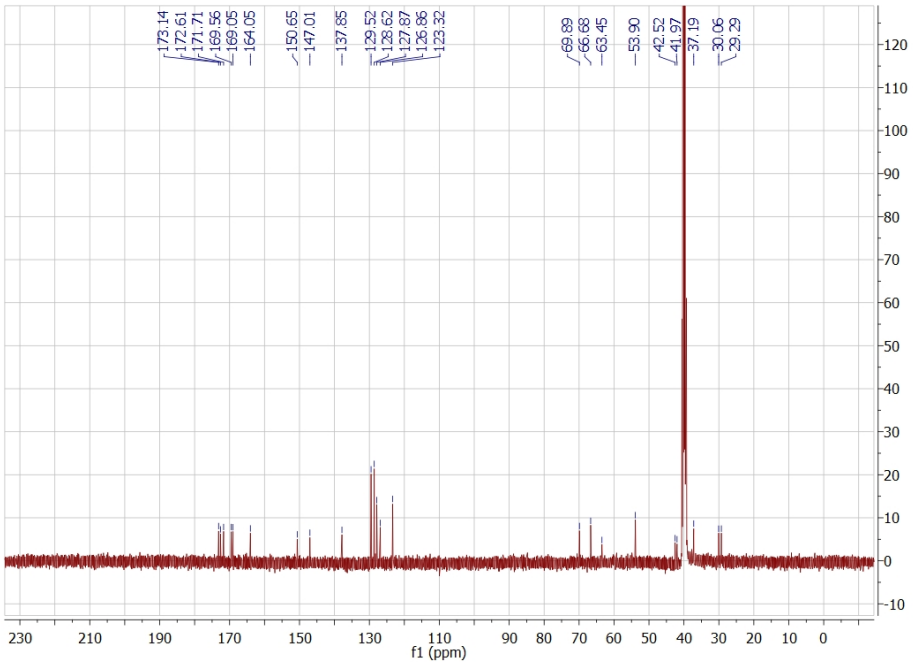

Figure S79. ^{13}C NMR of **1k** in DMSO-*d*$_6$.

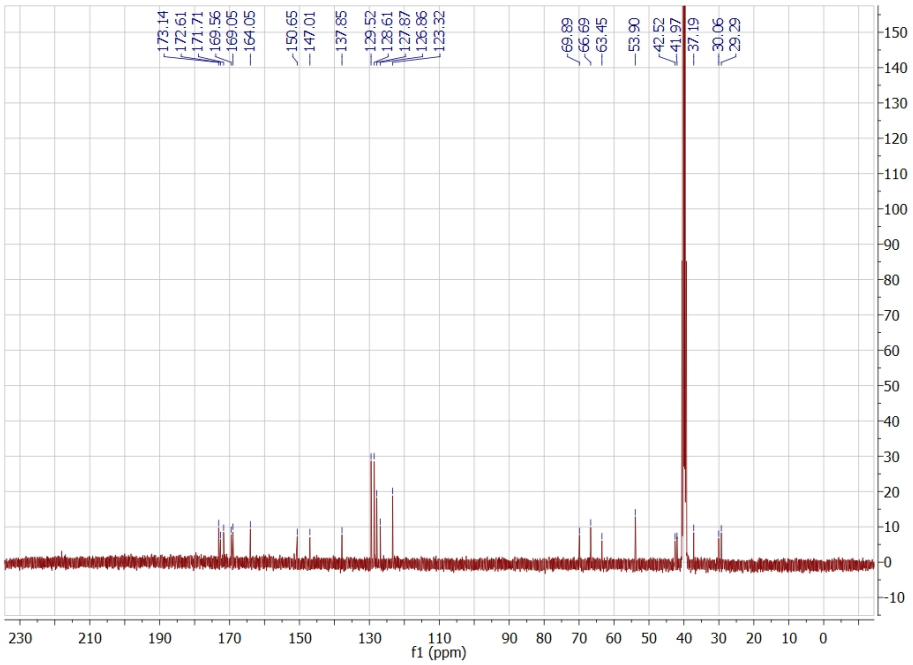

Figure S80. ^{13}C NMR of **1l** in DMSO-*d*$_6$.

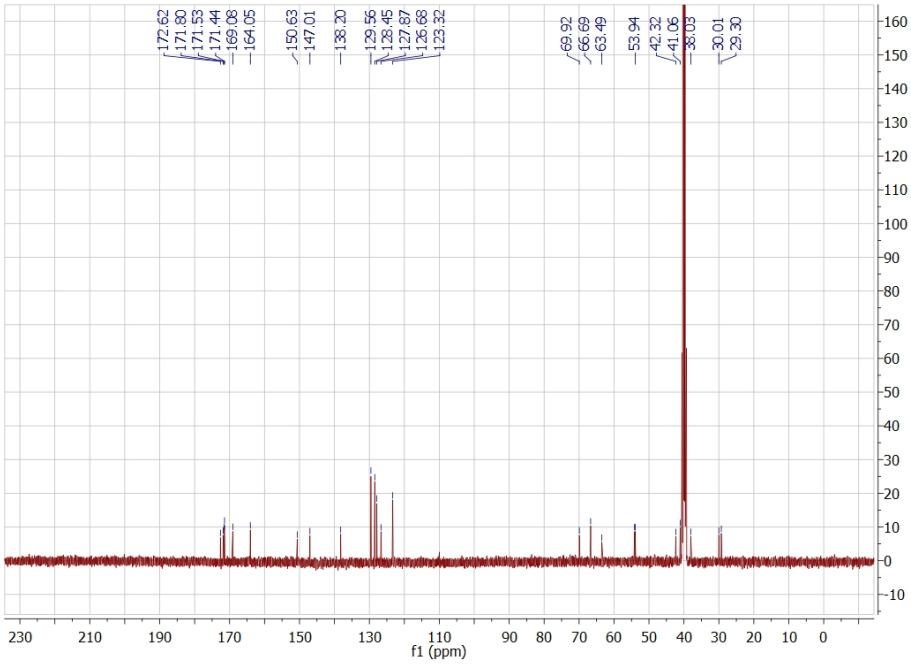

Figure S81. ^{13}C NMR of **1m** in DMSO-*d*$_6$.

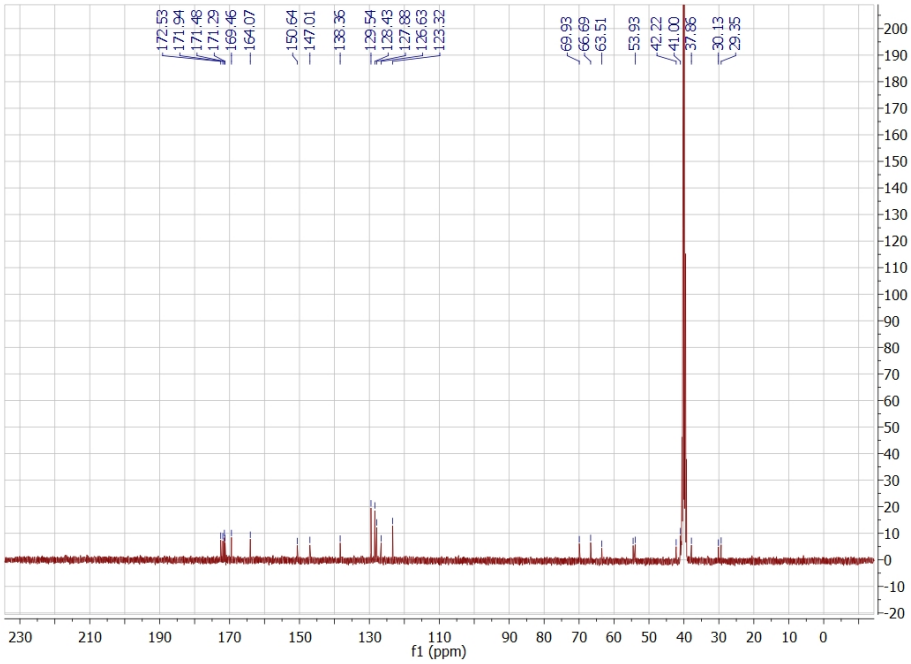

Figure S82. ^{13}C NMR of **1n** in DMSO-*d*$_6$.

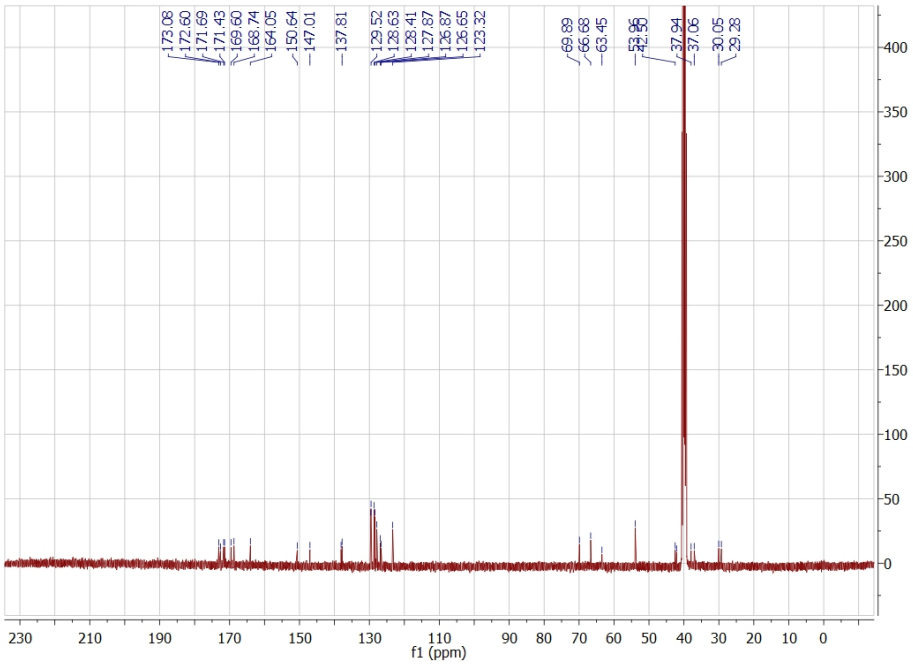

Figure S83. ^{13}C NMR of **1o** in DMSO-*d*$_6$.

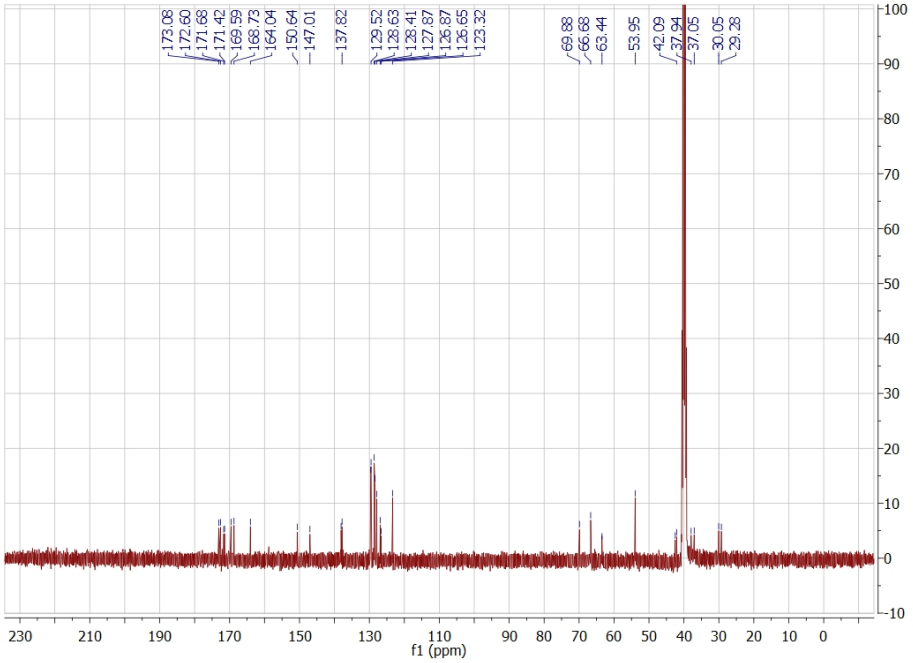

Figure S84. ^{13}C NMR of **1p** in DMSO-*d*$_6$.

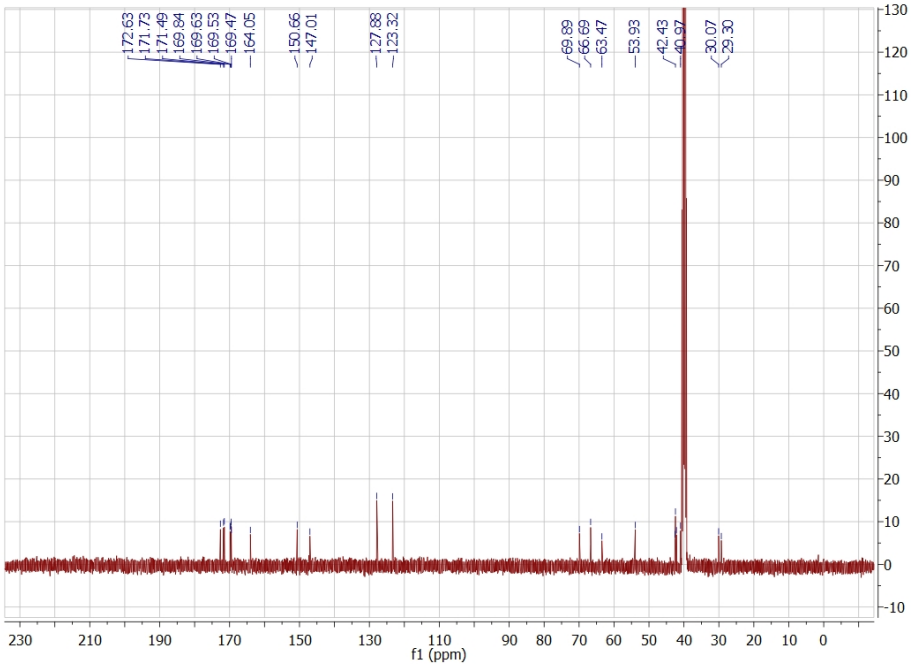

Figure S85. ^{13}C NMR of **1q** in DMSO-*d*$_6$.

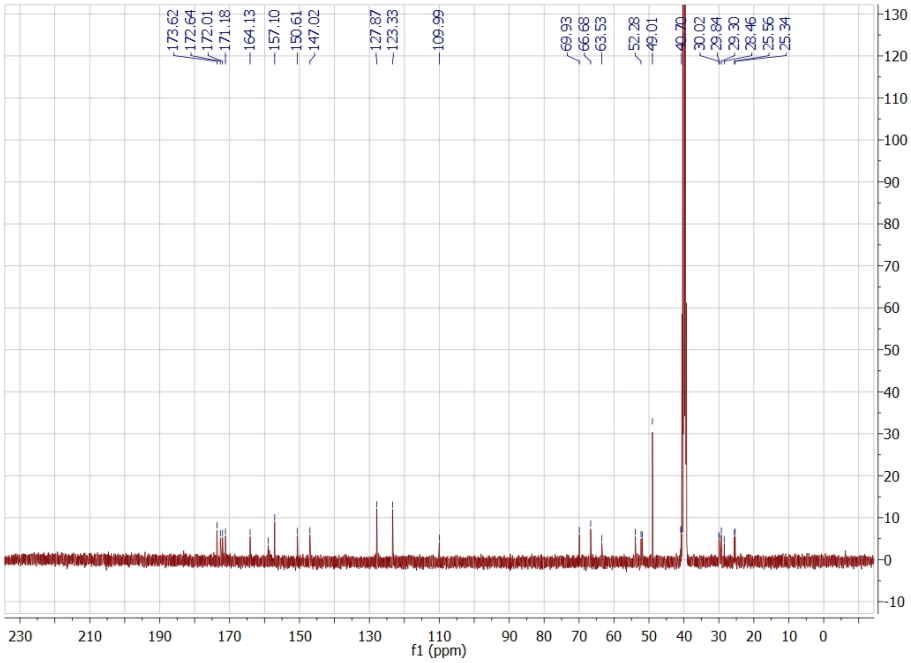

Figure S86. ^{13}C NMR of **2a** in DMSO-*d*$_6$.

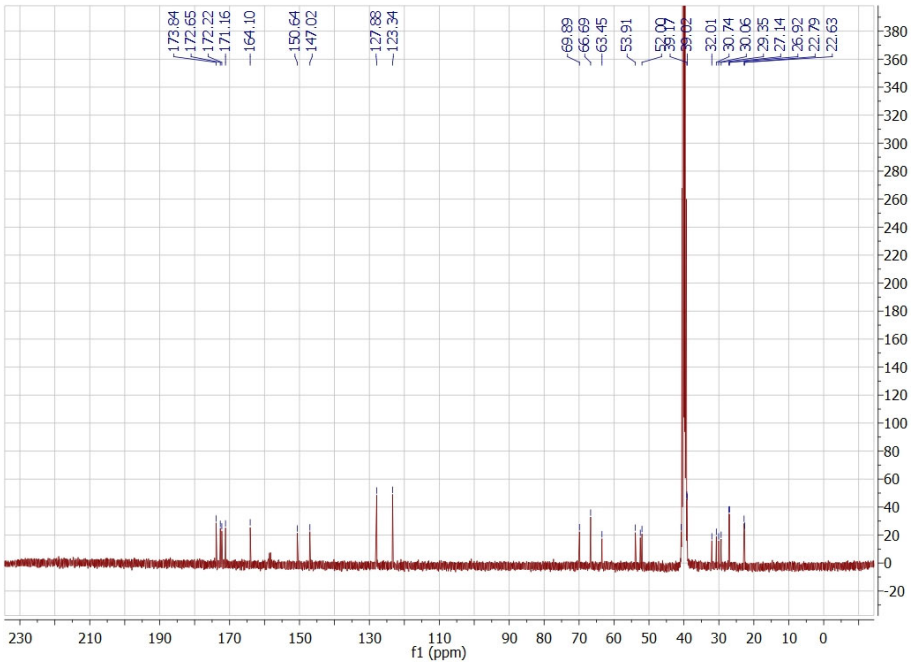

Figure S87. ^{13}C NMR of **2b** in DMSO-*d*$_6$.

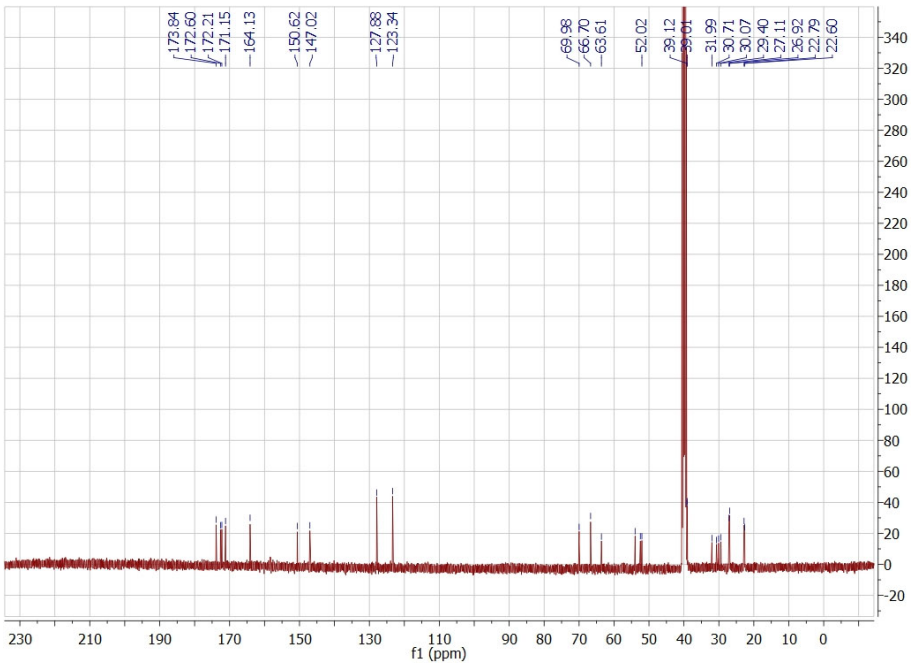

Figure S88. ^{13}C NMR of **2c** in DMSO-*d*$_6$.

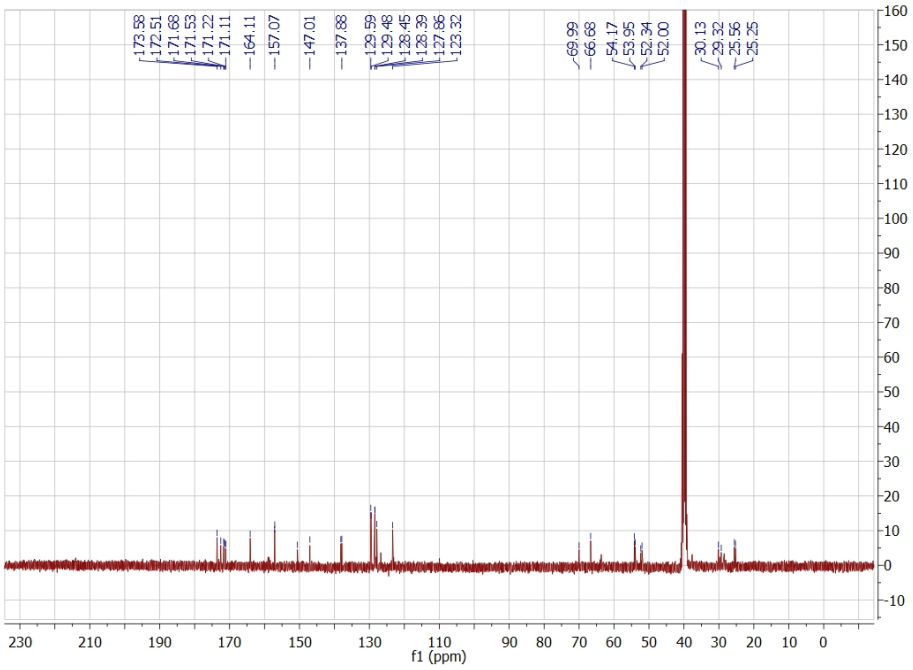

Figure S89. ^{13}C NMR of **2d** in DMSO-*d*$_6$.

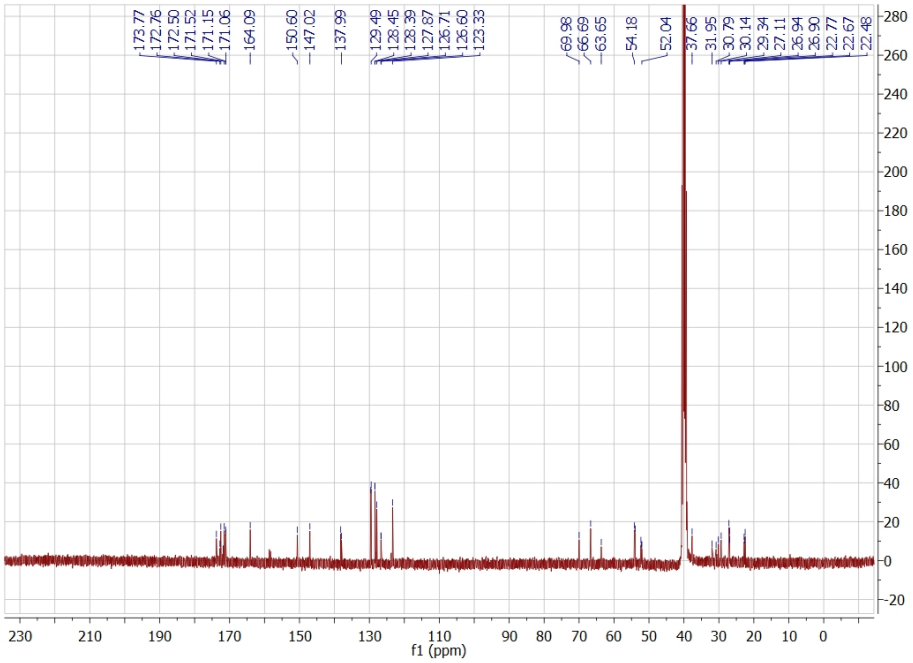

Figure S90. ^{13}C NMR of **2e** in DMSO-*d*$_6$.

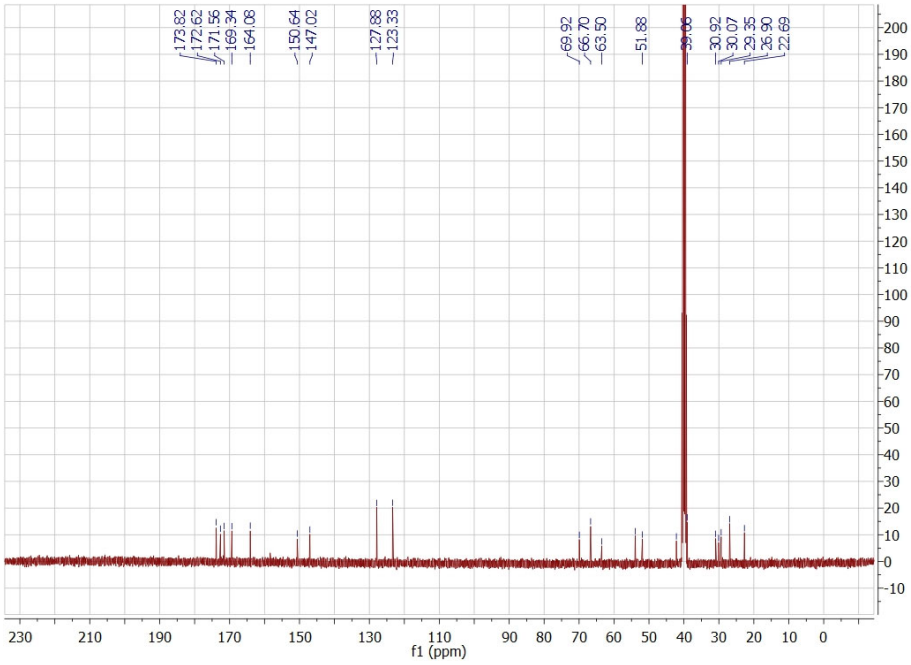

Figure S91. ^{13}C NMR of **2f** in DMSO-*d*$_6$.

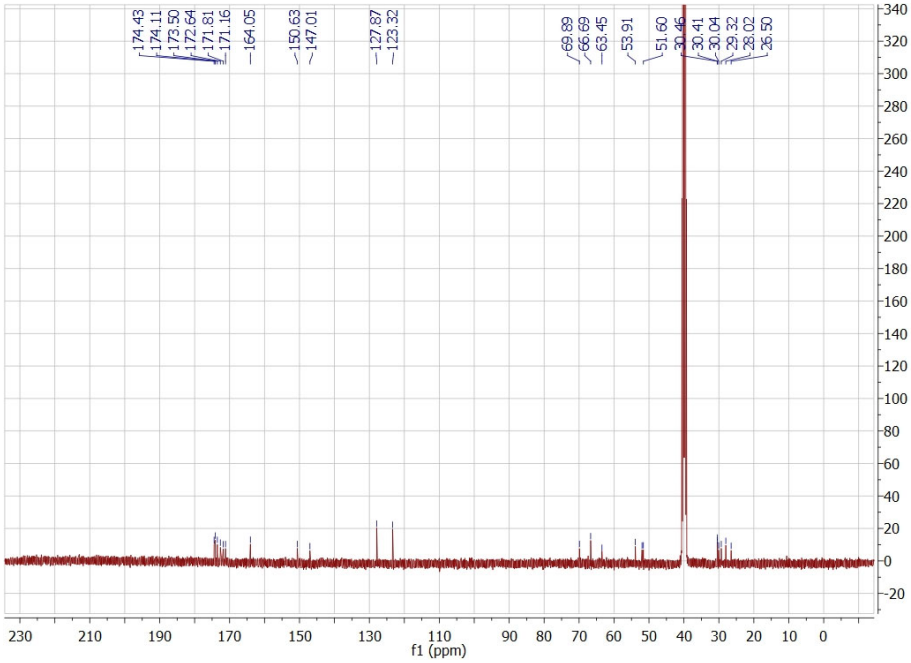

Figure S92. ^{13}C NMR of **2g** in DMSO-*d*$_6$.

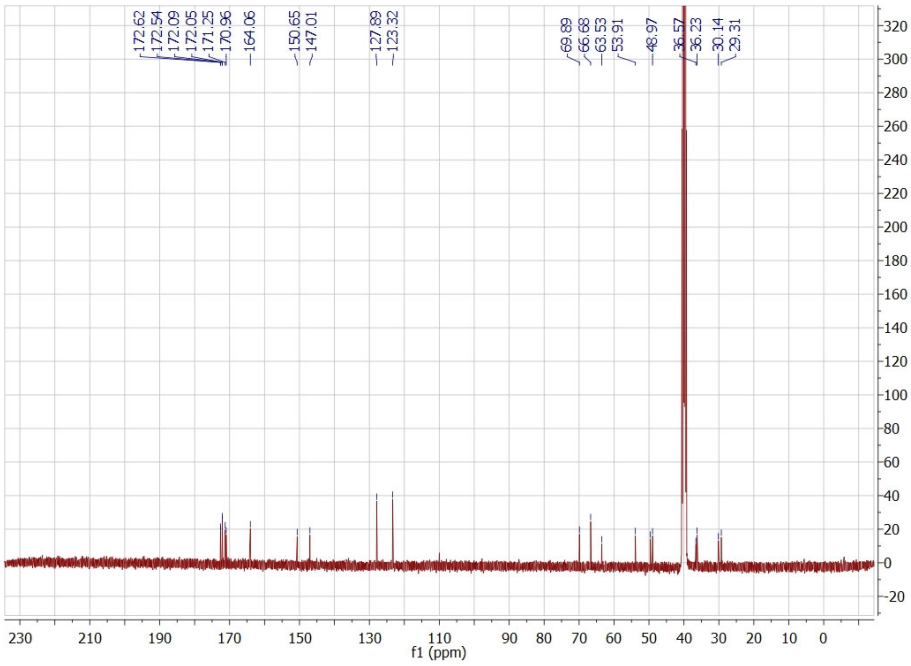

Figure S93. ^{13}C NMR of **2h** in DMSO-*d*$_6$.

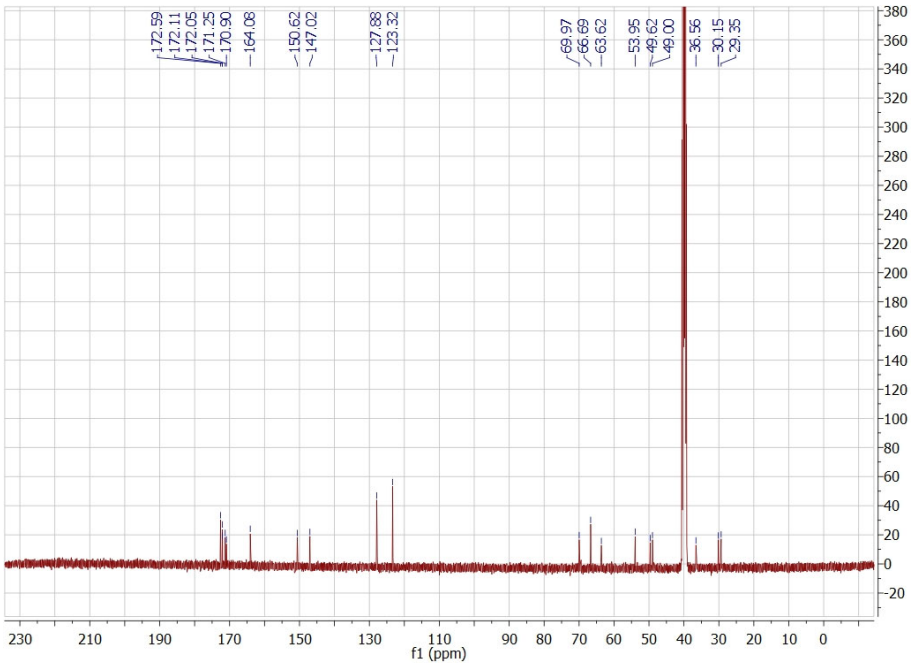

Figure S94. ^{13}C NMR of **2i** in DMSO-*d*$_6$.

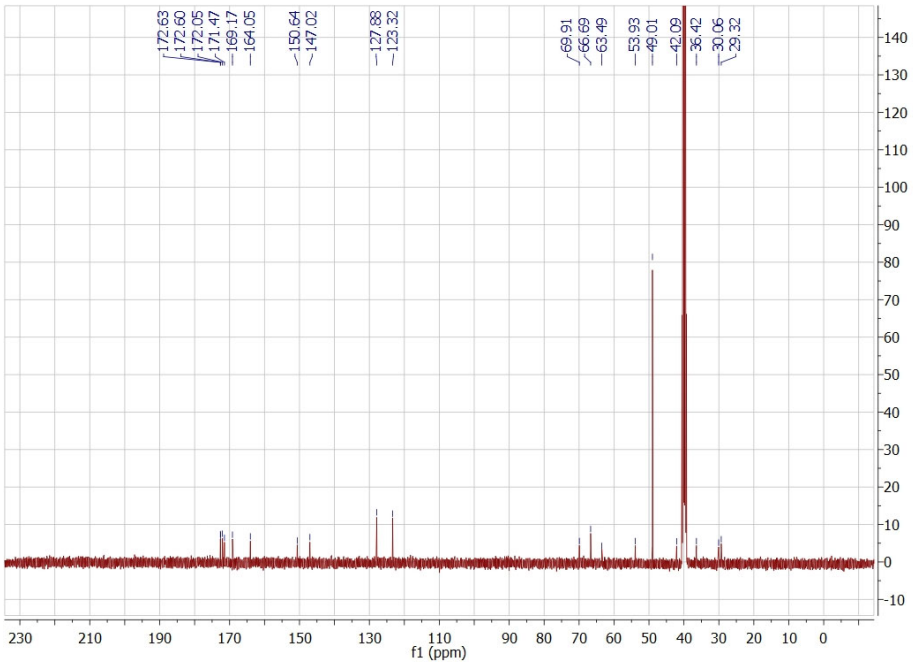

Figure S95. ^{13}C NMR of **2j** in DMSO-*d*$_6$.

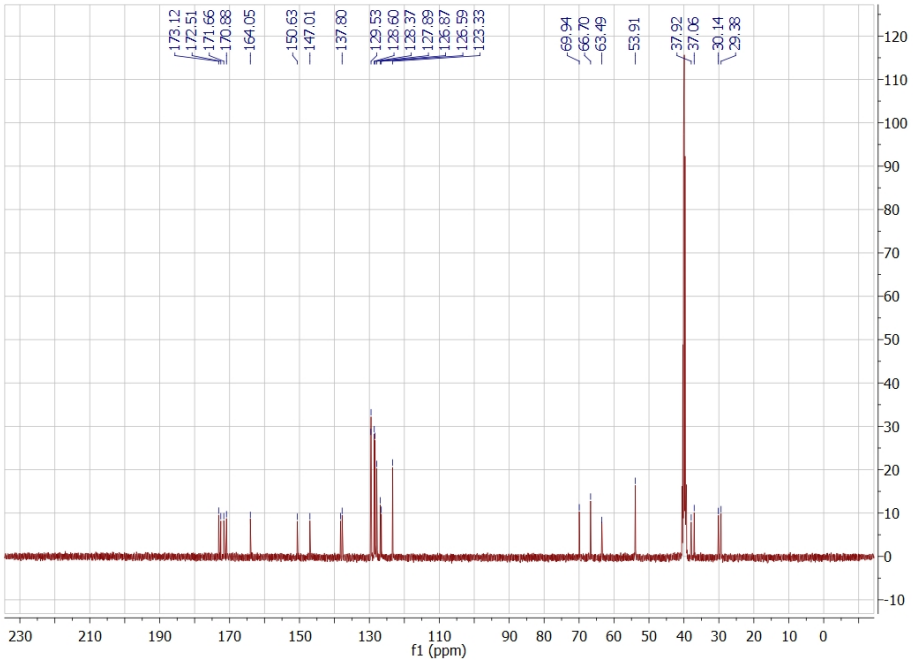

Figure S96. ^{13}C NMR of **3a** in DMSO-*d*$_6$.

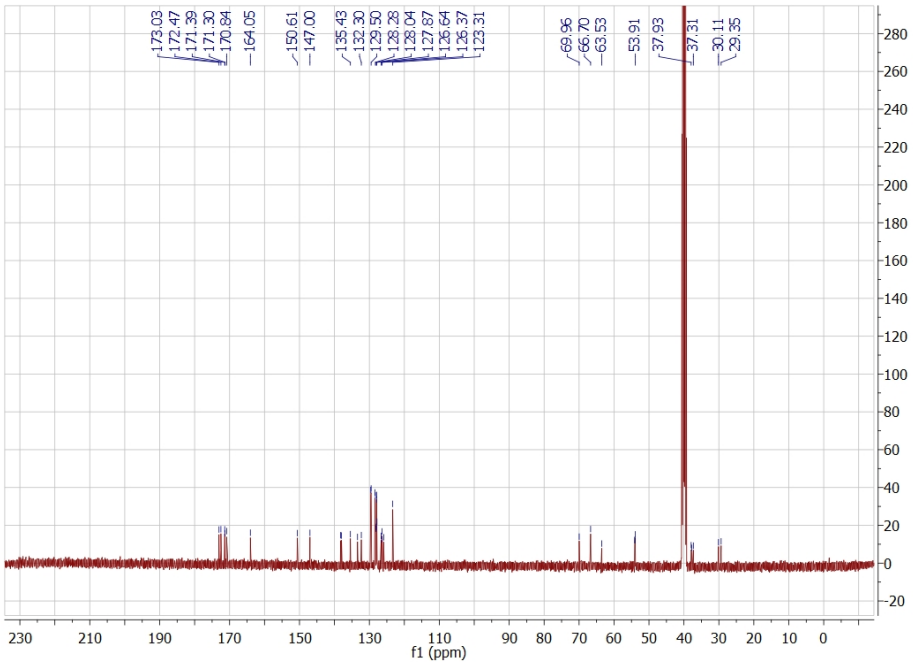

Figure S97. ^{13}C NMR of **3b** in DMSO-*d*$_6$.

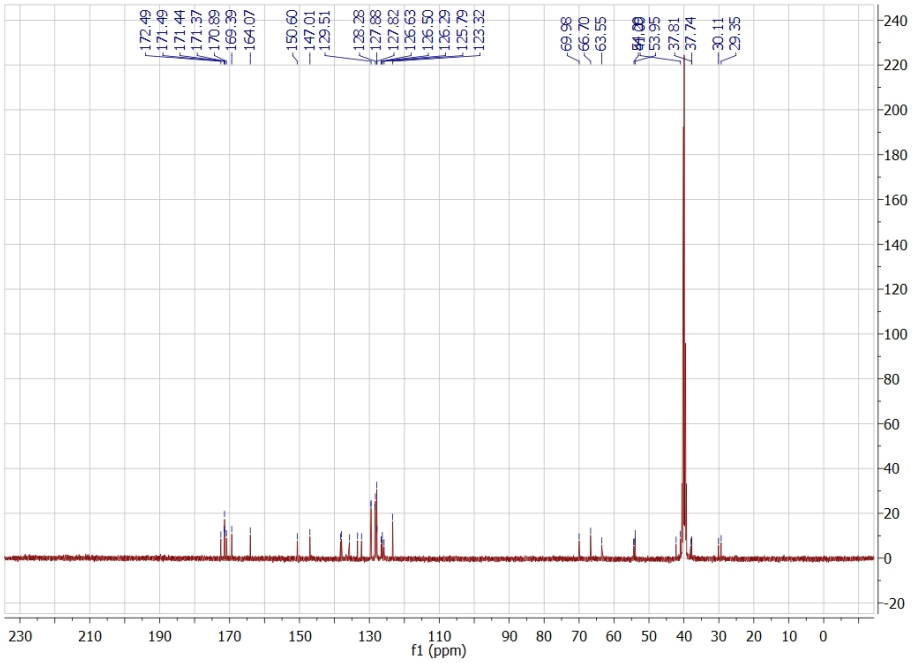

Figure S98. ^{13}C NMR of **3c** in DMSO-*d*$_6$.

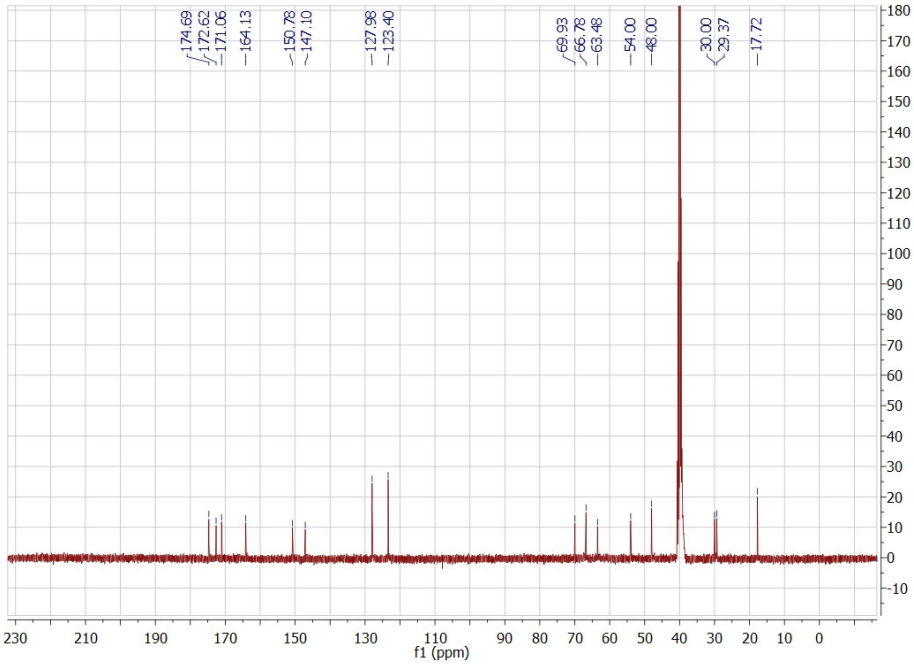

Figure S99. ^{13}C NMR of **4a** in DMSO-*d*$_6$.

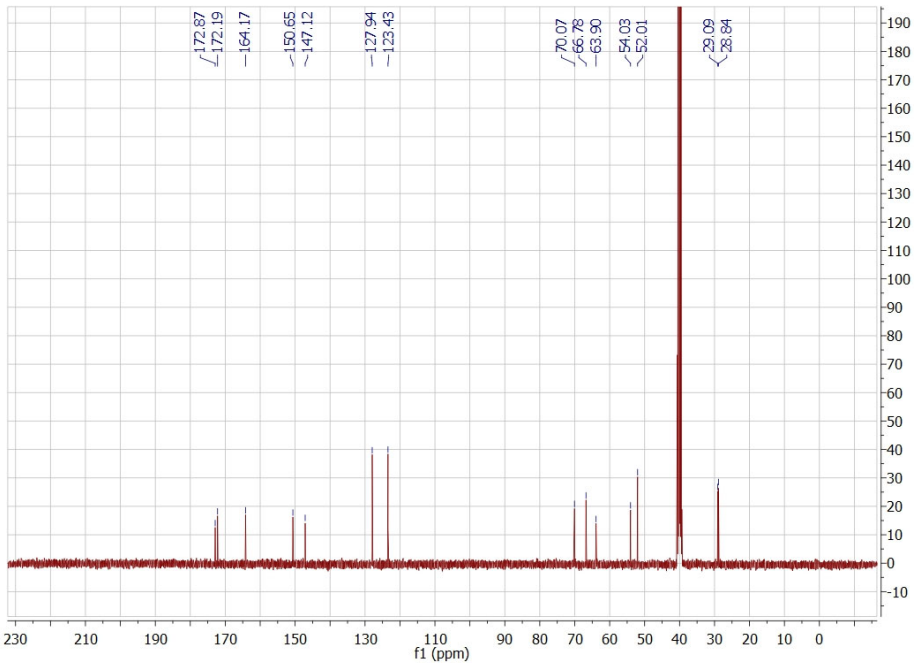

Figure S100. ^{13}C NMR of **4b** in DMSO-*d*$_6$.

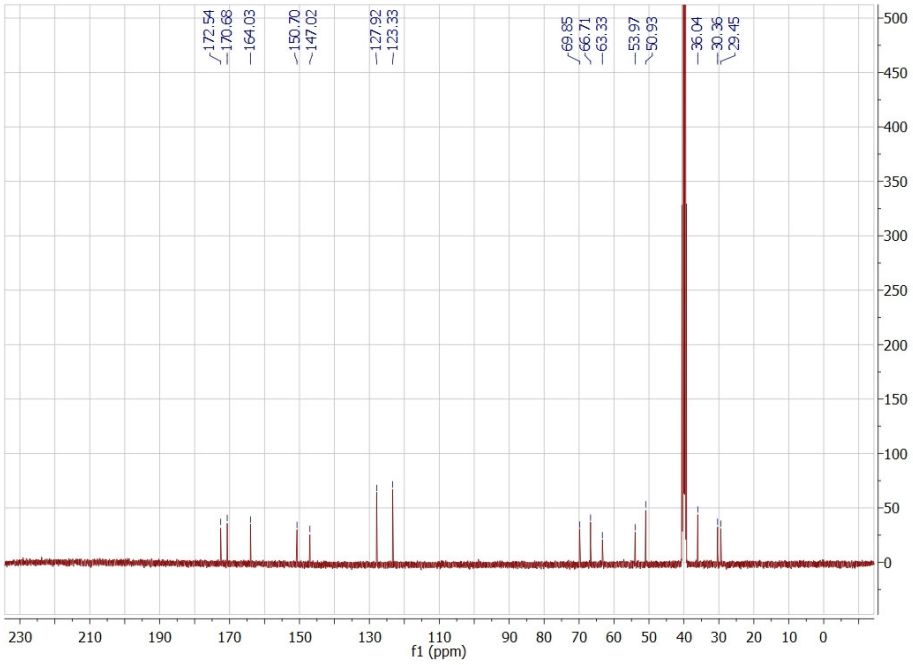

Figure S101. ^{13}C NMR of **4c** in DMSO-*d*$_6$.

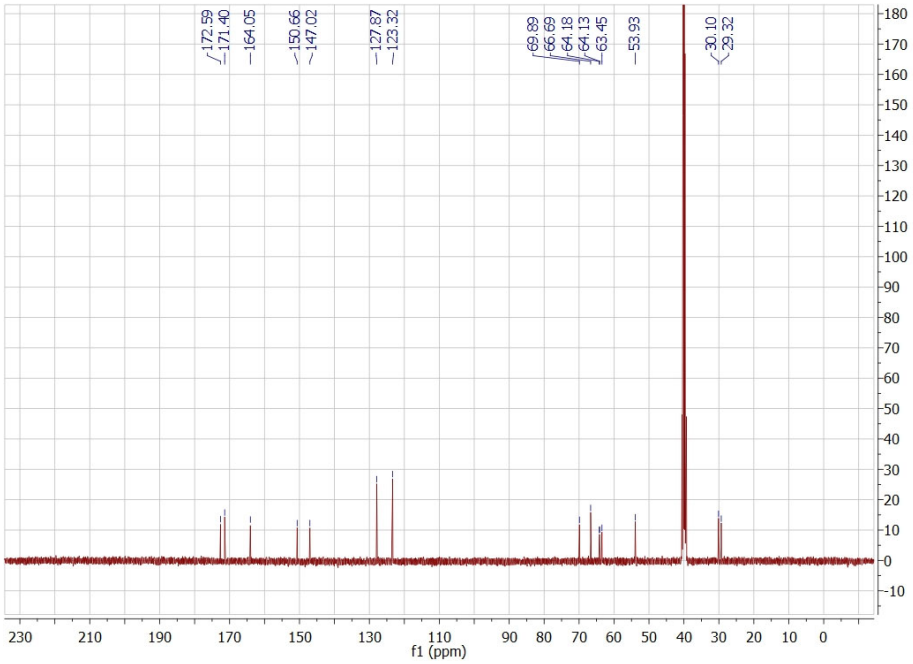

Figure S102. ^{13}C NMR of **4d** in DMSO-*d*$_6$.